ISSN 1881-7815 Online ISSN 1881-7823

BST
BioScience Trends

Volume 9, Number 4
August, 2015

IRCA
BSSA

IACMHR

www.biosciencetrends.com

BST
BioScience Trends

ISSN: 1881-7815
Online ISSN: 1881-7823
CODEN: BTIRCZ
Issues/Year: 6
Language: English
Publisher: IACMHR Co., Ltd.

BioScience Trends is one of a series of peer-reviewed journals of the International Research and Cooperation Association for Bio & Socio-Sciences Advancement (IRCA-BSSA) Group and is published bimonthly by the International Advancement Center for Medicine & Health Research Co., Ltd. (IACMHR Co., Ltd.) and supported by the IRCA-BSSA and Shandong University China-Japan Cooperation Center for Drug Discovery & Screening (SDU-DDSC).

BioScience Trends devotes to publishing the latest and most exciting advances in scientific research. Articles cover fields of life science such as biochemistry, molecular biology, clinical research, public health, medical care system, and social science in order to encourage cooperation and exchange among scientists and clinical researchers.

BioScience Trends publishes Original Articles, Brief Reports, Reviews, Policy Forum articles, Case Reports, News, and Letters on all aspects of the field of life science. All contributions should seek to promote international collaboration.

Editorial Board

Editorial Office

Pearl City Koishikawa 603,
2-4-5 Kasuga, Bunkyo-ku,
Tokyo 112-0003, Japan
Tel: +81-3-5840-8764
Fax: +81-3-5840-8765
E-mail: office@biosciencetrends.com

BioScience Trends

Editorial and Head Office

Pearl City Koishikawa 603, 2-4-5 Kasuga, Bunkyo-ku,
Tokyo 112-0003, Japan

Tel: +81-3-5840-8764, Fax: +81-3-5840-8765
E-mail: office@biosciencetrends.com
URL: www.biosciencetrends.com

CONTENTS

Volume 9, Number 4, 2015

Review

Original Articles

Brief Reports

Guide for Authors

Copyright

Mini-Review

DOI: 10.5582/bst.2015.01078

Substrates of the human oligopeptide transporter hPEPT2

Dongxin Zhao[1,*], Kui Lu[1,2,*]

[1] *School of Chemistry and Chemical Engineering, Henan University of Technology, Zhengzhou, China;*
[2] *Department of Materials and Chemical Engineering, Henan Institute of Engineering, Zhengzhou, China.*

Summary **Oligopeptide transporters serve important functions in nutrition and pharmacology. In particular, these transporters help maintain the homeostasis of peptides. The peptide-transporter PEPT2 is a high-affinity and low-capacity type oligopeptide transporter from the proton-coupled oligopeptide transporter family. PEPT2 has recently received attention because of its potential application in targeted drug delivery. PEPT2 is widely distributed in kidney, central nervous system, and lung of organisms. In general, all dipeptides, tripeptides, and peptide-like drugs such as β-lactam antibiotics and angiotensin-converting enzyme inhibitors could be mediated and transported as a substrate of PEPT2. The design of many extant drugs and prodrugs is based on the substrate structure of PEPT2 to accelerate absorption via peptide transporters. Thus, this paper summarizes the substrate features of PEPT2 to promote the rational design of drugs and prodrugs that target peptide transporters.**

Keywords: PEPT2, peptide, drug, substrate structure, regulation

1. Introduction

Proton-coupled oligopeptide transporters (POTs) are membrane proteins that can translocate various dipeptides, tripeptides, and peptide-like drugs across the biological membrane (*1,2*). The POT family, also called the solute carrier 15 family (SLC15), comprises four peptide transporters in mammals: PEPT1 (SLC15A1), PEPT2 (SLC15A2), PHT1 (SLC15A4), and PHT2 (SLC15A3). The peptide-transporter PEPT2 is widely expressed in various tissues, with predominant expression in the kidney, brain, lung, eye, prostate, astrocytes, spleen, uterus, and mammary gland (*3-6*). Given its 15 times higher affinity than PEPT1 to the same substrates, PEPT2 was characterized as a high-affinity, low-capacity transporter (*7,8*). PEPT2 can sequence-independently transport more than 400 dipeptides and 8,000 tripeptides, which are comprised of 20 essential L-α-amino acids and most D-enantiomers. Aside from peptides, drugs such as numerous aminocephalosporins, selected angiotensin-converting enzyme inhibitors, peptidase inhibitors, and various novel prodrugs can also be recognized by PEPT2 (*9-11*). Therefore, PEPT2 influences the uptake, efflux, and pharmacological effects of chemical substances, such as peptides and drugs (*12*).

The primary structure of PEPT2 has been deduced by molecular cloning studies in human and animals. As shown in Figure 1, human PEPT2 (hPEPT2) contains 12 transmembrane domains (TMDs) and an extracellular loop between TMDs 9 and 10, with the N- and C-termini facing the cytosol (*13,14*). The conserved Arg57, His121, Tyr56, Tyr64, and Tyr167 were essential for transport activity and substrate binding (*14*). And the putative substrate-binding domain in PEPT2 lays in the region TMDs 7, 8, and 9. The phenotypic characteristics of PEPT2 are determined by TMDs 1 to 9. The region between the centers of the TMDs 2 and 3 significantly contributes to the characteristic pH-dependency of transport. In addition, the large extracellular loop between TMDs 9 and 10 might not be responsible for substrate binding (*7,10,15*). And the amino acids were critical for functional divergence located in the hydrophobic region between predicted

**Address correspondence to:*
Dr. Dongxin Zhao, School of Chemistry and Chemical Engineering, Henan University of Technology, Locus Street, Hi-Tech Industrial Development Zone, Zhengzhou 450001, Henan, China.
E-mail: zhaodx798@163.com

Dr. Kui Lu, School of Material and Chemical Engineering, Henan Institute of Engineering, Zhengzhou 450007, Henan, China.
E-mail: luckyluke@126.com

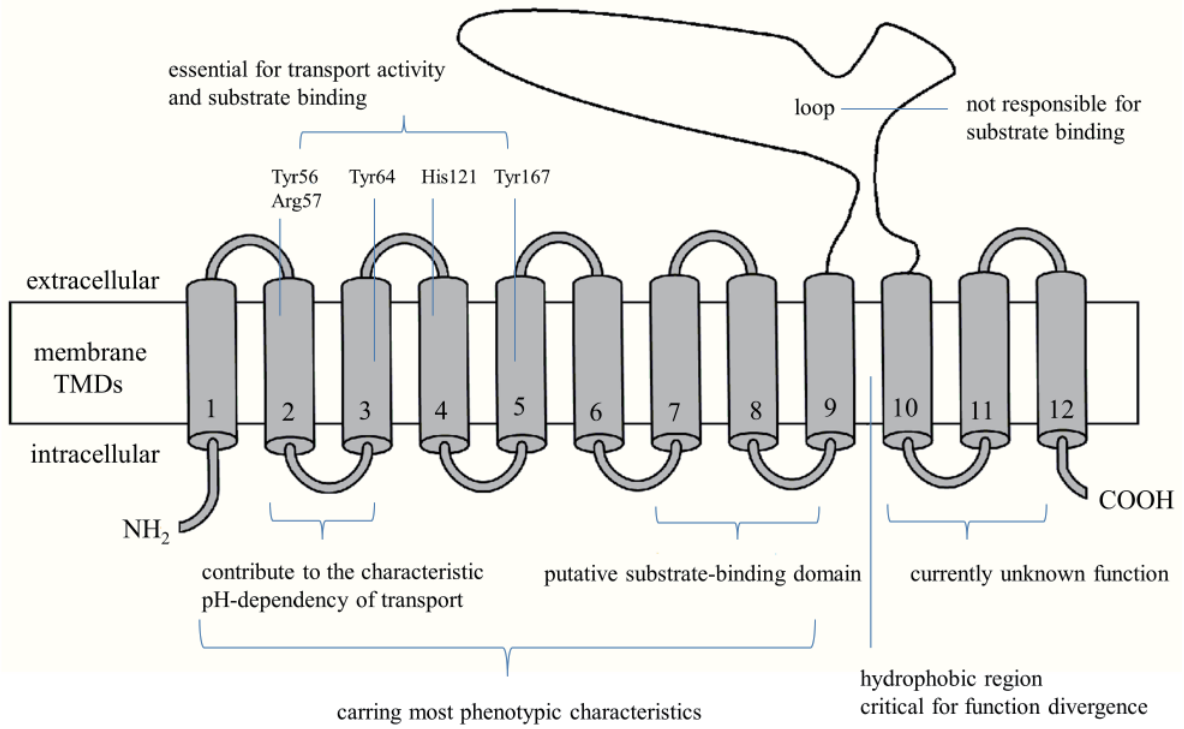

Figure 1. Functionally relevant domains of PEPT2 revealed by chimeric and mutant proteins.

TMDs 9 and 10 (*16*).

Functional studies on PEPT2 principally focused on the kidney and choroid plexus. In the kidney, PEPT2 is mainly found in the S3 segment of the tubule, but the renal PEPT2 is almost entirely responsible for the reabsorption of peptides and peptidomimetics (*10,11,16*). In the choroid plexus, PEPT2 is the only transporter responsible for the exposure of peptide and peptidomimetics in the cerebrospinal fluid (*17*). A few studies also detected PEPT2 in other organs. For example, PEPT2 might have an important role in the metabolism of the central nervous system (*18*), the delivery of peptides and peptidomimetics in human lung, and the reuptake of small peptides that accumulate from the hydrolysis of milk proteins in the mammary gland (*19*). Otherwise, PEPT2 alterations in various tissues could lead to the functional loss of transport activity. However, experiments demonstrated that PEPT2-null animals were healthy and fertile. In addition, neither clinical chemistry data obtained from plasma and urine samples nor general physiological measures indicated any significant metabolic perturbation (*4,20,21*). Therefore, the exact physiological role of PEPT2 warrants further studies.

Previous research determined the transport capability of PEPT2 through a systematic investigation of its structural influence on the uptake or transport of dipeptides and tripeptides, β-lactam antibiotics, and peptidase inhibitors in different organs (*4,22*). However, the function of PEPT2 remains unclear, and the structural features of its substrates are complex and incertain. In addition, a standard molecular structure model of the substrates has yet to be established. Accordingly, this review summarizes reports about the substrate structure of PEPT2 to understand the basic characteristics of PEPT2.

2. Substrate structure

As a high-affinity, low-capacity transporter, PEPT2 can transport almost all dipeptides, tripeptides and peptide-like drugs which differ in physicochemical characteristics, molecular mass, charge, and polarity. However, PEPT2 also displays specificity through its various substrate affinities depending on the particular substrate structure. This phenomenon is important when designing pharmacologically active compounds for delivery *via* PEPT2 because the substrate-binding sites provide freedom to accommodate molecules with unusual structures and pharmacological activities (*23*).

The molecular basis of the natural peptide and drug substrates of PEPT2 must be explored to understand the basic structural features of substrates (*24*). Rational and nonrational approaches have been applied to explain individual substrate specificities of PEPT2 and design compounds optimized for absorption by PEPT2. The essential structural elements of substrates will be discussed in detail below.

2.1. *α-Amino group*

A free α-amino may be essential for the substrate to be recognized by PEPT2. Many substrates have a free

α-amino group that shows high affinity to PEPT2. The α-amino group interacts with histidine residues of PEPT2 that may be involved in substrate recognition by peptide transporters (*25*). By contrast, reports also suggested that free α-amino may be unessential for recognition. For example, a study on the transport of quinapril, captopril, and enalapril showed that a free α-amino group is not an absolute requirement for substrate recognition by PEPT2 in the kidney (*26,27*). However, the substitution of this amino group by hydroxy or mercapto groups leads to loss of affinity. Thus, the presence of a free α-amino group is important but not mandatory for recognition by PEPT2.

2.2. *Peptide bond*

Peptide bond is an unessential group for recognition by PEPT2. The peptide bond of aminolevulinic acid (ALA) was replaced by a ketomethylene, which can serve as a substrate of PEPT2 (*27*). With a positively and a negatively charged head group separated by at least four methylene groups, omega-amino fatty acids can be transported by PEPT2 (*27*). Various compounds without peptide bond(s) also can be accepted as PEPT2 substrates. Such compounds include 4-aminophenylacetic acid, δ-amino levulinic acid, ω-amino fatty acid, aminoacid aryl amide, zidovudine, L-valyl ester of acyclovir, and valacyclovir (*28-31*), which strongly challenge the obligatory need for a peptide bond. However, only dipeptides and tripeptides with the trans-configuration of peptide bonds can be transported.

2.3. *N-terminal, C-terminal and carbonyl*

Groups at the ends of substrates may play important roles in recognition. The hydrophobicity of the N-terminal region of aminopenicillins increases affinity to PEPT2 (*27*). Anserine with an N-terminal β-amino acid displays a high affinity to PEPT2 (*32*). In addition, the hydroxyl group at the N-terminal phenyl ring of a few antibiotics may be involved in the interaction with PEPT2 (*25*). The terminal carboxylic group in substrates is not required for transport and can be replaced by an electrogenic group to form amino acid aryl amides (*10*). The presence of acidic amino acids in the amino terminus may result in greater reduction in affinity than the presence of the same amino acids in the C-terminus. However, the reverse effect has been observed for basic residues (*33*). Cephalosporins and penicillins with an N-terminal amino group and a hydroxyl group at the N-terminal phenyl ring promote high affinity. However, insufficient information is available regarding the influence of the C-terminal part (*34*).

The substrate affinity of the amino fatty acid substantially increases when an additional carbonyl group is incorporated into the backbone, as realized in delta-ALA (*27*). A comparison of the chemical structures of various substrates shows that the α- or β-amino carbonyl function is the common structure that exhibits a high affinity to PEPT2 (*35*). The affinity and transport currents of compounds can increase by more than 30-fold after introducing a single carbonyl group into the backbone (*22*).

These results demonstrate that a free amino-terminus, a correctly positioned backbone carbonyl group, and a carboxylic group positioned in a suitable distance from the intramolecular carbonyl function and the amino terminal head group are the major features for substrate recognition and transport by PEPT2. The higher the hydrophobicity of the N-terminal amino acid, the higher is the affinity to PEPT2.

2.4. *Side chain*

Side chains can considerably affect the recognition and affinity of substrates. In normal dipeptides and tripeptides, the substrate binding site in PEPT2 can accept various side chains of amino acids. However, side chains are accommodated in asymmetric binding pockets. The presence of a large aromatic hydrophobic group in the side chain of the N-terminal amino acid of dipeptides could evidently enhance the binding affinity of several derivatives to PEPT2 (*36*). The terminal carboxy group requires a distinct sterical location, and binding pockets that accommodate side chains show strong hydrophobicity-dependent stereoselectivity but are asymmetric (*22*). Dipeptides that contain hydrophobic side chains, particularly those of C-terminal residues, possess high affinities. These data suggest that the presence of hydrophobic side chains is an important factor that determines substrate affinity (*10, 33*).

2.5. *Stereoselectivity*

The probability of transport is decided by the 3D structure of the substrate. Statistics indicate that substrates are always transported in a stereoselective manner with a preference for L-α amino acids. However, the presence of D-amino acids results in the lack of uptake and transport of substrate. Peptides that solely contain D-amino acids do not bind with the substrate-binding domain as free amino acids, and peptides with four or more amino acids do not serve as substrates of PEPT2 (*5*). Dipeptides that contain proline are poor substrates because of the conformational difference to normal L-α-amino acids (*37*). As a typical L-amino acid alkyl ester, L-valine methyl ester could be recognized and transported by rat PEPT2 (rPEPT2) and shows high affinity (*29,38*). PEPT2 favors dipeptides with an amino acid in LL-configuration over those in DL-configuration. The stereoselectivity of the carrier protein is pronounced for dipeptides in LD-configuration. And DD-dipeptides

are unrecognized by PEPT2 (*39*). Similar to dipeptides, tripeptides with a D-configured N-terminal amino acid show lower affinities to PEPT2 than tripeptides in LLL-configuration. Tripeptides with LDL-configuration are low-affinity substrates of PEPT2, and DDD-configured tripeptides are unrecognized (*37,40*). These data show that L-α amino acids play important roles in the structure of substrates recognized by PEPT2.

2.6. *Basic structural characteristics of the substrates*

PEPT2 can transport many dipeptides, tripeptides, and drugs, but minimal differences in affinity exist among these compounds. Dipeptides with glycine and proline in the N-terminal position show lower affinities than other dipeptides. Tripeptides that contain hydrophobic amino acid residues show the highest affinity to PEPT2. The presence of charged or uncharged amino acids among other tripeptides also influences affinity to the H^+/peptide symporter PEPT2 (*37*).

Biegel *et al*. developed a comprehensive 3D quantitative structure activity relationship model based on 83 compounds (32 dipeptides and dipeptide derivatives, 27 tripeptides, and 24 β-lactam antibiotics) (*41*). The analyses reveal that a free N-terminal amino group, a high electron density around the carboxylic group in dipeptides or around the carbonyl group of the second amino acid in tripeptides, high electron densities at the first and third side chains, and the presence of hydrophobic side chains can significantly increase affinity to PEPT2.

PepT2 displays broad substrate selectivity and interacts with numerous drugs, including those without similar chemical structures such as peptides (*42*). Some drugs or prodrugs such as β-lactam antibiotic cephalexin, penicillins (*43*), 5-ALA (*44*), and valacyclovir (*29*) not only interact with PEPT2 but can also be transported.

A precise pharmacophore model is currently unavailable because of the lack of information regarding the 3D structure of the transporter proteins. However, preferred configurations and conformational features of PEPT2 substrates (Figure 2) should include the following:

1) A peptide backbone of two to three amino acid residues (*45*);

2) Dipeptides must be in zwitterionic forms, and the intramolecular distance between oppositely charged NH_2 and COOH head groups is > 500 and < 630 picometers (*46-48*);

3) A correctly positioned backbone carbonyl group (*28,41,48*);

4) A free amino group in α or β position;

5) Stereoselectivity with L-amino acids and trans-conformers being preferred (*37,39,40*);

6) Chiral centers at α-carbons and backbone torsion angles ψ, φ, and ω (*23,48*);

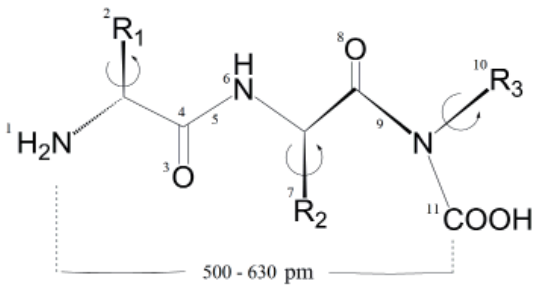

Figure 2. Molecular structures of selected pharmacologically compounds that may serve as substrates of PEPT2. 1. unessential, preferentially a free -NH_3^+; **2**. unessential, hydrophobic side chains can increase affinity but stereoselectivity; **3**. planar length-defined backbone from the N-terminal carbon to R2, with an incorporated backbone carbonyl function for hydrogen bonding; **4**. unessential, can be modified; **5**. unessential, only dipeptides and tripeptides with the trans-configuration can be transported; **6**. unessential, can be modified; **7**. unessential, hydrophobic side chains can increase affinity and stereoselectivity; **8**. unessential, more can increase affinity; **9**. non-required, can be modified; **10**. unessential, preferentially hydrophobic residues to increase affinity and stereoselectivity; **11**. unessential, can be replaced by stereoselective group.

7) Tripeptides with an uncharged amino acid residue in position 3.

8)Affinity of substrates could be improved by the presence of hydrophobic side chains or a C-terminal acid group.

In general, these data suggest that current models must be refined by trial and error until the 3D structure of transporter proteins is established. Furthermore, predictions of structure-affinity relationships and the substrate structure of transporter proteins on the basis of these models might promote the rational design of drugs and prodrugs targeting peptide transporters, and play major roles in treating various systemic diseases (*8*).

3. Regulation

Several reports focused on the function and substrate affinities of PEPT2. Meanwhile, minimal but important data are currently available on the regulation of PEPT2. For example, Mitsuoka *et al*. hypothesized that the growth of cancer cells could be suppressed by the inhibition of oligopeptide transporters under nutrient deficiency in vitro (*49*). Søndergaard and Bravo *et al*. reported that epidermal growth factor (EGF) has a strong inhibitory effect on rPEPT2 transport capacity (*50,51*). Otherwise, the mRNA and protein levels of PEPT2, amino acid homeostasis and drug pharmacokinetics could also be regulated by changes in thyroid function (*52,53*).

Takahashi *et al*. reported that 5/6 nephrectomized rats display unregulated mRNA and protein levels of PEPT2 at 2 weeks after surgery and downregulated mRNA level at 16 weeks after surgery. The up-regulation of PEPT2 expression promotes the reabsorption of small peptides and peptide-like drugs

across the brush-border membranes during chronic renal failure (*54*). Similarly, Tramonti *et al*. reported that a reduction in renal mass increases the expression of peptide transporters (influx) and P-glycoprotein (efflux) located at the brush border of renal tubular epithelial cells (*55*).

Sugiura *et al*. reported that the PDZ domain protein PDZK1 can affect the subcelluar localization and activity of PEPT2, thereby altering the membrane transport of various substrate compounds (*56*). Noshiro *et al*. also demonstrated that the capability of PDZK1 to couple PEPT2 to the Na^+/H^+ exchanger NHE3 may provide the necessary lumen-to-cell proton gradient (*57,58*). Boehmer *et al*. demonstrated that the serum and glucocorticoid-inducible kinase SGK1 and the Na^+/H^+ exchange regulating factor NHERF2 activated PEPT2 by stabilizing the transporter at the cell surface (*59*). Wenzel *et al*. reported that a reduction in cytosolic Ca^{2+} levels decreases the mRNA and protein levels of PEPT2, and kinase C changed the kinetic property of pig PEPT2 in a renal cell line (*60*).

And a few compounds also can inhibit the transport activity of PEPT2. These compounds include oral hypoglycemic agent nateglinide (*61*), the ACE inhibitor quinapril (*28*), cephalosporin (*62*), L-4,4′-biphenylalanine-L-proline (*36*), and amastatin (*63*). The shortage of information about regulation limits the development of drugs and prodrugs that target PEPT2. Therefore, the relevant factors that influence regulation warrant further research.

4. Summary and Perspective

Although the number of peptide transporters is fewer than that of amino acid transporters, numerous investigations have shown that PEPT2 plays an essential role in the absorption and reclamation of small peptides produced from the digestion of dietary proteins (*64*). The extensive substrate specificities of PEPT2 allow it to be exploited therapeutically for the delivery of peptides and peptidomimetic drugs in microbes and human (*23*). The design of many extant peptides and prodrugs is based on the substrates structure of the oligopeptide transporter to accelerate absorption *via* specific carrier proteins (*65*). Clinically relevant interactions between drugs and peptide transporter-mediated drugs are beginning to become an important aspect in therapy and toxicology (*66*).

Though PEPT2 appears to be a good target for the delivery of drugs because of the high affinity for peptides and drugs in tissues such as the kidney and lung, the structure of PEPT2 and related structure-function relationships are still unclear. Previous research demonstrated that PEPT2-null animals can still survive, therefore, the exact role of PEPT2 warrants further investigations.

In conclusion, PEPT2 not only plays important physiological and nutritional roles but also demonstrates pharmacokinetic and pharmacological significance. Further molecular clarification of the drug recognition mechanisms of PEPT2 will provide useful information for drug design and delivery systems to improve the efficiency of drug therapy.

Acknowledgements

The authors would like to thank the financial supports from the Chinese National Science Foundation (No. 21170254 and No. 21301050) and Innovation Scientists and Technicians Troop Construction Projects of Zhengzhou City (No. 10LJRC174).

References

1. Daniel H, Rubio-Aliaga I. An update on renal peptide transporters. Am J Physiol Renal Physiol. 2003; 284:F885-892.
2. Lee VH. Membrane transporters. Eur J Pharm Sci. 2000; 11(Suppl 2):S41-50.
3. Wang H, Fei YJ, Ganapathy V, Leibach FH. Electrophysiological characteristics of the proton-coupled peptide transporter PEPT2 cloned from rat brain. Am J Physiol. 1998; 275:C967-975.
4. Fujita T, Kishida T, Wada M, Okada N, Yamamoto A, Leibach FH, Ganapathy V. Functional characterization of brain peptide transporter in rat cerebral cortex: Identification of the high-affinity type H^+/peptide transporter PEPT2. Brain Res. 2004; 997:52-61.
5. Daniel H, Spanier B, Kottra G, Weitz D. From bacteria to man: Archaic proton dependent peptide transporters at work. Physiology (Bethesda). 2006; 21:93-102.
6. Wada M, Miyakawa S, Shimada A, Okada N, Yamanoto A, Fujita T. Functional linkage of H^+/peptide transporter PEPT2 and Na^+/H^+ exchanger in primary cultures of astrocytes from mouse cerebral cortex. Brain Res. 2005; 1044:33-41.
7. Wang M, Zhang X, Zhao H, Wang Q, Pan Y. Comparative analysis of vertebrate PEPT1 and PEPT2 genes. Genetica. 2010; 138:587-599.
8. Wang HP, Wang CL. Biological transporters as targets for new drug design. J Exp Clin Med. 2009; 1:31-38.
9. Terada T, Saito H, Sawada K, Hashimoto Y, Inui K. N-terminal halves of rat H^+/peptide transporters are responsible for their substrate recognition. Pharm Res. 2000; 17:15-20.
10. Rubio-Aliaga I, Daniel H. Mammalian peptide transporters as targets for drug delivery. Trends Pharmacol Sci. 2002; 23:434-440.
11. Verrey F, Singer D, Ramadan T, Vuille-dit-Bille RN, Mariotta L, Camargo SM. Kidney amino acid transport. Pflugers Arch. 2009; 458:53-60.
12. Terada T, Inui K. Peptide transporters: Structure, function, regulation and application for drug delivery. Curr Drug Metab. 2004; 5:85-94.
13. Fei YJ, Liu JC, Fujita T, Liang R, Ganapathy V, Leibach FH. Identification of a potential substrate binding domain in the mammalian peptide transporters PEPT1 and PEPT2 using PEPT1-PEPT2 and PEPT2-PEPT1 chimeras. Biochem Biophys Res Commun. 1998;

246:39-44.
14. Terada T, Irie M, Okuda M, Inui K. Genetic variant Arg57His in human H^+/peptide cotransporter2 causes a complete loss of transport function. Biochem Biophys Res Commun. 2004; 316:416-420.
15. Doring F, Martini C, Walter J, Daniel H. Importance of a small N-terminal region in mammalian peptide transporters for substrate affinity and function. J Membr Biol. 2002; 186:55-62.
16. Sala-Rabanal M, Loo DD, Hirayama BA, Wright EM. Molecular mechanism of dipeptide and drug transport by the human renal H^+/oligopeptide cotransporter hPEPT2. Am J Physiol Renal Physiol. 2008; 294:F1422-1432.
17. Hu Y, Ocheltree SM, Xiang J, Keep RF, Smith DE. Glycyl-L-glutamine disposition in rat choroid plexus epithelial cells in primary culture: Role of PEPT2. Pharm Res. 2005; 22:1281-1286.
18. Hu Y, Shen H, Keep RF, Smith DE. Peptide transporter 2 (PEPT2) expression in brain protects against 5-aminolevulinic acid neurotoxicity. J Neurochem. 2007; 103:2058-2065.
19. Pinsonneault J, Nielsen CU, Sadée W. Genetic variants of the human H^+/dipeptide transporter PEPT2: Analysis of haplotype functions. J Pharmacol Exp Ther. 2004; 311:1088-1096.
20. Rubio-Aliaga I, Frey I, Boll M, Groneberg DA, Eichinger HM, Balling R, Daniel H. Targeted disruption of the peptide transporter Pept2 gene in mice defines its physiological role in the kidney. Mol Cell Biol. 2003; 23:3247-3252.
21. Frey IM, Rubio-Aliaga I, Klempt M, Wolf E, Daniel H. Phenotype analysis of mice deficient in the peptide transporter PEPT2 in response to alterations in dietary protein intake. Pflugers Arch. 2006; 452:300-306.
22. Groneberg DA, Fischer A, Chung KF, Daniel H. Molecular mechanisms of pulmonary peptidomimetic drug and peptide transport. Am J Respir Cell Mol Biol. 2004; 30:251-260.
23. Inui K, Terada T, Masuda S, Saito H. Physiological and pharmacological implications of peptide transporters, PEPT1 and PEPT2. Nephrol Dial Transplant. 2000; 15(Suppl. 6):11-13.
24. Payne JW, Payne GM, Gupta S, Marshall NJ, Grail BM. Conformational limitations of glycylsarcosine as a prototypic substrate for peptide transporters. Biochim Biophys Acta. 2001; 1514:65-75.
25. Terada T, Saito H, Inui K. Interaction of beta-lactam antibiotics with histidine residue of rat H^+/peptide cotransporters, PEPT1 and PEPT2. J Biol Chem. 1998; 273:5582-5585.
26. Akarawut W, Lin CJ, Smith DE. Noncompetitive inhibition of glycylsarcosine transport by quinapril in rabbit renal brush border membrane vesicles: Effect on high-affinity peptide transporter. J Pharmacol Exp Ther. 1998; 287:684-690.
27. Döring F, Walter J, Will J, Föcking M, Boll M, Amasheh S, Clauss W, Daniel H. Delta-aminolevulinic acid transport by intestinal and renal peptide transporters and its physiological and clinical implications. J Clin Invest. 1998, 101:2761-2767.
28. Biegel A, Gebauer S, Hartrodt B, Knütter I, Neubert K, Brandsch M, Thondorf I. Recognition of 2-aminothiazole-4-acetic acid derivatives by the peptide transporters PEPT1 and PEPT2. Eur J Pharm Sci. 2007; 32:69-76.
29. Ganapathy ME, Huang W, Wang H, Ganapathy V, Leibach FH. Valacyclovir: A substrate for the intestinal and renal peptide transporters PEPT1 and PEPT2. Biochem Biophys Res Commun. 1998; 246:470-475.
30. Masereeuw R, Russel FG. Therapeutic implications of renal anionic drug transporters. Pharmacol Ther. 2010; 126:200-216.
31. Han HK, Amidon GL. Targeted prodrug design to optimize drug delivery. AAPS Pharmsci. 2000; 2:E6.
32. Geissler S, Zwarg M, Knütter I, Markwardt F, Brandsch M. The bioactive dipeptide anserine is transported by human proton-coupled peptide transporters. FEBS J. 2010; 277:790-795.
33. Biegel A, Knütter I, Hartrodt B, Gebauer S, Theis S, Luckner P, Kottra G, Rastetter M, Zebisch K, Thondorf I, Daniel H, Neubert K, Bransdch M. The renal type H^+/peptide symporter PEPT2: Structure-affinity relationships. Amino Acids. 2006; 31:137-156.
34. Biegel A, Gebauer S, Brandsch M, Neubert K, Thondorf I. Structural requirements for the substrates of the H^+/peptide cotransporter PEPT2 determined by three-dimensional quantitative structure-activity relationship analysis. J Med Chem. 2006; 49:4286-4296.
35. Terada T, Sawada K, Irie M, Saito H, Hashimoto Y, Inui K. Structural requirements for determining the substrate affinity of peptide transporters PEPT1 and PEPT2. Pflugers Arch. 2000; 440:679-684.
36. Knütter I, Hartrodt B, Tóth G, Keresztes A, Kottra G, Mrestani-Klaus C, Born I, Daniel H, Neubert K, Brandsch M. Synthesis and characterization of a new and radiolabeled high-affinity substrate for H^+/peptide cotransporters. FEBS J. 2007; 274:5905-5914.
37. Chen XZ, Zhu T, Smith DE, Hediger MA. Stoichiometry and kinetics of the high-affinity H^+-coupled peptide transporter PepT2. J Biol Chem. 1999; 274:2773-2779.
38. Sawada K, Terada T, Saito H, Hashimoro Y, Iuni KI. Recognition of L-amino acid ester compounds by rat peptide transporters PEPT1 and PEPT2. J Pharmacol Exp Ther. 1999; 291:705-709.
39. Theis S, Hartrodt B, Kottra G, Neubert K, Daniel H. Defining minimal structural features in substrates of the H^+/peptide cotransporter PEPT2 using novel amino acid and dipeptide derivatives. Mol Pharmacol. 2002; 61:214-221.
40. Theis S, Knütter I, Hartrodt B, Brandsch M, Kottra G, Neubert K, Daniel H. Synthesis and characterization of high affinity inhibitors of the H^+/peptide transporter PEPT2. J Biol Chem. 2002; 277:7287-7292.
41. Biegel A, Gebauer S, Brandsch M, Neubert K, Thondorf I. Structural requirements for the substrates of the H^+ / peptide cotransporter PEPT2 determined by three-dimensional quantitative structure-activity relationship analysis. J Biol Chem. 2006; 49:4286-4296.
42. Botka CW, Wittig TW, Graul RC, Nielsen CU, Higaka K, Amidon GL, Sadée W. Human proton/oligopeptide transporter (POT) genes: Identification of putative human genes using bioinformatics. AAPS Pharmsci. 2000; 2:E16.
43. Lin H, King N. Demonstration of functional dipeptide transport with expression of PEPT2 in guinea pig cardiomyocytes. Pflugers Arch. 2007; 453:915-922.
44. Novotny A, Stummer W. Aminolevulinic acid and the blood-brain barrier—a review. Med Laser Appl. 2003; 18:36-40.
45. Kamal MA, Keep RF, Smith DE. Role and relevance of PEPT2 in drug disposition, dynamics, and toxicity. Drug

Metab Pharmacokinet. 2008; 23:236-242.
46. Döring F, Will J, Amasheh S, Clauss W, Ahlbrecht H, Daniel H. Minimal molecular determinants of substrates for recognition by the intestinal peptide transporter. J Biol Chem. 1998; 273:23211-23218.
47. Fei YJ, Nara E, Liu JC, Boyd CA, Ganapathy V, Leibach FH. Preferential recognition of zwitterionic dipeptides as transportable substrates by the high-affinity peptide transporter PEPT2. Biochim Biophys Acta. 1999; 1418:344-351.
48. Payne JW, Grail BM, Gupta S, Ladbury JE, Marshall NJ, O'Brien R, Payne GM. Structural basis for recognition of dipeptides by peptide transporters. Arch Biochem Biophys. 2000; 384:9-23.
49. Mitsuoka K, Kato Y, Miyoshi S, Murakami Y, Hiraiwa M, Kubo Y, Nishimura S, Tsuji A. Inhibition of oligopeptide transporter suppress growth of human pancreatic cancer cells. Eur J Pharm Sci. 2010; 40:202-208.
50. Søndergaard HB, Bravo SA, Nielsen CU, Frokjaer S, Brodin B. Cloning of the pig PEPT2 (pPEPT2) and characterization of the effects of epidermal growth factor (EGF) on pPEPT2-mediated peptide uptake in the renal porcine cell line LLC-PK1. Eur J Pharm Sci. 2008; 33:332-342.
51. Bravo SA, Nielsen CU, Amstrup J, Frokjaer S, Brodin B. Epidermal growth factor decreases PEPT2 transport capacity and expression in the rat kidney proximal tubule cell line SKPT0193 cl.2. Am J Physiol Renal Physiol. 2004; 286:F385-393.
52. Döring F, Schmitt R, Bernhardt WM, Klapper M, Bachmann S, Daniel H, Groneberg DA. Hypothyroidism induces expression of the peptide transporter PEPT2. Biol Chem. 2005; 386:785-790.
53. Lu H, Klaassen C. Tissue distribution and thyroid hormone regulation of Pept1 and Pept2 mRNA in rodents. Peptides. 2006; 27:850-857.
54. Takahashi K, Masuda S, Nakamura N, Saito H, Futami T, Doi T, Inui K. Upregulation of H^+-peptide cotransporter PEPT2 in rat remnant kidney. Am J Physiol Renal Physiol. 2001; 281:F1109-1116.
55. Tramonti G, Xie P, Wallner EI, Danesh FR, Kanwar YS. Expression and functional characteristics of tubular transporters: P-glycoprotein, PEPT1, and PEPT2 in renal mass reduction and diabetes. Am J Physiol Renal Physiol. 2006; 291:F972-980.
56. Sugiura T, Kato Y, Kubo Y, Tsuji A. Mutation in an adaptor protein PDZK1 affects transport activity of organic cation transporter OCTNs and oligopeptide transporter PEPT2. Drug Metab Pharmacokinet. 2006; 21:375-383.
57. Noshiro R, Anzai N, Sakata T, Miyazaki H, Terada T, Shin HJ, He X, Miura D, Inui K, Kanai Y, Endou H. The PDZ domain protein PDZK1 interacts with human peptide transporter PEPT2 and enhances its transport activity. Kidney Int. 2006; 70:275-282.
58. El-Sheikh AA, Masereeuw R, Russel FG. Mechanisms of renal anionic drug transport. Eur J Pharmacol. 2008; 585:245-255.
59. Boehmer C, Palmada M, Klaus F, Jeyaraj S, Lindner R, Laufer J, Daniel H, Lang F. The peptide transporter PEPT2 is targeted by the protein kinase SGK1 and the scaffold protein NHERF2. Cell Physiol Biochem. 2008; 22:705-714.
60. Wenzel U, Diehl D, Herget M, Kuntz S, Daniel H. Regulation of the high-affinity H^+/peptide cotransporter in renal LLC-PK1 cells. J Cell Physiol. 1999; 178:341-348.
61. Terada T, Sawada K, Saito H, HashimotoY, Inui K. Inhibitory effect of novel oral hypoglycemic agent nateglinide (AY4166) on peptide transporters PEPT1 and PEPT2. Eur J Pharmacol. 2000; 392:11-17.
62. Ganapathy ME, Prasad PD, Mackenzie B, Ganapathy V, Leibach FH. Interaction of anionic cephalosporins with the intestinal and renal peptide transporters PEPT1 and PEPT2. Biochim Biophys Acta. 1997; 1324:296-308.
63. Xiang J, Jiang H, Hu Y, Smith DE, Keep RF. Kyotorphin transport and metabolism in rat and mouse neonatal astrocytes. Brain Res. 2010; 1347:11-18.
64. Terada T, Shimada Y, Pan X, Kishimoto K, Sakurai T, Doi R, Onodera H, Katsura T, Imamura M, Inui K. Expression profiles of various transporters for oligopeptides, amino acids and organic ions along the human digestive tract. Biochem Pharmacol. 2005; 70:1756-1763.
65. Balakrishnan A, Jain-Vakkalagadda B, Yang C, Pal D, Mitra AK. Carrier mediated uptake of L-tyrosine and its competitive inhibition by model tyrosine linked compounds in a rabbit corneal cell line (SIRC)-strategy for the design of transporter/receptor targeted prodrugs. Int J Pharm. 2002; 247:115-125.
66. Endres CJ, Hsiao P, Chung FS, Unadkat JD. The role of transporters in drug interactions. Eur J Pharm Sci. 2006; 27:501-517.

(Received June 3, 2015; Revised July 29, 2015; Re-revised August 19, 2015; Accepted August 22, 2015)

Original Article

DOI: 10.5582/bst.2015.01075

Prevalence of 7 virulence genes of *Legionella* strains isolated from environmental water sources of public facilities and sequence types diversity of *L. pneumopila* strains in Macau

Lina Xiong[1,2], Hongbo Zhao[2], Ziyao Mo[2,*], Lei Shi[1]

[1] *School of Light Industry and Food Sciences, South China University of Technology, Guangzhou, Guangdong, China;*
[2] *The First Affiliated Hospital of Guangzhou Medical University, Guangzhou Institute of Respiratory Disease, State Key Laboratory of Respiratory Disease, Guangzhou, Guangdong, China.*

Summary **In this study, we analyzed 7 virulence genes in 55 *Legionella* species (including 29 *L. pneumophila* and 26 non-*L. pneumophila* strains) which isolated from environmental water sources of the public facilities in Macau by using PCR and real-time PCR. In addition, 29 *Legionella pneumophila* isolates were subjected to genotyping by sequence-based typing scheme and compared with the data reported. The detection rate of *flaA*, *pilE*, *asd*, *mip*, *mompS*, *proA* and *neuA* genes in the *L. pneumophila* were 100.0%, respectively. The *neuA* gene was not detected in the non-*L. pneumophila* strains, but *flaA*, *pilE*, *asd*, *mip*, *mompS*, and *proA* genes could be amplified with a positive rate of 15.4%, 15.4%, 53.8%, 38.5%, 15.4%, and 38.5%, respectively. The results from real-time PCR were generally consistent with that of PCR. Those *L. pneumophila* strains were assigned into 10 sequence types (STs) and ST1 (9/29) was the dominant STs. Four new STs were found to be unique in Macau. The analysis of population structure of *L. pneumophila* strains which isolated from Macau, Guangzhou and Shenzhen indicated that the similar clones were existed and ST1 was the most prevalent STs. However, the distribution of the subtypes isolated from Macau was not the same extensive as those from Guangzhou and Shenzhen. The different detection rates of the 7 virulence genes in different species of *Legionella* might reflect their own potential for environmental adaptability and pathogenesis. And the data analyzed from STs diversity indicated the Macau *L. pneumophila* possessed obvious regional specificity and high genetic diversity.**

Keywords: Sequence-based typing, population structure, phylogenetic relationship

1. Introduction

Legionella species, commonly found in the environment, are the major causative agents of Legionnaire's disease and Pontiac fever. They have been found to not only induce lung infection, but also to cause dysfunction of other organs, such as the heart, kidney and central nervous system (*1*). To date, more than 50 species of *Legionella* have been described (*2*). Among of them, 20 species are recognized as human pathogens. *L. pneumophila* was identified as primary culprit for Legionnaire's disease. In recent years, several studies related to the presence of *Legionella* have been reported in southern Chinese cities, such as Guangzhou, Shenzhen, Jiangmen and Hong Kong (*3,4*). However, no data of *Legionella* from Macau were published. In May of 2010, a case of *Legionella* infection emerged, which was vigorously suspected to be caused by local *Legionella* species since the patient did not previously travel abroad. We investigated and detected the existence of *Legionella* in natural and artificial water environments in Macau in the summer (from May to July) of the same year. A total of 55 isolates of *Legionella* were isolated from air conditioning cooling towers, fountains and

**Address correspondence to:*
Dr. Ziyao Mo, The First Affiliated Hospital of Guangzhou Medical University, Guangzhou Institute of Respiratory Disease, State Key Laboratory of Respiratory Disease, No. 151, YanJiangXi Road, YueXiu District, Guangzhou 510120, Guangdong, China.
E-mail: moziyao@gird.cn

surface waters in public facilities of Macau (*5*).

In the present study, seven virulence genes (*flaA*, *pilE*, *asd*, *mip*, *mompS*, *proA* and *neuA*) responsible for the expression of adherence, invasion, colonization and cytotoxin production (*6,7*), were detected in all 55 strains isolated from Macau. For comparison, the PCR and the real-time PCR were applied to detect the genes simultaneously. In addition, sequence-based typing (SBT), a powerful epidemiological method recognized by the European Working Group for Legionella Infections (EWGLI) as a "gold standard" tool, was used for the *L. pneumophila* strains. The population structure and phylogenetic relationship of *L. pneumophila* strains isolated from Macau were analyzed and compared to those from near cities such as Guangzhou and Shenzhen. This investigation will help us to learn more about the characteristics of the Macau *Legionella* isolates, provide the possibility to trace and control for a large area of epidemic and appropriate precaution strategy against *Legionella* infection.

2. Materials and Methods

2.1. *Legionella strains*

A total of 55 *Legionella* strains were collected from 43 water samples including air conditioning cooling towers (27 samples), fountains (13 samples) and surface waters (3 samples) in public sites of Macau. *Legionella* species were identified by serological agglutination with Legionella Latex Agglutination Kit (PRO-LAB, Weston, USA) based on manufacturer instructions and fatty acid analysis was performed with the Sherlock microbial identification system (software version 6.0, MIDI, USA; Microbial ID, Inc., Newark, Del).

2.2. *Preparation of DNA*

The strains were cultured with buffered charcoal yeast extract (BCYE) ager plates at 37°C in 5% CO_2. A single colony of *Legionella* was picked from the plate and resuspended into 100 µL sterilized ultrapure water. DNA was then extracted by one thaw-freeze cycle (99°C for 10 min and 4°C for 5 min). After briefly centrifuged, the supernatant was measured with a spectrophotometry at 260 nm in triplicates using A260/A280 ratio (NanoDropTM 1000, Thermo Scientific) then used as the DNA template for PCR and real-time PCR.

2.3. *Detection of pathogenic genes by PCR and real-time PCR*

The PCR primers were based on EWGLI recommended (*8,9*). PCR conditions were the same as described by Gaia *et al*. (*8*) with minor modification. PCR was performed in a mixture (50 µL) consisting of 25 µL of 2× SuperStar PCR mix (GenStar Biosolution, Beijing, China), 5 pmol each primers, 100 ng of the template. Sterile distilled water was added to make 50 µL. The products were detected by electrophoresis and purified using the DNA Gel Extraction Kit (Axygen USA).

To establish a more sensitive, higher speciality and easier operation detecting method, a real-time PCR was applied at the present study. The primers used in real-time PCR were designed based on sequences from GenBank accession numbers X83232 (*flaA*), AF048690 (*pilE*), AF034213 (*asd*), AJ496269 (*mip*), AF078136 (*mompS*), M32884 (*proA*) and AJ007311 (*neuA*). The primers sequences were list in Table S1. For amplifications, 50 ng template was mixed with 12.5 µL 2× SYBR Premix EX Taq™ II (Perfect Real Time, Takara, Japan), and 5 pmol each of the forward and the reverse primers in a final volume of 25 µL. The reaction conditions were 5 s at 95°C and 30 s at 60°C for 40 cycles. Sterilized water was used as a template for the blank control for both PCR reactions.

2.4. *Sequence-based typing*

The purified PCR products were sequenced by Beijing Genomics Institute (Beijing, China). SBT using loci *flaA*, *pilE*, *asd*, *mip*, *mompS*, *proA* and *neuA* was performed according to the EWGLI scheme (*8,9*). Genotype analysis was based on the standard SBT method given by the EWGLI with these 7 genes. The nucleotide sequences obtained were confirmed by the SBT database available on the EWGLI website (*http://www.ewgli.org/*), and the sequences were compared with those in the SBT database from the website (*http://www.hpabioinformatics.org.uk/legionella/legionella_sbt/php/sbt_homepage.php*).

2.5. *Population structure and phylogenetic analysis*

The minimum spanning trees (MST) were conducted by the BioNumerics software (version 7.1; Applied Maths, Kortrijk, Belgium). In MST, the ST that possesses the most number of single-locus variants is defined as the founder ST. The clusters of relative STs that originate from a common ancestor are considered as the clone groups or complexes. The single genotype that does not correspond to any other clone groups is classified as singleton. The sequence types are represented by the circles. The size of circle indicates the number of the particular strains. The relationship of the different circles is present with the connecting lines.

The concatenated sequence in phylogenetic analysis was prepared with the seven loci of the initial SBT scheme according to their locations on the chromosome by BioEdit (*http://www.mbio.ncsu.edu/BioEdit/bioedit.html*). Based on the concatenated sequence, the evolutionary relationship between STs was conducted using the neighbour-joining method with Tamura

Table 1. Detection rate of seven genes in *Legionella* strains isolated from Macao

Species	No. of strains	No. of positive strains													
		flaA		*pilE*		*asd*		*mip*		*mompS*		*proA*		*neuA*	
		P[a]	R[b]	P	R	P	R	P	R	P	R	P	R	P	R
L. pneumophila	29	29	27	29	29	29	29	29	28	29	29	29	29	29	29
L. adelaidensis	1	0	0	0	0	0	0	0	0	0	0	0	0	0	0
L. rubrilucens	3	1	0	0	0		0	0	0	1	1	0	0	0	0
fluoribacter-gormanii	3	0	0	2	1	3	0	0	0	0	0	0	0	0	0
L. shakespearei	5	0	0	0	2	5	4	5	3	1	3	5	4	0	3
L. feeleii	6	0	0	0	0	0	0	0	0	1	4	0	0	0	2
L. wadsworthii	3	2	2	0	0	3	1	0	0	0	0	1	3	0	0
L.quateirensis	5	1	0	2	2	3	0	5	3	1	4	5	3	0	0
		Detection rate of seven genes with three different methods (%)													
L. pneumophila	29	100	93.1	100	100	100	100	100	96.5	100	100	100	100	100	100
No-*L. pneumophila*	26	15.4	7.69	15.4	19.2	53.8	19.2	38.5	23.1	15.4	46.2	42.3	38.5	0	19.2

[a]PCR; [b]Real-time PCR.

Table 2. Sequences-Based Typing of *L. pneumophila* strains from Macao

SBT type	*flaA*	*pilE*	*asd*	*mip*	*mompS*	*proA*	*neuA*	Serotype (no.)	No. of isolate
1	1	4	3	1	1	1	1	Lp1(5)LP14(4)	9
160	11	14	16	16	15	13	9	Lp1(1)Lp14(1)	2
566	16	4	3	1	1	1	1	Lp1(2)Lp14(1)	3
752	22	4	3	1	1	1	1	Lp1	1
1119	2	10	14	10	21	4	3	Lp1	2
1417	8	6	34	9	2	8	209	Lp14	4
01[a]	11	14	16	25	15	13	206	Lp14	1
02[a]	11	4	16	16	15	13	9	Lp1	1
03[a]	1	4	3	5	11	1	15	Lp14	4
04[a]	11	4	16	12	15	13	9	Lp1(1)Lp14(1)	2

[a] New ST type assigned by SBT database of EWGIL.

3-parameter model by MEGA v5.05.

3. Results

3.1. *Legionella isolates*

A total of 55 isolates of *Legionella* were isolated from air conditioning cooling towers (96.8%), fountains (1.8%) and surface waters (1.8%). Among them, *L. pneumophila* accounted for 29 isolates, approximately 52.7% of all isolates, whereas *Legionalla* species other than *L. pneumophila* accounted for 47.3% of the total. Among the 29 *L. pneumophila* species, the serotype 1 strains accounted for 44.8%, whereas serotype 14 accounted for 55.2%. *L. feeleii* was the dominant species (23.1%) among 26 non-*L. pneumophila* species, followed by *L. shakespearei* and *L. quateirensis*, which severally accounted for 19.2%. The above indicated that *Legionella* species were widely distributed in the public environment of Macau and *L. pneumophila* occupied the major proportion.

3.2. *Different prevalence of pathogenic genes in Legionella species*

In 29 *L. pneumophila* strains, *flaA*, *pilE*, *asd*, *mip*, *mompS*, *proA* and *neuA* genes were 100% detected (Table 1). In 26 non-*L. pneumophila*, other genes included *flaA*, *pilE*, *asd*, *mip*, *mompS*, and *proA* which tested as 15.4%, 15.4%, 53.8%, 38.5%, 15.4% and 38.5%. However, the *neuA* gene failed to amplify. The positive results of the three genes *asd*, *mip* and *proA* in non-*L. pneumophila* focused on the *L. quateirensis* and *L. shakespearei* strains.

For *L. pneumophila* strains, the results of real-time PCR were almost same as that of PCR, but the positive rate of *flaA* and *mip* genes were 93.1% and 96.5% (Table 1). The positive results for seven genes of non-*L. pneumophila* from real-time PCR exhibited some differences with that from PCR. Genes of *flaA*, *asd*, *mip* and *proA* showed a little lower sensitive while *pilE*, *mompS* and *neuA* genes were with more sensitive. In summary, the detection rates of seven genes were high in *L. pneumophila* strains and relatively low in non-*L. pneumophila* strains.

3.3. *Sequence-based typing*

The 29 environmental *L. pneumophila* strains could be divided into 10 STs (Table 2), including 3 singletons, in which one was ST752 and the other two were new STs (ST01 and 02). According to the EWGLI SBT

database submitted in March 2014, there were four new STs unique to Macao. The ST with the largest number of isolates was ST1 (9/29, 31.0%), followed by ST1417 and ST03 (4/29, 13.8%), ST566 (3/29, 10.3%), then ST160, ST1119 and ST04 (2/29, 6.9%). There were 36 alleles were identified across the 7 loci. At the individual loci level, *mip* gene provided the most alleles. Seven alleles were obtained from *mip* gene, whereas six alleles were obtained using *flaA* and *neuA* genes, five from the *mompS* gene, and four from *pilE*, *asd* and *proA* genes. The results revealed that ST1 was the main ST-type and *mip* gene showed greatest genetic diversity in Macau.

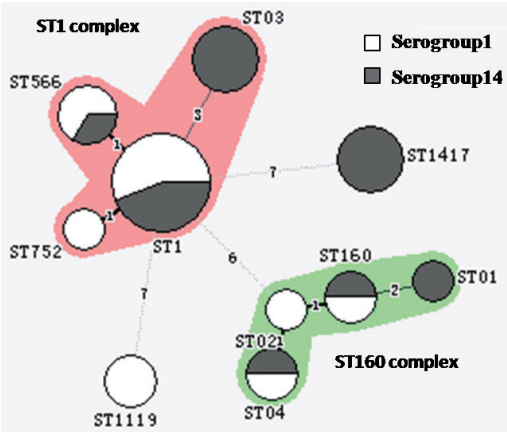

Figure 1. MST analysis of 29 *L. pneumophila* strains isolated in Macau. STs are represented by circles. The size of each circle indicates the number of isolates within this particular type; the STs are shown beside the circles and the number of isolates in each ST is shown in the circles. The branch distance is shown on the connecting line. This links STs or sets of STs with a branch distance less than or equal to 3 within a single ST complex.

3.4. *Population structure and Phylogenetic analysis*

All 10 STs identified from Macau were analysed for their population structure with the minimum spanning trees (Figure 1). Among them, 8 STs formed two clone complexes, and the other 2 different STs were determined to be singletons with four or more gene variants. The ST1 complex was a bigger clone group, including four STs groups containing 17 isolates. ST1 was suggested to be a primary founder, since there were 9 ST1 (9/17, 52.9%), the highest number of isolates in the complex. The other three STs in the ST1 complex were either single-locus variant or double-locus variants to ST1. In the other clone group ST160 complex, there were 4 STs with 6 isolates. Three (ST01, 02 and 04) of four new STs unique to Macao were found in this complex, while ST03 belonged to the ST1 complex.

The 29 strains in the study with the addition of 116 isolates from Guangzhou (*10*), and 52 isolated from Shenzhen (*11*) were put together and analysed again with minimum spanning tree by the BioNumerics software (Figure 2). They were identified as 47 STs, of which, 43 STs were grouped into eight clonal complexes. The other 4 STs (ST59, 114, 238, 1054) were singletons. Only ST1, ST 160 and ST752 were found in the three areas. The isolates from Macau were distributed mainly in two large clone complexes, I and II. Only one Macau STs could be found in the complexes III and VIII.

Clone complex I, the largest clone group in these three cities, contained the ST1 complex from Macau. There were four main STs, ST150, ST154, ST159 and ST160 in clone complex II, in which most of STs were single-locus or double-locus variants to ST154

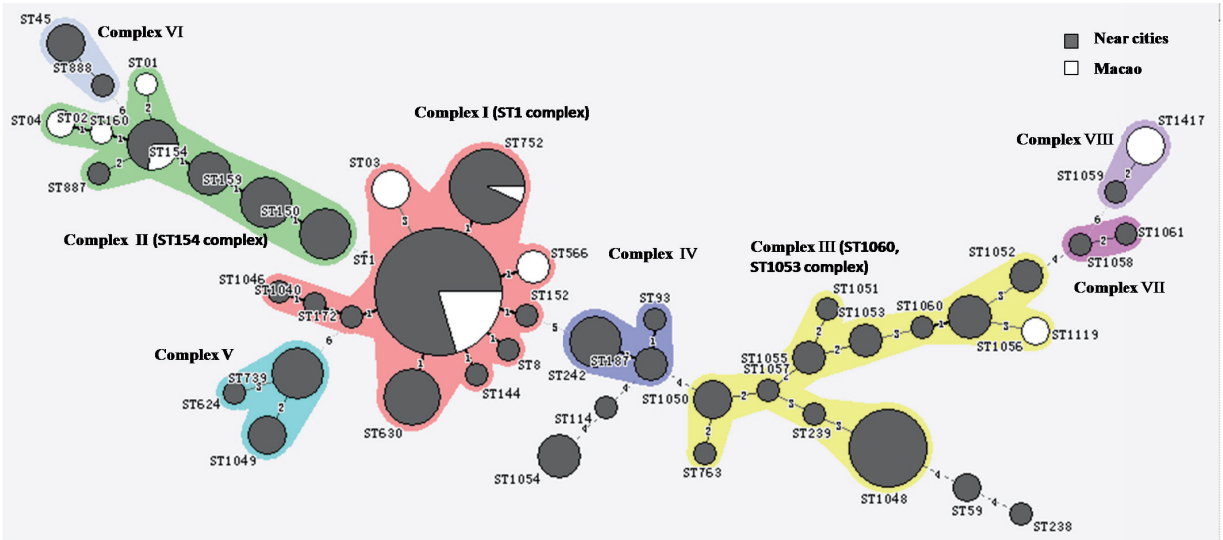

Figure 2. MST analysis of 197 *L. pneumophila* strains isolated from Macau, Guangzhou and Shenzhen. STs are represented by circles. The size of each circle indicates the number of isolates within this particular type; the STs are shown beside the circles. The heavy solid black lines connect two types within a single variant locus, the light solid black lines connect double-locus variants, the light solid gray lines connect triple-locus variants, the gray dashed lines connect quadruple-locus variants, and the dotted lines connect variants over quadruple-locus. The branch distance is shown on the connecting line. The colors of the halo surrounding the STs denote types that belong to the same clonal group.

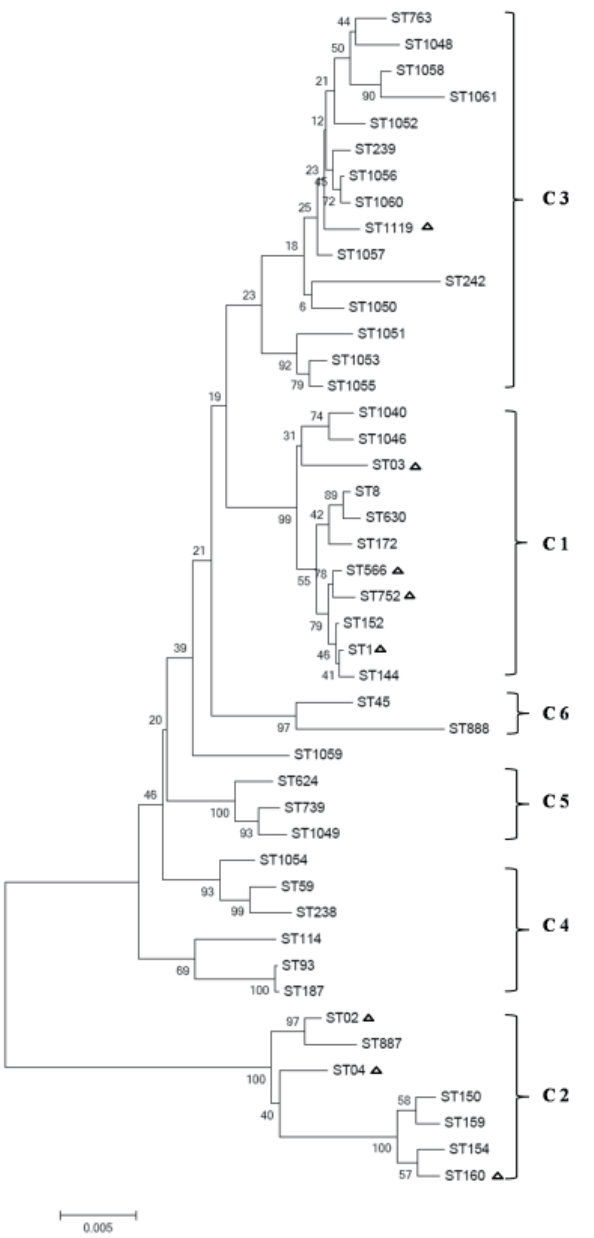

Figure 3. Phylogenetic analysis of the *L. pneumophila* STs isolated from Macau, Guangzhou and Shenzhen. The tree was constructed with MEGA v5.05. STs of strains isolated from Macao are labeled by black triangles. The scale bar indicates genetic distances between sequences. The percentages of replicate trees in which the associated STs clustered together in the bootstrap test are shown next to the branches. The evolutionary distances are in the units of the number of base substitutions per site.

or ST160. Clone complex III was another large group, which composed of the most STs with double-locus or triple-locus variants each other. The STs in the other four small clone complexes, IV to VII were from Shenzhen and Guangzhou, but not Macau.

STs phylogenetic analysis was conducted using a neighbor-joining method with the Tamura 3-parameter model based on concatenated sequences of SBT alleles. Because ST01 and ST1417 were obtained the *neuA* allele with new primers, the results of their phylogenetic analysis were unfaithful. The other STs were divided into six groups (C1-C6) by the neighbor-joining analysis (Figure 3). These groups generally had a one-to-one correspondence with the six clonal complexes (complexes I to VI) determined by BioNumerics software. It was unexpected that the single C3 group identified by MEGA v5.05 contained both clonal complexes (III and VII). The distribution of Macau STs wasn't as wide as that of STs from near cities Guangzhou and Shenzhen, and ST1 was the preponderant STs among these three cities.

4. Discussion

We have previously studied the distribution and species of environmental *Legionella* isolates from Macau in detail (*5*). In this work, our main objective has been to analyze the prevalence of seven virulence genes of this species and reveal the STs distribution of *L. pneumophila* isolates from Macau. Furthermore, the *L. pneumophila* isolates from Macau were compared with the isolates from Guangzhou and Shenzhen. Our findings revealed the high prevalence of these seven virulence genes in *L. pneumophila* strains and low prevalence in non-*L. pneumophila*. Additionally, our study also indicated that STs had several unique allelic profiles and ST1 is the predominant ST-type in Macau.

The seven genes detected in this study are closely related to bacterial signal transduction, virulence, and adaptive capacity (*6,12-14*). The different detection rates of these genes revealed the relationships between each virulence gene or combinations of these genes and the various species of *Legionella* in Macau. The high prevalence of these genes in *L. pneumophila* strains and low prevalence in non-*L. pneumophila* strains might reflect their own ability to adapt to the external environment and their strong pathogenicity to human beings. Some reports have shown that non-*L. pneumophila* could cause a variety of organ dysfunction (*15*). However, studies focused on detection of virulence genes associated with non-*L. pneumophila* strains are rarely found. This study represents the first detection for these seven virulence genes from both *L. pneumophila* and non-*L. pneumophila* strains which might provide a reliable basis to evaluate the pathogenic potential of the strains and their adaptability to the local environment.

In this study, the real-time PCR was also applied for its high level of efficiency and ability for specialization, as well as for its ability to multiply amplify the target genes and its ease of operation. The results from real-time PCR were generally consistent with that of PCR. The data suggested that real-time PCR, instead of conventional PCR, should be used to detect these seven genes, especially for large-scale investigation. If the PCR products needed to be collected for other purposes, or used to perform a test to compare and verify the relevant multi-alleles, both tests could be

used together. Since the primers designed for real-time PCR were not appropriate for all *L. pneumophila* and non-*L. pneumophila* strains, a future study is needed to further investigate this issue.

These 29 *L. pneumophila* isolates were classified with the method recommended by EWGLI and four new STs were found unique to Macau. Within the 10 Macao STs, ST1 is the predominant ST-type (9/29, 31.0%). The result was similar to the report in Japan where STI consisted of 29% of environmental isolates (*16*). In a recent study conducted in the United States, ST1 accounted for 25% and 49% of the number of the sporadic and environmental isolates, respectively (*17*). In one study conducted in England and Wales, ST1 was the most frequent STs, accounting for 35% of the number of *L. pneumophila* environmental isolates (*18*). From the *L. pneumophila* serogroup 1 isolates from potable systems, cooling towers, and hot springs in China, ST1 were reported to be about 14.3%, to 53.1% and 92.3%, respectively (*19*). For *L. pneumophila* strains, ST1 (1, 4, 3, 1, 1, 1) is predominant in environmental samples, widely distributed around world (*18,20,21*). The Macau SBT analysis of *L. pneumophila* strains isolated from the public sites revealed the same ST-type characterization.

In the study, the loci *mip* and *flaA* offered more alleles in Macau's samples. The number of each allele presented by EWGLI from all over the world showed that the *mompS* locus provided the maximum number of alleles, *neuA-Ah* provided the next most, and *mip*, *asd*, *proA* and *pilE*, *flaA* provided the minimum. One report in South Korea showed that the *mompS* locus had the most alleles (*2*). Similarly, another study conducted in Canada obtained the same result that locus *mompS* provided the most alleles (*22*). However, one study on SBT of *L. pneumophila* strains in mainland China indicated that *mip* and *flaA* individually provided the most alleles in the isolates from cooling water and hot spring water (*19*). This might be attributed to the geographical correlation which could lead to the emergence of these results. Additionally, it might also reflect that the homology that exists between strains from Macau and mainland China.

Meanwhile, in order to understand the population structure and phylogeny of the *L. pneumophlia* strains isolated from Macau, the minimum spanning tree and the neighbor-joining method were respectively applied to compare Macau STs to those identified from nearby cities of Guangzhou and Shenzhen. All STs from these three cities were divided into eight clone complexes in the minimum spanning tree, and six groups could be seen by the neighbor-joining method. Consistent results from these two similar methods suggested that the phylogenetic analysis could be selected either individually or simultaneously. Among eight complexes generated in the minimum spanning tree, only four were related to Macau STs. The subtype distribution of *L. pneumophlia* strains isolated from Macau was not as extensive as that from other cities (*20,22,23*). However, in complex I, ST1 from Macau was the major STs involved in, which reflects the concentration of local types. This supports that ST1 is the most common hereditary character of *L. pneumophlia* strains and extensively distributed all over the world. The majority of isolates from Macau kept also represented this distrubution. In this study, four new STs were found for the first time. It is convinced of that more new STs will be reported in further investigation. After a detailed study using phylogenetic analysis and population structure, the high diversity and specificity of *L. pneumophlia* strains isolated from Macau were observed. Since ST154 has been proven to be relevant to *Legionnella* epidemiology (*1,2*), the closely connected ST04, ST02 and ST160, should bring significant attention and research interest.

To summarize, this study enables, for the first time, the ability to realize the prevalence of seven virulence genes of *Legionella* in Macau, to characterize the *L. pneumophila* environment isolates with SBT methodology, and to create a database of Macau's *L. pneumophila* profiles for use in epidemiological surveillance efforts. The findings of this study also contribute to the EWGLI-SBT database and to the knowledge of *L. pneumophila* diversity in southern China. Further studies are needed to reveal the relationships between each pathogenic gene or combinations of these genes and the pathogenicity of *Legionella*, and to analyze the correlation between environmental and clinical strains of *Legionella*.

Acknowledgements

This work was supported by a grant from the State Key Lab of Respiratory Disease, Guangzhou Medical College (2012-2014) and MACAO - Science and Technology Development Fund (039/2007/A3).We thank Miss Elizabeth Li for her great help with revising the article.

References

1. Helbig JH, Uldum SA, Bernander S, Lück PC, Wewalka G, Abraham B, Gaia V, Harrison TG. Clinical utility of urinary antigen detection for diagnosis of community-acquired, travel-associated, and nosocomial legionnaires' disease. J Clin Microbiol. 2003; 41:838-840.
2. Lee HK, Shim JI, Kim HE, Yu JY, Kang YH. Distribution of *Legionella* species from environmental water sources of public facilities and genetic diversity of *L. pneumophila* serogroup 1 in South Korea. Appl Environ Microbiol. 2010; 76:6547-6554.
3. Tsang KW, Ho PL, Ooi GC, *et al*. A cluster of cases of severe acute respiratory syndrome in Hong Kong. N Engl J Med. 2003; 348:1977-1985.
4. Guo J, Liang T, Hu C, Lv R, Yang X, Cui Y, Song Y, Yang R, Zhu Q, Song Y. Sequence types diversity of *Legionella pneumophila* isolates from environmental

water sources in Guangzhou and Jiangmen, China. Infect Genet Evol. 2015; 29:35-41.
5. Zhao HB, Guan WD, Yang ZF, Lu X, Shi L, Cai F, Mo ZY. Detection and fatty acid analysis of public sites *Legionella* isolated from Macau. Ao Men Ke Ji Da Xue Xue Bao. 2011; 5:106-15. (in Chinese)
6. Cianciotto NP. Type II Secretion and *Legionella* Virulence. Curr Top Microbiol Immunol. 2013; 376:81-102.
7. Fields BS, Benson RF, Besser RE. *Legionella* and Legionnaires' disease: 25 years of investigation. Clin Microbiol Rev. 2002; 15:506-526.
8. Gaia V, Fry NK, Afshar B, Lück PC, Meugnier H, Etienne J, Peduzzi R, Harrison TG. Consensus sequence-based scheme for epidemiological typing of clinical and environmental isolates of *Legionella pneumophila*. J Clin Microbiol. 2005; 43:2047-2052.
9. Ratzow S, Gaia V, Helbig JH, Fry NK, Lück PC. Addition of *neuA*, the gene encoding N-acylneuraminate cytidylyl transferase, increases the discriminatory ability of the consensus sequence-based scheme for typing *Legionella pneumophila* serogroup 1 strains. J Clin Microbiol. 2007; 45:1965-1968.
10. Liang T. Population genetics analysis of *Legionella pneumophlia* isolated from Guangzhou by using sequence-based typing. M.Sc. Thesis. Liaoning University. 2012. (in Chinese)
11. Yuan M, Yuan YM, Yu MH, Duan Y. Sequenced-based typing research for *Legionella* pneumophila isolated from the cooling tower in Shenzhen. Huan Jing Yu Jiang Kang Za Zhi. 2010; 5:423-434. (in Chinese)
12. Khweek AA, Caution K, Akhter A, Abdulrahman BA, Tazi M, Hassan H, Majumdar N, Doran A, Guirado E, Schlesinger LS, Shuman H, Amer AO. A bacterial protein promotes the recognition of the *Legionella pneumophila* vacuole by autophagy. Eur J Immunol. 2013; 43:1333-1344.
13. Case CL, Kohler LJ, Lima JB, Strowig T, de Zoete MR, Flavell RA, Zamboni DS, Roy CR. Caspase-11 stimulates rapid flagellin-independent pyroptosis in response to *Legionella pneumophila*. Proc Natl Acad Sci U S A. 2013; 110:1851-1856.
14. Girard A, Roques E, Massie B, Archambault D. Flagellin in fusion with human rotavirus structural proteins exerts an adjuvant effect when delivered with replicating but non-disseminating adenovectors through the intrarectal route. Mol Biotechnol. 2014; 56:394-407.
15. Leggieri N, Gouriet F, Thuny F, Habib G, Raoult D, Casalta JP. *Legionella longbeachae* and endocarditis. Emerg Infect Dis. 2012; 18:95-97.
16. Amemura-Maekawa J, Kikukawa K, Helbig JH, Kaneko S, Suzuki-Hashimoto A, Furuhata K, Chang B, Murai M, Ichinose M, Ohnishi M, Kura F. Distribution of monoclonal antibody subgroups and sequence-based types among *Legionella pneumophila* serogroup 1 isolates derived from cooling tower water, bathwater, and soil in Japan. Appl Environ Microbiol. 2012; 78:4263-4270.
17. Donohue MJ, O'Connell K, Vesper SJ, Mistry JH, King D, Kostich M, Pfaller S. Widespread molecular detection of *Legionella pneumophila* Serogroup 1 in cold water taps across the United States. Environ Sci Technol. 2014; 48:3145-3152.
18. Harrison TG, Afshar B, Doshi N, Fry NK, Lee JV. Distribution of *Legionella pneumophila* serogroups, monoclonal antibody subgroups and DNA sequence types in recent clinical and environmental isolates from England and Wales (2000-2008). Eur J Clin Microbiol Infect Dis. 2009; 28:781-791.
19. Qin T, Zhou H, Ren H, Guan H, Li M, Zhu B, Shao Z. Distribution of sequence-based types of *Legionella pneumophila* serogroup 1 strains isolated from cooling towers, hot spring, and potable water systems in China. Appl Environ Microbiol. 2014; 80:2150-2157.
20. Borchardt J, Helbig JH, Lück PC. Occurrence and distribution of sequence types among *Legionella pneumophila* strains isolated from patients in Germany: Common features and differences to other regions of the world. Eur J Clin Microbiol Infect Dis. 2008; 27:29-36.
21. Chasqueira MJ, Rodrigues L, Nascimento M, Marques T. Sequence-based and monoclonal antibody typing of *Legionella pneumophila* isolated from patients in Portugal during 1987-2008. Euro Surveill. 2009; 14:29-35.
22. Reimer AR, Au S, Schindle S, Bernard KA. *Legionella pneumophila* monoclonal antibody subgroups and DNA sequence types isolated in Canada between 1981 and 2009: Laboratory Component of National Surveillance. Eur J Clin Microbiol Infect Dis. 2010; 29:191-205.
23. Underwood AP , Jones G, Mentasti M, Fry NK, Harrison TG. Comparison of the *Legionella pneumophila* population structure as determined by sequence-based typing and whole genome sequencing. BMC Microbiol. 2013; 13:302.

(Received June 1, 2015; Revised July 29, 2015; Re-revised August 9, 2015; Accepted August 9, 2015)

Supplemental data

Table S1. Sequence of primers designed for detecting virulence genes used in real-time PCR

Gene	Primers (5'-3')	Product size (bp)
flaA	F: GATGCTACGTCTGCCTAT R: CCTGCGGTTCCACCTATT	119
pilE	F: CGATGCTCATGCCACATT R: CCGTTCGGAGTTGTTTGC	120
asd	F: AAGCGGTTCATCTGGAGT R: TGCTGTGGGATAACTTGC	119
mip	F: AAATGCCATCGTTCCTG R: AGAAGCTGCGAAATCAGT	164
mompS	F: TGCCATCGTTCCTGAGTT R: GACCAGAAGCTGCGAAAT	164
proA	F: GGTGCTGTAGTTTCAACG R: GTGGCATTCTTACTGTGC	143
neuA	F: TGCCTTGCAGTCGTCTTG R: TCCGTGGCTAAATCTTCC	123

Primer designed with the sequences downloaded from EWGLI (http://www.ewgli.org/) as a template. *F* forward, *R* reverse.

Original Article

DOI: 10.5582/bst.2015.01060

High copy numbers and N terminal insertion position of influenza A M2E fused with hepatitis B core antigen enhanced immunogenicity

Xincheng Sun[1,2], Yunlong Wang[1,3,4,*], Caiwen Dong[2], Jinqiang Hu[2], Liping Yang[5]

[1] *Basic Medical School of Zhengzhou University, Zhengzhou, Henan, China;*
[2] *College of Food and Biological Engineering, Zhengzhou University of Light Industry, Zhengzhou, Henan, China;*
[3] *Bioengineering Research Center of Henan Province, Zhengzhou, Henan, China;*
[4] *Henan Biotechnology Research Centre, Zhengzhou, Henan, China;*
[5] *Basic Medical School of Henan University of Traditional Chinese Medicine, Zhengzhou, Henan, China.*

Summary **The extra domain of influenza M2 protein (M2e) is almost completely conserved among all influenza A virus subtypes. M2e is a promising candidate target for the development of a broad-spectrum recombinant influenza A vaccine. However, the immunogenicity of M2e needs to be improved. Copy numbers of M2e and its fusion expression with different carrier proteins may affect its immunopotency. In this study, we designed and created different constructs through genetic fusion of M2e (MSLLTEVETPTRSEWECRCSDSSD) (A/California/05/2009 (H1N1)) with the N-terminus (HBcAg1−149aa+Cys) by insertion in the N-terminus Hepatitis B Core (HBc) antigen 1−149aa and Middle 78-81aa of HBcAg1-149aa to construct a recombinant M2e-based vaccine candidate. These chimeric sequences were expressed in *Escherichia coli*. We constructed fusion proteins containing influenza A H1N1 influenza virus (2009), as well as one, two, and three copies of M2e and hepatitis B core antigen1-149aa amino acid-optimized codon inserted N and its intermediate. The recombinant protein was expressed and purified. Western blot analysis was employed to evaluate the expression of the M2e recombinant protein containing different copy numbers of M2e. Mice were immunized for two times with the purified fusion protein HBc/M2e BALB/c. Serum levels of M2e antibody gradually increased along with increase in immunity. The levels of different fusion protein M2e antibodies increase with increasing M2e copy number. In addition, the protein antibody level in the N terminal fusion protein is higher than that in intermediate fusion.**

Keywords: Influenza A (H1N1), M2e, HBc, vaccine

1. Introduction

Influenza is a common acute respiratory infectious disease in humans. Influenza epidemics result in millions of infections worldwide, including an estimated 250,000 to 500,000 deaths per year (*1*). The influenza virus is divided into three types (*i.e.*, A, B, and C) according to the antigenic difference of the viral nucleoprotein and the matrix protein. The vast majority of influenza cases are caused by the influenza virus types A or B. Influenza C seldom results in infection and pandemics (*2*). Vaccination is the most effective prophylaxes to control the spread of influenza. Influenza vaccine antigens (HA, NA), especially the HA antigen, can induce protective neutralizing antibodies and have a very important role in immunity. Given that the HA antigen often continues to mutate (including antigenic drift and shift), the choice of vaccine strain should also result in a corresponding change; otherwise, the vaccine prevention effect cannot be assured, even without much effect (*2-4*). Inactivated vaccines produced in embryon*ated hen eggs have several serious disadvantages (e.g.*, egg supply, matching vaccine strains, unwanted antigenic variants, and contamination with egg derived protein) that may decrease vaccine efficiency (*5*). Ideally, a flu vaccine should contain epitopes conserved in all influenza isolates to be effective against all strains of influenza A (*6*).

The influenza virus matrix protein 2 (M2) is the third

**Address correspondence to:*
Dr. Yunlong Wang, Basic Medical School of Zhengzhou University, 100 Science Avenue, Zhengzhou, Henan-450001, China.
E-mail: biowyl68@126.com

outer membrane protein. The extracellular domain of M2 (M2e) contains 23 amino acids at the N end of influenza A virus M2 and is highly conserved in the influenza A virus, particularly in subtypes of human influenza A virus (*7-8*). At present, no significant difference has been found among the M2e proteins of all influenza A viruses in population prevalence. Antibodies specific to M2e can provide a cross-protective effect against different subtypes. Passive immunization with these antibodies has reduced viral replication in the lungs of mice infected with influenza A virus (*9*). Therefore, the development of a universal influenza vaccine that can provide cross-protective effect against different subtypes has attracted considerable research interest (*10-12*).

M2e is poorly immunogenic during natural infection (*13*). However, some approaches can be applied to enhance its immunogenicity. M2e has been linked to different carriers, including hepatitis B virus core (HBc) (*14,15*), TLR5 ligand flagellin (*16*), keyhole limpet hemocyanin (*17*), and virus-like particles (VLPs) (*18-20*). These M2e-based vaccines could provide highly effective protection in animal models. Fusion proteins containing different copies of M2e epitope have demonstrated that high epitope density significantly enhances M2e-specific immunogenicity and protection (*8*). These studies have provided methods to enhance the immunogenicity of the M2e epitope. Nevertheless, studies on enhancing the immunogenicity of M2e-based vaccines in inducing better protective responses are important. Increasing epitope density enhances humoral immune response in systemic immunization. When M2e is linked to an appropriate carrier, such as HBc particles, the immunized mice achieve complete protection, which increases with the copy numbers of M2e epitope carried on the VLPs (*21-23*). However, regardless of epitope density, determining the effects of different M2e sequences, insertion position in the HBcAg, and type of HBcAg on the level of antibodies and its immunopotency is necessary. The emergence of the new influenza virus A strain H1N1 originated form swine in the human population in 2009 has demonstrated the potential pandemic threat of influenza viruses (*24*).

In this study, we designed and created a number of different constructs through genetic fusion of M2e (MSLLTEVETPTRSEWECRCSDSSD) (A/California/05/2009 (H1N1)) with the N-terminus and middle 78-81aa of (HBcAg1−149aa+Cys) by insertion in the immuno-dominant loop of HBc antigen (HBcAg1−149aa+Cys). These chimeric sequences were expressed in *Escherichia coli*, purified, and then analyzed as a recombinant fusion protein.

2. Materials and Methods

2.1. *PCR amplification and DNA cloning*

The fragment containing M2e (MSLLTEVETPTRSEWE CRCSDSSD 24 aa) gene and HBcAg1-149aa+Cys was amplified through PCR with the T7 primers from the CMM3/CMN3 plasmid, which carries the M2e gene from the influenza A virus (A/California/05/2009(H1N1)) and HBcAg(1-149aa+Cys) (Figure 1).

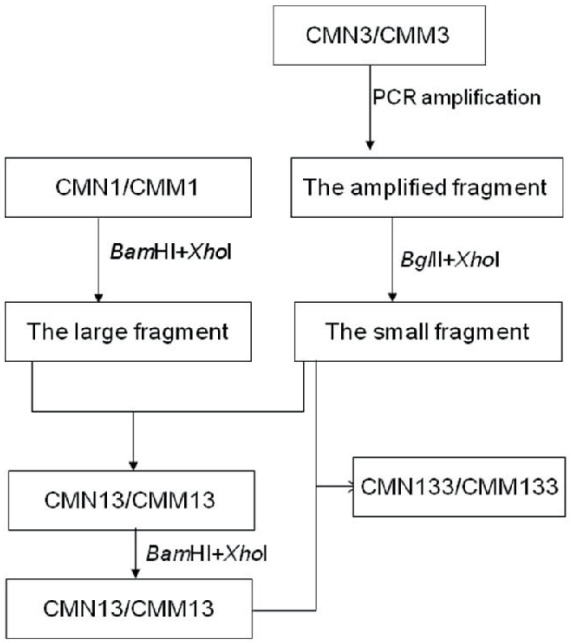

Figure 1. Contraction of the recombinant fusion gene.

PCR was carried out in a 50 μL reaction mixture containing 2× Pre-mix (25 μL), specific primers (10 pmol), 1.0 U of pfu DNA polymerase (Takara Biotechnology (Dalian) Co., Ltd., China), and 100 ng of CMM3/CMN3 plasmid as template. Amplification program was set at 94°C for 5 min, followed by 35 cycles at 94°C for 30 s, 53°C for 45 s, 72°C for 1 min, and a final extension at 72°C for 5 min. The resulting PCR products were analyzed using 1.0% (w/v) agarose gel electrophoresis.

The amplified fragments, M2e and HBcAg(1-149aa+Cys), were gel-purified using high purity PCR product purification kit (Roche, Germany) and digested with *Bgl*II and *Xho*I restriction enzymes. The fragments that underwent electrophoresis and gel-purification were named F-CMM3 and F-CMN3.

The pET30a-CMM1 and pET30a-CMN1 plasmid DNA were digested with *BamH*II and *Xho*I restriction enzymes, analyzed, and then gel-purified using the same methods as described above. The products were again gel-purified and ligated using T4 DNA ligase (Takara Biotechnology (Dalian) Co., Ltd., China) to form a recombinant vector named pET30a-CMM13/CMN13, which contains two copies of M2e. The pET30a-CMN13 and pET30a- CMM133 were identified using PCR (Figure 2).

The identified pET30a-CMN13 and pET30a-CMM133 were digested with *BamH*II and *Xho*I restriction enzymes, analyzed, and the large fragment was gel-purified using the same method as described above. The digested and purified large fragments

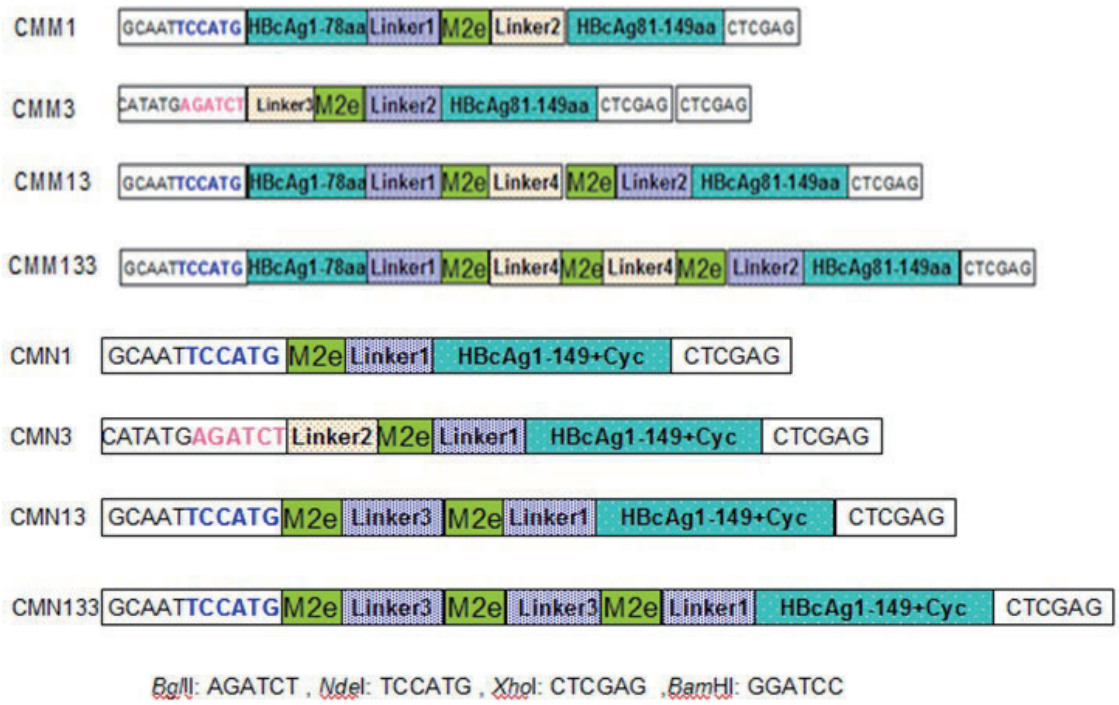

Figure 2. Schematic of the construction of M2e tandem copies.

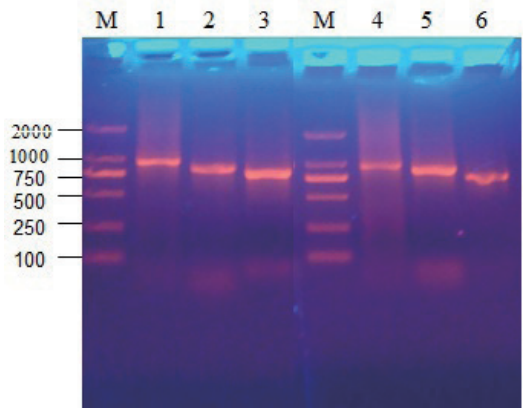

Figure 3. PCR analysis of the constructed CMN133 and CMM133 plasmid on 1.0% (w/v) agarose gel. M: DL2000 DNA Marker; 1: CMM133; 2: CMM13; 3: CMM1; 4: CMN133; 5: CMN13; 6: CMN1.

of pET30a-CMN13, F-CMM3, and F-CMN3 were respectively ligated using T4 DNA ligase to form recombinant vectors named pET30a-CMN133 and pET30a-CMN133, which contain three copies of M2e and one copy of HBcAg(1-149aa+Cys). The connected product was transformed to DH5a *E. coli*. The pET30a-CMN133 and pET30a-CMM133 fragments were identified using PCR (Figure 3).

2.2. *Transformation of BL21 and selection of transformants*

Recombinant vectors were purified from the transformed cells under the selection of 30 mg/mL Kanamycin antibiotics (Takara Biotechnology (Dalian) Co., Ltd., China) and after the restriction analysis was confirmed using sequencing reaction.

2.3. *Expression and purification of recombinant protein in BL21(DE3)*

CMN1, CMM1, and CMN133CMN133 were respectively transformed into BL21 *E. coli*. A single colony was picked and grown in 3.5 mL LB supplemented with 30 mg/mL Kanamycin, and shaken for 16 h at 37°C and 200 rpm. A 500 µL culture was added with 500 µL of 15% (v/v) sterile glycerol and stored at 20°C. To express CMN1, CMM1, and CMN133CMN133, each tube (35 µL) of glycerol stock was expanded to a starter culture of 3.5 mL LB+Kana and shaken overnight at 37°C. The culture was then expanded to 1000 mL LB+Kana induction, and grown to OD600 0.5 at 37°C. Protein expression was induced with 30 µM isopropyl β-D-1-thiogalactopyranoside (IPTG) for 6 h. The culture medium (1 mL) was sampled for assessment of expression using sodium dodecyl sulfate polyacrylamide gel electrophoresis (SDS-PAGE).

The cells were harvested and re-suspended in a 300 µL of 0.05 M PB buffer. After incubation, the cell wall was disrupted by ultrasonication (Branson sonifier 450) for 30 min at 250% to 300%, 550 W, with 10 s pulses and 5 s pauses for each cycle; the entire process was executed on ice. The broken cells were centrifuged at 10,000 g for 20 min at 4°C to separate the soluble and insoluble proteins. The insoluble protein or inclusion body was dissolved in the denaturing solubilization buffer (50 mM NaH_2PO_4, 300 mM NaCl, 8 M urea, pH 8.0). The soluble protein and dissolved-inclusion body

were analyzed using 12% SDS-PAGE. The presence of tagged-6×His fused recombinant protein was further confirmed using Western blot.

2.4. *Purification of fusion protein*

The recombinant protein CMN1, CMM1, and CMN133CMN133 with 6×His tagged at the C-terminus was purified by affinity chromatography under denaturing conditions. A column containing 1 g of nickel sulfate was equilibrated with four bed volumes of denaturing solubilization buffer. The solubilized-inclusion body was diluted at a ratio of 1:2 in the denaturing solubilization buffer containing 20 mM imidazole before being added into a column and being allowed to flow by gravity. The resin was washed thrice using four bed volumes of denaturing solubilization buffer containing 20 mM imidazole and one bed volume of denaturing solubilization buffer containing 50 mM imidazole. The recombinant CMN1, CMM1, and CMN133CMN133 were separated using 12% SDS-PAGE through a discontinuous Tris-glycine buffer system (pH 8.3).

2.5. *SDS-PAGE and Western blot analysis*

Protein samples were separated using 12% SDS-PAGE. The gel was stained with Coomassie brilliant blue R-250 and a broad-range low molecular weight marker (Takara Biotechnology (Dalian) Co., Ltd., China) was used to estimate protein size. For Western blot analysis, separated proteins were transferred onto a polyvinylidene difluoride (PVDF) membrane using transfer buffer (39 mmol/L glycine, 48 mmol/L Tris base, 0.037% SDS) and was incubated in the blocking buffer (0.01 M TBS pH 7.4, 3% bovine serum albumin) for about 30 min. Subsequently, the membrane was washed for five times with a washing buffer (0.01 M TBS pH7.4, 0.1% Tween 20), and then with ddH_2O. The membrane was then probed with horse-radish peroxidase-conjugated anti-penta-His Ab (Sangon Biotech (shanghai) Co., Ltd., China) for 30 min, and then washed again with washing buffer and deionized water. The PVDF membrane was dyed in the solution [30 mL of ddH_2O, 200 μL of 1.5 M Tris base (pH8.8), 200 μL of 1.0 M Tris base (pH 6.8), 200 μL of $NiSO_4$, 100 μL of H_2O_2, and 10 mg of diaminobenzidine (DAB)]. Protein bands were revealed by their exposure to substrate DAB (Sangon Biotech (shanghai) Co., Ltd., China).

2.6. *Immunization*

Female Balb/C mice (45 day-old) were intraperitoneally immunized with CMN1, CMN133, CMM1, and CMM133 (100 μg/per mouse) in incomplete Freund's adjuvant, aluminum adjuvant, or PBS at a final volume of 200 μL. The animals were randomly divided into five groups (*i.e.*, PBS, CMN1, CMN133, CMM1, and CMM133), with 10 mice in each group. A booster immunization was administered with the same immunogen after two weeks. Sera were collected 14 days after final immunization. Two immunizations were administered two weeks apart.

2.7. *Antibody detection*

The M2e-specific antibodies were detected using enzyme-linked immunosorbent assay (ELISA). Briefly, 96-well microtiter plates were coated with 50 μL of M2e peptide (5 μg/mL) in PBS for 2 h at room temperature and blocked with PBS containing 0.25% gelatin. Serum samples were serially diluted and added, followed by 1 h of incubation at room temperature. After extensive washes, the bound antibodies were detected sequentially by adding 1:2,000 diluted horse-radish peroxidase-linked anti-mouse antibodies and substrate o-phenylenediamine dihydrochloride peroxide solution (Sangon Biotech (shanghai) Co., Ltd., China). Absorbance at 450 nm was recorded.

Identification of the isotypes of M2e-specific antibodies was carried out as previously described (*25*).

3. Results

3.1. *Construction of recombinant fusion plasmid, pCMN133*

Influenza A virus M2e and HBc (HBcAg1-149aa+Cys) fusion genes were PCR amplified using T7 sequence primers from pET30a CMN3 plasmid. The purified fusion genes (named FM2EHBV) and pET30a CMN1 were digested, purified, and combined to form the fusion gene, pET30a-CMN13, which encoded two copies of M2e and HBcAg1-149aa+Cys protein in a single open reading frame (ORF). FM2EHBV digested with *Bgl*II and *Xho*I restriction enzymes and the purified large fragment of pET30a-CMN13 digested with *Bam*HI and *Xho*I were combined to form the fusion gene pET30a-CMN13 3, which encoded three copies M2e and HBcAg1-149aa+Cys protein in a single ORF (Figure 2).

Cloning of three copies of M2e-HBcAg1-149aa+Cys sequence into the multiple cloning site of pET30 plasmid resulted in the expression of a larger fusion protein that contained His-tag and -linker (9aa: GGGGSGGGG).

3.2. *Expression, purification, and confirmation of recombinant M2e-HBc fusion protein*

M2e-HBc/6×His gene in *E. coli* cells was confirmed using PCR and gene-specific primers. Several confirmed colonies were further induced for expression of the fusion protein under the direction of a Lac

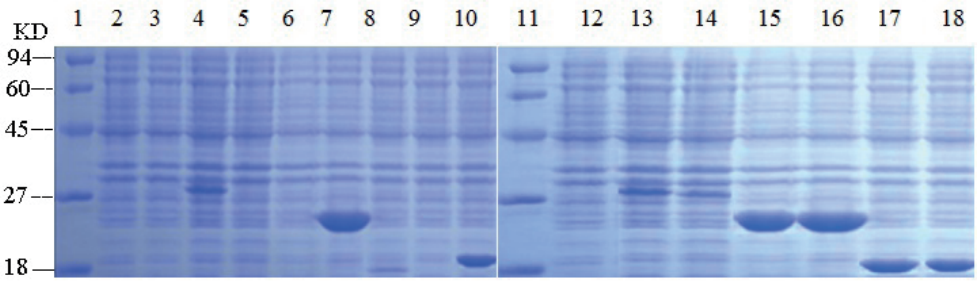

Figure 4. Analysis of recombinant M2e HBV/6×His fusion protein in the culture media by SDS-PAGE. Lane 1: Marker. Lane 2: Sample from CMN133 *E. coli* prior to IPTG induction. Lane 3: Supernatant from CMN133 *E. coli* after 4 h of IPTG induction. Lane 4: Sediment of from CMN133 after 4 h of IPTG induction. Lane 5: Sample from CMN13 *E. coli* prior to IPTG induction. Lane 6: Supernatant from CMN13 *E. coli* after 4 h of IPTG induction. Lane 7: Sediment from CMN13 *E. coli* after 4 h of IPTG induction. Lane 8: Sample from CMN1 *E. coli* prior to IPTG induction. Lane 9: Supernatant from CMN1 *E. coli* after 4 h of IPTG induction. Lane 10: Sediment from CMN1 *E. coli* after 4 h of IPTG induction. Lane 11: Marker. Lane12: Sample from BL21 (DE3). Lane 13: Supernatant from CMM133 after 4 h of IPTG induction. Lane 14: Sediment from CMM133 after 4 h of IPTG induction. Lane 15: Supernatant of from CMM13 after 4 h of IPTG induction. Lane 16: Sediment from CMM13 after 4 h of IPTG induction. Lane 17: Supernatant from CMM1 after 4 h of IPTG induction. Lane 18: Sediment from CMM1 after 4 h of IPTG induction.

promoter by adding IPTG. The culture was sampled after being induced for 4 h for the final analysis using SDS-PAGE. As illustrated in Figure 4, a protein band corresponding to the expression of the recombinant fusion protein with an approximate molecular weight of 30 kDa was detected in all three samples, but was absent in the uninduced cells. However, the recombinant protein expression was slightly higher. Moreover, the fusion of vector-derived 6×His tag to the C-terminus of the expressed protein provided the possibility of its one-step purification through the Ni-NTA columns (Figure 4).

3.3. *Confirmation of the recombinant M2e-HBc fusion protein*

To confirm the purified protein, the purified recombinant proteins CMN1, CMN133, CMM1, and CMM133 were transferred to a PVDF membrane and treated with M2e monoclonal antibody. A band with the expected size (23 and 30 kDa) was revealed in the lane of the purified protein, which corroborated its accuracy, as shown in Figure 5. A single copy and three copies of the protein were successfully expressed and had the antigenicity of M2e.

3.4. *ELISA result*

To detect four kinds of purified protein using ELISA, the purified single copy and three copies of the fusion protein were coated and detected using anti M2e monoclonal antibody preparation, with four kinds of fusion proteins from 1:10,000, 1:20,000, 1:40,000, 1:80,000, and 1:160,000. The results (Figure 6) showed that the fusion protein in dilution 1:40,000 were active, and that a single copy of the fusion protein exhibited activity below three copies of protein. The three copies of protein in the N-terminus fusion protein were slightly higher than that in the middle of the insertion of the HBc antigen protein.

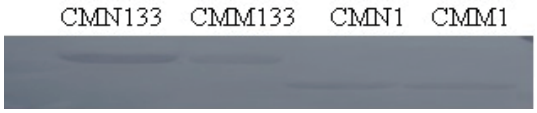

Figure 5. Western blot of the purified recombinant protein.

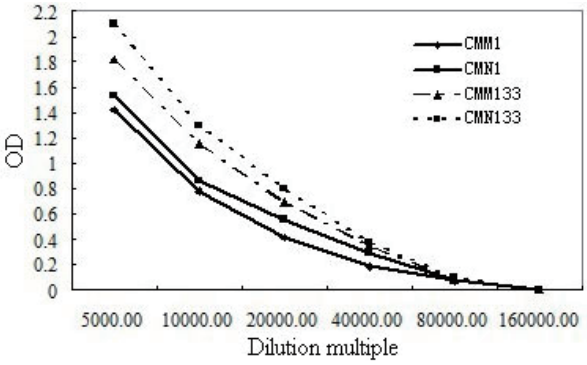

Figure 6. ELISA detection of M2e.

3.5. *Detection of serum titer of mice*

The titer of the serum anti-M2e antibody was detected using indirect ELISA two weeks after each immunization and before the final immunization. This was executed after the mice have been immunized with purified single copy and three copies of M2e protein. The experimental results showed that the CMN1, CMN133, CMM1, and CMM133 groups could produce anti M2eIgG antibody in the induced mice. The antibody titer increased with the number of strengthening immunity. The three copies of M2e were significantly better than the single copy at two weeks after the first immunization. No significant differences were observed between CMN1 and CMM1 and CMM133 and CMN133. Alternatively, significant differences were observed among the antibody titer of CMN1, CMM1, CMN133, and CMM133 at four weeks after the final immunization (Figure 7).

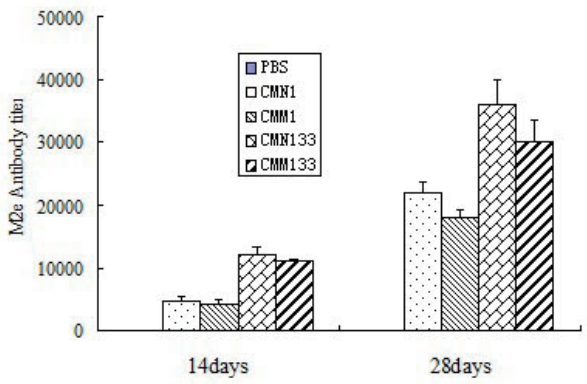

Figure 7. Detection result of serum titer of mice.

4. Discussion

M2e-based universal influenza vaccines have attracted research interest because of the highly conservative character of the sequence of M2e membrane protein in all influenza A isolates (*20*). Results of several preclinical studies with M2e protein, with or without carriers, have already proven the successful protection of M2e-based vaccinated animal models against the lethal challenge of heterologous and homologous influenza A virus.

HBc particles have been used as virus-like display scaffolds since 1980s (*26*). In the last 30 years, the most successful application of this scaffold is the influenza vaccine ACAM-FLU-A produced by Sanofi Pasteur and the malaria (*Plasmodium falciparum*) vaccine MalariVax (ICC-1132) produced by Apovia (*27,28*). These particles have been expressed in *E. coli* with the HBc as the foreign insertion site, and they have already been subjected to phase I clinical trials.

However, the M2e-based immunization effect against influenza virus differs under various conditions of expression strategy, immune pathway, and animal model. Host-specific variations were also observed in M2e sequences among influenza strains from different hosts. Thus, evaluating whether M2e-based immunization could provide protection against the 2009 pandemic H1N1 is necessary.

In this study, we successfully constructed the aforementioned plasmids bearing one copy, three copies of M2e, and HBc (HbcAg1-149aa+Cys). These fusion proteins were expressed in *E. coli*. Considering the senior conformation and structural features of M2 protein, the linker arm of GGGGSGGGG in the fusion proteins was located between M2e and HBc (HBcAg1-149aa+Cys). A single cysteine residue was added to the C-terminus to provide additional stabilization (*29*). All of the purified proteins of CMN1, CMM1, CMN133, and CMM133 in incomplete Freund's adjuvant can induce production of IgG antibody against M2e. Higher epitope density engendered higher antibody levels. The ELISA showed that the increase in M2e copies results in an increase in level of the immune serum antibody. The insertion position of M2e in the HBc affects the antibody level.

In conclusion, our study provided evidence for the construction of the M2e-HBcAg1-149aa+Cys fusion sequence. The sequence had been successfully expressed in *E. coli*, and the purified protein induced the production of antibodies against M2e. These fusion proteins are potential candidates for developing influenza vaccine. However, further investigation is necessary to evaluate the in vivo protective potential of the resulting protein.

Acknowledgements

This work was supported by a grant from the key scientific and technological research project of Henan Province (142102310062) and scientific and technological research project of Zhengzhou City (141PPTGG347).

References

1. Ryan J, Zoellner Y, Gradl B, Palache B, Medema J. Establishing the health and economic impact of influenza vaccination within the European Union 25 countries. Vaccine. 2006; 24:6812-6822.
2. Palese P. Influenza: Old and new threats. Nat Med. 2004; 10:82-87.
3. Scalera NM, Mossad SB. The first pandemic of the 21st century: A review of the 2009 pandemic variant influenza A (H1N1) virus. Postgrad Med. 2009; 5:43-47.
4. Kilbourne ED. Influenza pandemics of the 20th century. Emerg Infect Dis. 2006; 12:9-14.
5. Subbarao K, Matsuoka Y. The prospects and challenges of universal vaccines for influenza. Trends Microbiol. 2013; 21:350-358.
6. Denis J, Acosta-Ramirez E, Zhao Y, Block T M, Gish R, Guo H, Mehta A, Cuconati A, Thomas London W, Guo JT. Chronic hepatitis B: What should be the goal for new therapies. Antiviral Res. 2013; 98:27-34.
7. De Filette M, Fiers W, Martens W, Birkett A, Ramne A, Löwenadler B, Lycke N, Jou WM, Saelens X. Improved design and intranasal delivery of an M2e-based human influenza A vaccine. Vaccine. 2006; 24:6597-6601.
8. Liu W, Zou P, Ding J, Lu Y, Chen YH. Sequence comparison between the extracellular domain of M2 protein human and avian influenza A virus provides new information for bivalent influenza vaccine design. Microbes Infect. 2005; 7:171-177.
9. Turley CB, Rupp RE, Johnson C, Taylor DN, Wolfson J, Tussey L, Kavita U, Stanberry L, Shaw A. Safety and immunogenicity of a recombinant M2e–flagellin influenza vaccine (STF2.4xM2e) in healthy adults. Vaccine. 2011; 29:5145-5152.
10. Ebrahimi SM, Tebianian M. Influenza A viruses: Why focusing on M2e-based universal vaccines. Virus Genes. 2011; 42:1-8.
11. De Filette M, Martens W, Smet A, Schotsaert M, Birkett A, Londoño-Arcila P, Fiers W, Saelens X. Universal influenza A M2e-HBc vaccine protects against disease

even in the presence of pre-existing anti-HBc antibodies. Vaccine. 2008; 26:6503-6507.
12. Subbarao K, Matsuoka Y. The prospects and challenges of universal vaccines for influenza. Trends Microbiol. 2013; 7:350-358.
13. Feng J, Zhang M, Mozdzanowska K, Zharikova D, Hoff H, Wunner W, Couch RB, Gerhard W. Influenza A virus infection engenders a poor antibody response against the ectodomain of matrix protein 2. Virol J. 2006; 3:102.
14. Blokhina EA, Kuprianov VV, Stepanova LA, Tsybalova LM, Kiselev OI, Ravin NV, Skryabin KG. A molecular assembly system for presentation of antigens on the surface of HBc virus-like particles. Virology. 2013; 20:293-300.
15. Arora U, Tyagi P, Swaminathan S, Khanna N. Virus-like particles displaying envelope domain III of dengue virus type 2 induce virus-specific antibody response in mice. Vaccine. 2013; 31:873-878.
16. Talbot HK, Rock MT, Johnson C, Tussey L, Kavita U, Shanker A, Shaw AR, Taylor DN. Immunopotentiation of trivalent influenza vaccine when given with VAX102, a recombinant influenza M2e vaccine fused to the TLR5 ligand flagellin. PLoS One. 2010; 5:e14442.
17. Reese KA, Lupfer C, Johnson RC, Mitev GM, Mullen VM, Geller BL, Pastey M. A novel lactococcal vaccine expressing a peptide from the M2 antigen of H5N2 highly pathogenic avian influenza A virus prolongs survival of vaccinated chickens. Vet Med Int. 2013; 5:1-8.
18. Kim MC, Lee YN, wang HS, Lee YT, Jung YJ, Cho MK, Kim YJ, Lee JS, Ha SH, Kang SM. Influenza M2 virus-like particles confer a broader range of cross protection to the strain-specific pre-existing immunity. Vaccine. 2014; 32:5824-5831.
19. Wang L, Hess A, Chang TZ, Wang YC, Champion JA, Compans RW, Wang BZ. Nanoclusters self-assembled from conformation-stabilized influenza M2e as broadly cross- protective influenzavaccines. Nanomedicine. 2014; 10:473-482.
20. Lee YN, Kim MC, Lee YT, Wang HS, Cho MK, Lee JS, Ko EJ, Kang SM. AS04-adjuvanted virus-like particles containing multiple M2 extracellular domains of influenza virus confer improved protection. Vaccine. 2014; 32:4578-4585.
21. Zhang X, Liu M, Liu C, Du J, Shi W, Sun E, Li H, Li J, Zhang Y. Vaccination with different M2e epitope densities confers partial protection against H5N1 influenza A virus challenge in chickens. Intervirology. 2011; 54:290-299.
22. Zhou C, Zhou L, Chen YH. Immunization with high epitope density of M2e derived from 2009 pandemic. Vaccine. 2012; 30:3463-3469.
23. De Filette M, Min Jou W, Birkett A, Lyons K, Schultz B, Tonkyro A, Resch S, Fiers W. Universal influenza A vaccine: Optimization of M2-based constructs. Virology. 2005; 337:149-161.
24. Smith GJ, Vijaykrishna D, Bahl J. Lycett SJ, Worobey M, Pybus OG, Ma SK, Cheung CL, Raghwani J, Bhatt S, Peiris JS, Guan Y, Rambaut A. Origins and evolutionary genomics of the 2009 swine-origin H1N1 influenza A epidemic. Nature. 2009; 459:1122-1125.
25. Wu F, Huang JH, Yuan XY, Huang WS, Chen YH. Characterization of immunity induced by M2e of influenza virus. Vaccine, 2007; 25:8868-8873.
26. Kilbourne ED. Influenza pandemics of the 20th century. Emerg Infect Dis. 2006; 12:9-14.
27. Lee JS, Kwon YM, Wang HS, Lee YN, Ko EJ, Yoo SE, Kim MC, Kim KH, ChoMK, Lee YT, Lee YR, Quan FS, Kang SM. Baculovirus-expressed virus-like particle vaccine in combination with DNA encoding the fusion protein confers protection against respiratory syncytial virus. Vaccine. 2014; 32:5866-5874.
28. Kushnir N, Streatfield SJ, Yusibov V. Virus-like particles as a highly efficient vaccine platform: Diversity of targets and production systems and advances in clinical development. Vaccine. 2012; 17:58-83.
29. Kaminaka K, Matsuda J, Nozaki C. Influenza virus M2e with additional cysteine residues shows enhanced immunogenicity and protection against lethal virus challenge. Viral Immunol. 2013; 4:291-295.

(Received April 24, 2015; Revised July 27, 2015; Re-revised July August 24, 2015; Accepted August 24, 2015)

Original Article

DOI: 10.5582/bst.2015.01092

Products of dentin matrix protein-1 degradation by interleukin-1β-induced matrix metalloproteinase-3 promote proliferation of odontoblastic cells

Naoko Hase[1,*], Nobuaki Ozeki[1,*], Taiki Hiyama[1], Hideyuki Yamaguchi[1], Rie Kawai[1], Ayami Kondo[2], Kazuhiko Nakata[1], Makio Mogi[1,]**

[1] *Department of Endodontics, School of Dentistry, Aichi Gakuin University, Nagoya, Aichi, Japan;*
[2] *Department of Medicinal Biochemistry, School of Pharmacy, Aichi Gakuin University, Nagoya, Japan.*

Summary **We have previously reported that interleukin (IL)-1β induces matrix metalloproteinase (MMP)-3-regulated cell proliferation in mouse embryonic stem cell (ESC)-derived odontoblast-like cells, suggesting that MMP-3 plays a potentially unique physiological role in regeneration by odontoblast-like cells. MMPs are able to process virtually any component of the extracellular matrix, including collagen, laminin and bioactive molecules. Because odontoblasts produce dentin matrix protein-1 (DMP-1), we examined whether the degraded products of DMP-1 by MMP-3 contribute to enhanced proliferation in odontoblast-like cells. IL-1β increased mRNA and protein levels of odontoblastic marker proteins, including DMP-1, but not osteoblastic marker proteins, such as osteocalcin and osteopontin. The recombinant active form of MMP-3 could degrade DMP-1 protein but not osteocalcin and osteopontin *in vitro*. The exogenous degraded products of DMP-1 by MMP-3 resulted in increased proliferation of odontoblast-like cells in a dose-dependent manner. Treatment with a polyclonal antibody against DMP-1 suppressed IL-1β-induced cell proliferation to a basal level, but identical treatment had no effect on the IL-1β-induced increase in MMP-3 expression and activity. Treatment with siRNA against MMP-3 potently suppressed the IL-1β-induced increase in DMP-1 expression and suppressed cell proliferation ($p < 0.05$). Similarly, treatment with siRNAs against Wnt5a and Wnt5b suppressed the IL-1β-induced increase in DMP-1 expression and suppressed cell proliferation ($p < 0.05$). Rat KN-3 cells, representative of authentic odontoblasts, showed similar responses to the odontoblast-like cells. Taken together, our current study demonstrates the sequential involvement of Wnt5, MMP-3, DMP-1 expression, and DMP-1 degradation products by MMP-3, in effecting IL-1β-induced proliferation of ESC-derived odontoblast-like cells.**

Keywords: Embryonic stem cell, odontoblast, Wnt5

1. Introduction

Because matrix metalloproteinases (MMPs) are able to process virtually any component of the extracellular matrix (ECM), including collagen, laminin, and bioactive molecules, it has been suggested that MMPs may be important in inflammatory conditions, such as rheumatoid arthritis, metastasis and periodontitis (*1,2*). In particular, MMP-3 (known as stromelysin-1) has a wide substrate specificity and is capable of degrading many types of ECM proteins, such as collagen types II, III, IV, IX, and X, proteoglycans, fibronectin, laminin, and elastin (*1,2*), rendering MMP-3 crucial in connective tissue and bone remodeling (*3,4*). However, while it is intuitive that dental pulp destruction may be a function of MMPs, our previous study reported that MMP-3 actually accelerates wound healing following dental pulp injury (*5,6*). This observation indicates that MMP-3 may instead be involved in ECM

*These authors contributed equally to this works.
***Address correspondence to:*
Dr. Makio Mogi, Department of Medicinal Biochemistry, School of Pharmacy, Aichi Gakuin University, 1-100 Kusumoto, Chikusa-ku, Nagoya, Aichi 464-8650, Japan.
E-mail: makio@dpc.agu.ac.jp

degradation, especially in dentin, and in the subsequent morphogenesis, wound repair (*5,6*) and angiogenesis (*5-7*) of the inflamed tissue.

Interleukin (IL)-1β detected in inflamed dental pulp, is associated with periapical disease (*8*) and is apparently essential to the pathogenesis of acute pulpitis. Notably, treatment with IL-1β induces potent expression of *MMP-3* in dental pulp, a tissue that contains large numbers of odontoblasts (*7*). We also reported that proinflammatory cytokine IL-1β-induced MMP-3 activity is associated with cell proliferation of purified odontoblast-like cells derived from mouse embryonic stem cells (ESCs) and induced pluripotent stem cells (iPSCs) (*9,10*). Thus, IL-1β-induced MMP-3 appears to be pivotal in the pathophysiology of inflamed dental pulp containing rich odontoblasts. However, the signaling cascade underpinning this stimulation is yet to be elucidated.

Because performing experiments using purified odontoblast-like cells derived from mouse iPSCs (*11*) and ESCs (*12*), we have developed excellent *in vitro* models in which to examine the mechanisms of wound healing following exposure to proinflammatory cytokines (*9,10*). We have also previously reported that a proinflammatory cytokine mixture of IL-1β, tumor necrosis factor-α, and interferon-γ, or IL-1β alone, can induce MMP-3 activity in rat dental pulp cells, and result in a potent increase in cell proliferation (*13,14*). Taken together, these studies suggest that MMP-3 induced by the proinflammatory cytokine IL-1β contributes to the pathophysiology of inflamed dental pulp containing rich odontoblast cells.

It is unclear how IL-1β cytokine-induced MMP-3 regulates odontoblast-like cell proliferation. Recent reports demonstrate that IL-1β-induced MMP-3 is associated with the secreted glycoprotein Wnt signaling pathway (*15*). We have also demonstrated that IL-1β-induced MMP-3-regulated proliferation of mouse ESC-derived odontoblastic cells is mediated by the Wnt5a- and 5b-signaling pathways (*16*). Although compelling evidence remains to be shown, we speculate that an ECM-derived degradation product generated by MMP-3 might induce cell proliferation; however, the substrates of MMP-3 that induce cell proliferation remain to be identified.

Odontoblasts are essentially dentin-secretory cells that produce pre-dentin, an ECM formed by type I collagen as the major organic component (about 90%), together with noncollagenous proteins, including glycoproteins, proteoglycans, and dentin phosphoproteins, such as dentin matrix protein-1 (DMP-1), which constitute relatively specific markers for dentin (*17,18*). Therefore, odontoblasts are surrounded by collagen and dentin matrix proteins. A recent report has demonstrated that ECM, especially the dentin matrix protein component, contains functional proteins that have been previously defined as solely intracellular (*19*). However, DMP-1, which has a role in matrix mineralization, can act as both an intra- and extracellular-signaling molecule, thus impacting odontoblast differentiation (*20,21*). To date, functional data, especially in respect to the proliferative roles of MMP-3 signaling and DMP-1 in mouse odontoblasts, remains scarce. Therefore, further studies are required to completely understand the intracellular role of DMP-1 in odontoblasts.

Here, we examine whether DMP-1 degradation products by MMP-3 are associated with the proliferation of odontoblasts, as may be encountered in inflamed dental pulp. We show for the first time, that MMP-3 up-regulates dentin matrix protein degradation in our odontoblast-like cells, and leads to increased cell proliferation.

2. Materials and Methods

2.1. *Products*

Mouse recombinant IL-1β was obtained from PeproTech (Rocky Hill, NJ, USA). Mouse recombinant DMP-1 and osteopontin were obtained from R&D Systems Inc. (Minneapolis, MN, USA) and osteocalcin was obtained from Uscn Life Science Inc. (Wuhan Hubei, China). Anti-DMP-1 polyclonal antibody was obtained from Abcam (ab103203; Cambridge, UK). Recombinant mouse MMP-3 (Pro-form) was obtained from R&D Systems Inc., and was activated by treating with 1 mM 4-aminophenyl mercuric acetate in all experiments.

2.2. *Cell culture*

The mouse ESC cell line, E14Tg2a (*22*), was a kind gift from Dr. Randall H. Kramer (University of California San Francisco, San Francisco, CA, USA) and was maintained as described previously (*23*). Purified ESC-derived odontoblast-like cells were obtained as previously reported (*12*). These differentiated cells displayed odontoblast-like physiological characteristics, for example calcification activity and alkaline phosphatase activation, up to day 21 of culture. Authentic rat odontoblast-like cells (KN-3) (*24*) were kindly provided by Dr. Chiaki Kitamura (Kyushu Dental College, Kitakyushu, Japan) and were maintained as described previously (*24*). Mouse osteoblast-like MC3T3-E1 cells were obtained from the Riken BioResource Center Cell Bank (Ibaraki, Japan) and were cultured as previously described (*25,26*). These cells were used throughout the study as a negative control.

2.3. *Cell proliferation assay*

Cell proliferation was evaluated using the BrdU-cell proliferation enzyme-linked immunosorbent assay (ELISA; Roche Applied Science, Mannheim, Germany) as described previously (*25,26*). Cells were seeded

into 96-well tissue culture plates at a density of 1×10^5 cells/cm^2.

2.4. *Real-time quantitative polymerase chain reaction analysis*

Real-time quantitative polymerase chain reaction (qPCR) for all samples and standards was performed in triplicate in 96-well optical microtiter plates with ~25 ng of RNA, 0.25 µL of RT Mix (Qiagen Quantitect RT Mix), 1.25 µL of 20× Primer/Probe Mix, and 12.5 µL of Mastermix (Qiagen Quantitect RT-PCR Kit) in a 25 µL reaction volume. The following primer/probe sets were used: mouse DMP-1, Mm01208363_m1; rat DMP-1, Rn01450122_m1; human osteocalcin [*BGLAP*] (mouse available), Hs01587814_g1; rat osteocalcin [*BGLAP*], Rn00566386_g1; mouse osteopontin [*SPP1*], Mm00436767_m1; rat osteopontin, Rn00681031_m1; Assays-On-Demand™ (Applied Biosystems, Carlsbad, CA, USA). Standards and samples were mixed with the PCR reagents, loaded into the 96-well microtiter plate and sealed with optical film (Applied Biosystems). TaqMan samples were subjected to thermal cycling conditions with the following parameters: an initial holding stage of 30 min at 50°C (for RNA reverse transcription), 15 min at 95°C (to activate HotStarTaq polymerase enzyme), then 40 cycles of 15 s at 94°C/60 s at 60°C. Gene expression was quantified relative to a standard curve. Glyceraldehyde-3-phosphate dehydrogenase (GAPDH) and 18S amplicon rRNA were employed as housekeeping genes and used as normalization controls to account for variations in the amount of total RNA in each sample. For each experimental sample, the amount of target and endogenous reference was determined from the appropriate standard curve. The amount of target was then divided by the amount of endogenous reference to obtain a normalized target value. Ct (threshold cycle values) for samples and housekeeping genes were extrapolated from the standard curve to produce an arbitrary value of expression, the ratio of which (sample/housekeeping gene) within a given tissue sample was plotted as the relative mRNA expression level.

2.5. *Western blot analysis*

DMP-1, MMP-3, Osteocalcin, Osteopontin, Wnt5a, and Wnt5b protein levels in the cell lysate were determined by western blot analysis. Cells were cultured for 24 h with or without IL-1β, lysed, and the protein lysate separated on sodium dodecyl sulfate polyacrylamide gels (12%). Western blot analysis was then performed using anti-DMP-1 (ab103203; Abcam), anti-MMP-3, anti-osteocalcin, anti-osteopontin, anti-Wnt5a, anti-Wnt5b, and anti-β-tubulin polyclonal antibodies (sc-6839, sc-18322, sc-10593, sc-365370, sc-109464, and sc-9935, respectively; Santa Cruz Biotechnology Inc., Santa Cruz, CA, USA). The anti-MMP-3 antibody showed no significant cross-reactivity with other MMPs (data not shown). Visualization and quantification of blotted protein bands were performed with Multi Gauge-Ver3.X software (Fujifilm, Tokyo, Japan).

2.6. *Measurement of MMP-3 activity*

The protocol for measuring MMP-3 activity has been described previously (*10,13,16,27*) and is now a commercially available MMP-3 activity assay kit (SensoLyte™ 520 MMP-3 assay kit; AnaSpec, San Jose, CA, USA). Prior to detection, MMP-3 was immunoprecipitated from the culture medium using a goat anti-MMP-3 antibody (sc-6839, Santa Cruz Biotechnology Inc.) and protein A/G–agarose for 6 h at 4°C. After centrifugation, the agarose pellets were suspended in an MMP-3 assay buffer containing the MMP-3 substrate, 5-FAM-Arg-Pro-Lys-Pro-Val-Glu-Nva-Trp-Arg-Lys- QXL™520-NH_2 fluorescence resonance energy transfer peptide, as supplied in the assay kit. MMP-3 activity was then determined according to the manufacturer's instructions (*28*).

2.7. *Silencing of Wnt5a, Wnt5b and MMP-3 genes by siRNA transfection*

The Wnt5a, Wnt5b and MMP-3 siRNAs for gene silencing were acquired commercially (sc-41113, sc-155357 and sc-37265, respectively; Santa Cruz Biotechnology Inc.) and transfected into cultured cells using a siRNA reagent system (Santa Cruz Biotechnology Inc.) according to the manufacturer's protocol. An anti-GAPDH siRNA and an anti-control siRNA, with no known homogeny for any vertebrate sequence (Thermo Scientific, Lafayette, CO, USA), were used as positive and negative controls, respectively.

2.8. *Statistical analysis*

Data presented in bar graphs are the mean ± standard deviation (S.D.) of four independent experiments. Statistical significance was assessed using the Mann-Whitney *U*-test. A value of $p < 0.05$ was considered as statistically significant.

3. Results

3.1. *IL-1β induction of DMP-1 mRNA and protein expression*

The ESC-derived odontoblast-like cell line was cultured in the presence of four concentrations of IL-1β (0, 0.25, 2.5, and 25 ng/mL). Induction of DMP-1, osteocalcin, and osteopontin mRNA and protein were assessed using real-time qPCR (Figures 1A-1C) and western blot analysis (Figures 1A-1C, far lower panels), respectively. mRNA and protein levels of the odontoblastic marker

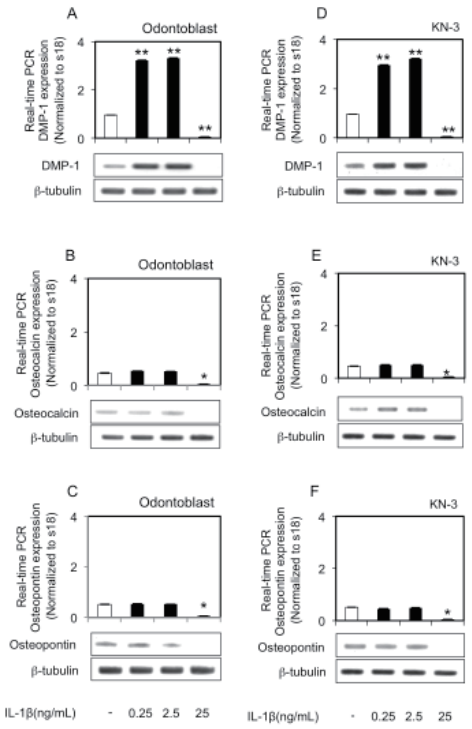

Figure 1. IL-1β-induced expression of DMP-1, osteocalcin, and osteopontin mRNA and protein in odontoblast-like cells. ESC-derived odontoblast-like cells and KN-3 odontoblast cells were incubated with IL-1β (0, 0.25, 2.5, and 25 ng/mL). Real-time qPCR expression of DMP-1, osteocalcin and osteopontin mRNA relative to control (S18 mRNA) using ESC-derived odontoblast-like cells (A-C) and KN-3 cells (D-F). Data represent the mean ± S.D. of four independent experiments. $^{*}p < 0.05$, $^{**}p < 0.01$. Lower panels show western blot analysis of DMP-1, osteocalcin, osteopontin, and β-tubulin protein levels following stimulation with IL-1β. Blots shown are representative of three independent experiments.

DMP-1 were increased in the presence of 0.25 ng/mL and 2.5 ng/mL IL-1β, but not at 25 ng/mL.

To assess whether the induction of DMP-1 by IL-1β is a specific response in ESC-derived odontoblast-like cells, we evaluated the expression of other osteoblastic markers, including osteocalcin and osteopontin proteins, following treatment with the same concentrations of extracellular IL-1β (0, 0.25, 2.5, and 25 ng/mL). However, there were no significant increases in mRNA levels of these markers in response to IL-1β (Figures 1B and 1C). KN-3 odontoblast cells showed similar responses to the ESC-derived odontoblast-like cells (Figures 1D-1F).

3.2. *MMP-3 degraded DMP-1 protein in vitro*

When exogenous active MMP-3 was mixed with recombinant mouse DMP-1, prior to incubation at 37°C for 2 h, the intensity of both DMP-1 protein bands decreased in a time-dependent-manner, as visualized by western blot, indicating that DMP-1 as a dentin matrix component could be the substrate for MMP-3 (Figure 2A). Interestingly, the other bone matrix protein components and osteoblast markers, osteocalcin and osteopontin, showed no differences, suggesting that

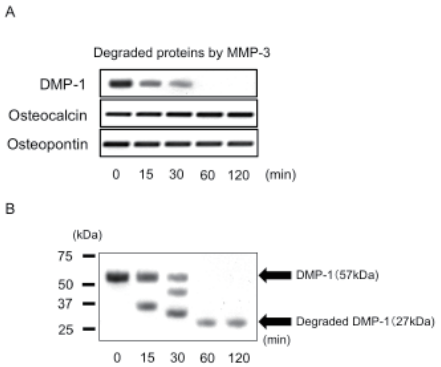

Figure 2. Time-dependent degradation of bone matrix proteins DMP-1, osteocalcin, and osteopontin by MMP-3. (A) Western blotting analysis of proteins incubated with exogenous active MMP-3 and recombinant mouse DMP-1, osteocalcin and osteopontin for 0, 0.25, 0.5, 1, and 2 h using a molar ratio of 1:1 at 37°C, respectively. **(B)** Western blotting analysis of proteins incubated with exogenous active MMP-3 and recombinant mouse DMP-1 with Coomassie brilliant blue staining for 0, 0.25, 0.5, 1, and 2 h using a molar ratio of 1:1 at 37°C. Before Western blot analysis, MMP-3 was immunoprecipitated by incubation with anti-MMP-3 polyclonal antibody and protein A/G Sepharose for 1 h at 4°C. Visualization of blotted protein bands was performed with Multi Gauge-Ver3.X software (Fujifilm). Blots shown are representative of three independent experiments.

MMP-3 could not degrade these proteins under similar conditions. In addition, when activated MMP-3 and recombinant DMP-1 were incubated at 37°C, mature DMP-1 (57 kDa) decreased time-dependently, but the degraded product of DMP-1 (27 kDa) appeared for up to 2 h (Figure 2B).

3.3. *Effect of exogenous degraded product of DMP-1 protein by MMP-3 on cell proliferation*

Subsequent experiments used ESC-derived odontoblast-like cells (E14Tg2a) in comparison to rat KN-3 cells. We tested whether exogenous degraded products of DMP-1 by MMP-3 could enhance cell proliferation in odontoblast-like cells. DMP-1 and the active form of MMP-3 were mixed, incubated and added to the anti-MMP-3 polyclonal antibody. Protein A/G sepharose was then added and this was spun down to remove MMP-3. When the supernatant (containing DMP-1 degradation products) was added to odontoblast-like cells, cell proliferation was slightly increased ($p < 0.05$; Figures 3A and 3B). Therefore, we confirmed that the enhanced effect on cell proliferation was dependent on the degraded products of DMP-1 and not exogenous MMP-3 (Figure 3A). We also confirmed that the addition of DMP-1 had no effect on cell proliferation in odontoblast-like cells (Figures 3C and 3D). Therefore, the degraded products of DMP-1 were required for cell proliferation. KN-3 cells showed similar responses to the ESC-derived odontoblast-like cells (Figures 3B and 3D). The supernatant was confirmed to have no MMP-3 activity (Figure 3E). Interestingly, DMP-1 products had no proliferative effect on mouse osteoblastic MC3T3-E1 cells (Figure 3F).

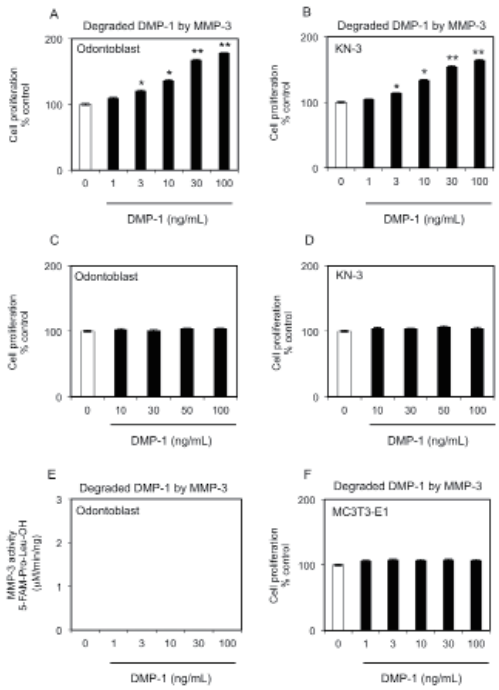

Figure 3. Effect of DMP-1 degradation products by MMP-3 on cell proliferation. Effect of exogenous DMP-1 degradation products by MMP-3 on cell proliferation of ESC-derived odontoblast-like cells **(A)** and KN-3 cells **(B)**. **(C)** Effect of exogenous DMP-1 protein on cell proliferation of ESC-derived odontoblast-like cells **(D)** and KN-3 cells. **(E)** Determination of MMP-3 activity in the supernatant containing DMP-1 degradation products by MMP-3. One unit of MMP-3 activity is defined as 1 μM of 5-FAM-Pro-Leu-OH formed/min/ng enzyme at 37°C. **(F)** Effect of DMP-1 degradation products by MMP-3 on MC3T3-E1 cell proliferation.

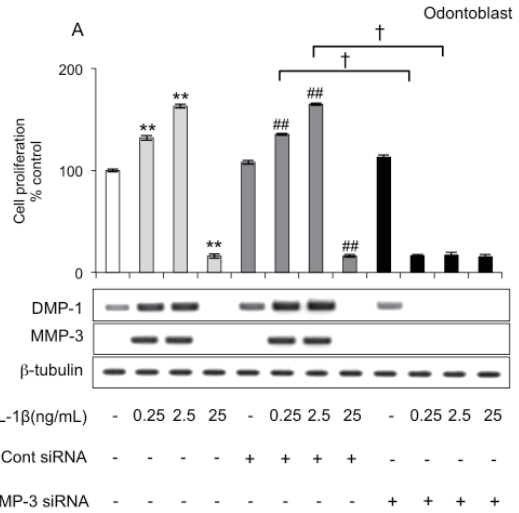

Figure 4. Effect of anti-mouse DMP-1 polyclonal antibody on IL-1β-induced MMP-3 expression and cell proliferation. ESC-derived odontoblast-like cells **(A** and **C)** and KN-3 cells **(B** and **D)** were treated for 24 h with anti-DMP-1 polyclonal antibody, stimulated with IL-1β (0, 0.25, 2.5, and 25 ng/mL), then analyzed by BrdU-cell proliferation ELISA (for cell proliferation; A and B graphs, upper panels), MMP-3 activity **(C** and **D)** and western blotting (for MMP-3 protein expression; **C** and **D**, far lower panels). β-Tubulin was used as a housekeeping protein in the western blots. $^{**}p < 0.01$ *vs*. control; $^{\#\#}p < 0.01$ as indicated by the bracket. Cell proliferation was estimated by BrdU-ELISA. ELISA data represent the mean ± S.D. of four independent experiments. $^{*}p < 0.05$ and $^{**}p < 0.01$.

3.4. *Effect of anti-DMP-1 polyclonal antibody on IL-1β-induced MMP-3 expression and cell proliferation*

Because there is no commercially available mouse DMP-1 siRNA, we employed a specific anti-DMP-1 polyclonal antibody to determine if the proliferation effects observed with IL-1β stimulation were mediated by DMP-1. Cells were pretreated with an anti-DMP-1 polyclonal antibody, and then stimulated with IL-1β as described above. Western blot analysis of MMP-3 protein expression confirmed that the antibody had no effect on the IL-1β-induced MMP-3 activity (Figure 4C). Anti-DMP-1 polyclonal antibody had no effect on the expression of β-tubulin (loading control). Using the same culture conditions, we tested the effect of an anti-DMP-1 polyclonal antibody on IL-1β-induced changes in cell proliferation. DMP-1 silencing considerably decreased the number of proliferating odontoblast-like cells following IL-1β stimulation when compared with untreated cells ($p < 0.01$; Figure 4A). The reduction in proliferative potential was estimated to be ~60% and up to the basal level, suggesting that IL-1β-induced cell proliferation required DMP-1 protein in odontoblast-like cells.

Using the same culture conditions, KN-3 cells showed a similar response to ESC-derived odontoblast-like cells (Figures 4B and 4D).

3.5. *Effect of anti-MMP-3 siRNA on IL-1β-induced DMP-1 expression and cell proliferation*

We replicated the above experiments using anti-MMP-3 siRNA. This reagent efficiently down-regulated the DMP-1 protein expression induced by IL-1β (0.25 and 2.5 ng/mL; $p < 0.01$; Figure 5A). Conversely, the control siRNA had no such effect (Figure 5A). Silencing the MMP-3 gene also significantly decreased IL-1β-stimulated cell proliferation ($p < 0.01$; Figure 5A) as described previously (*9,10*). Taken together, these data suggest that IL-1β-induced DMP-1 expression depends on the expression of MMP-3 in odontoblast-like cells. Using the same culture conditions, KN-3 cells showed similar responses to the ESC-derived odontoblast-like cells (Figure 5B).

3.6. *Effect of anti-Wnt5a and -Wnt5b siRNA on IL-1β-induced DMP-1 expression and cell proliferation*

We replicated the above experiments using anti-Wnt5a and -Wnt5b siRNA. These reagents efficiently down-regulated the DMP-1 protein expression induced by IL-1β (0.25 and 2.5 ng/mL; $p < 0.01$; Figures 6A and 6B). Conversely, the control siRNA had no such effect (Figures 6A and 6B). Silencing the Wnt5 gene also significantly decreased IL-1β-stimulated cell proliferation ($p < 0.01$;

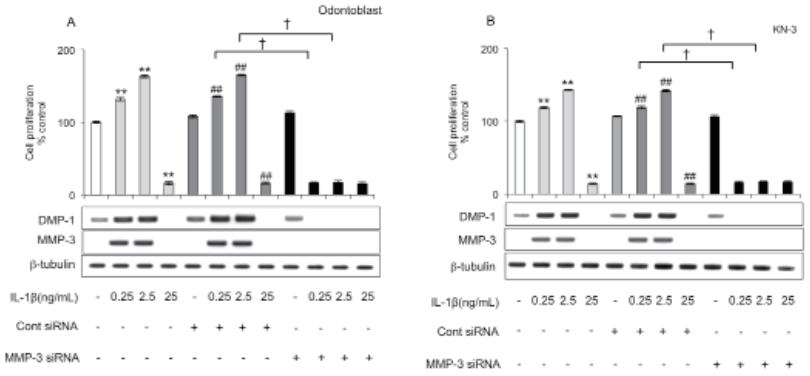

Figure 5. Effect of MMP-3 siRNA on IL-1β-induced DMP-1 expression and cell proliferation. ESC-derived odontoblast-like cells **(A)** and KN-3 cells **(B)** were transfected for 24 h with MMP-3 siRNA, stimulated with IL-1β (0, 0.25, 2.5, and 25 ng/mL), then analyzed by BrdU-cell proliferation ELISA (for cell proliferation) and western blotting (for DMP-1 and β-tubulin protein expression). $^{**}p < 0.01$ *vs*. control; $^{\#\#}p < 0.01$ *vs*. control siRNA; $^{\dagger}p < 0.01$, as indicated by the bracket.

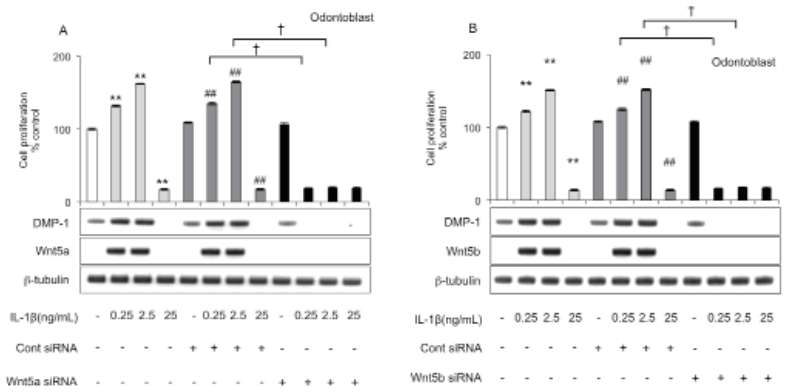

Figure 6. Effect of Wnt5a and Wnt5b siRNA on IL-1β-induced DMP-1 expression and proliferation in ESC-derived odontoblast-like cells. ESC-derived odontoblast-like cells were transfected for 24 h with Wnt5a or Wnt5b siRNA, stimulated with IL-1β (0, 0.25, 2.5, and 25 ng/mL), then analyzed by BrdU-cell proliferation ELISA (for cell proliferation) and western blotting (for DMP-1 protein expression). β-Tubulin was used as a housekeeping protein in the western blots. $^{**}p < 0.01$ *vs*. control; $^{\#\#}p < 0.01$ *vs*. control siRNA; $^{\dagger}p < 0.01$, as indicated by the bracket.

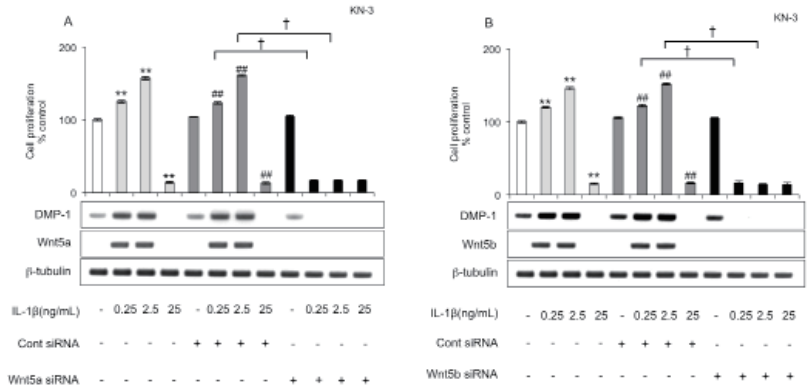

Figure 7. Effect of Wnt5a and Wnt5b siRNA on IL-1β-induced DMP-1 expression and proliferation in KN-3 cells. KN-3 cells were transfected for 24 h with Wnt5a or Wnt5b siRNA, stimulated with IL-1β (0, 0.25, 2.5, and 25 ng/mL), then analyzed by BrdU-cell proliferation ELISA (for cell proliferation) and western blotting (for DMP-1 protein expression). β-Tubulin was used as a housekeeping protein in the western blots. $^{**}p < 0.01$ *vs*. control; $^{\#\#}p < 0.01$ *vs*. control siRNA; $^{\dagger}p < 0.01$, as indicated by the bracket.

Figures 6A and 6B). Taken together, these data suggest that IL-1β-induced DMP-1 expression depends on the expression of Wnt5 in odontoblast-like cells. Using the same culture conditions, KN-3 cells showed similar responses to the ESC-derived odontoblast-like cells ($p < 0.01$; Figures 7A and 7B).

In line with our previous report (*29*), we examined the sequential order in which Wnt5, MMP-3 and DMP-1 are expressed in odontoblast-like cells using western blot analysis and siRNA silencing. This signaling cascade appeared to be IL-1β→Wnt5→MMP-3→DMP-1→DMP-1 degradation products by MMP-3, and intimately involved in the cell proliferation of ESC-derived odontoblast-like cells (Figure 8).

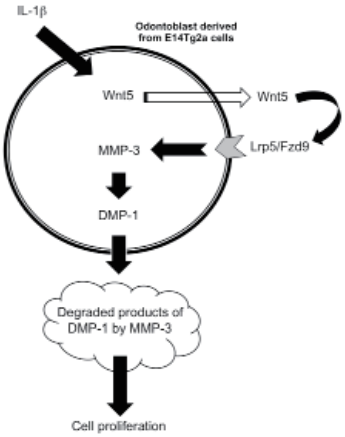

Figure 8. Schematic illustrating the putative signaling pathway by which IL-1β stimulates MMP-3 activity to induce cell proliferation in ESC-derived odontoblast-like cells.

4. Discussion

We have demonstrated previously that the proinflammatory cytokine IL-1β induces MMP-3-regulated cell proliferation in odontoblast-like cells and in KN-3 cells (*9,10*). While recent reports demonstrate that IL-1β-induced MMP-3 is associated with the secreted glycoprotein Wnt signaling pathway (*30,31*), we also confirmed that Wnt5a and Wnt5b are associated with IL-1β-induced proliferation in odontoblast-like cells derived from mouse ESCs (*16*). However, the mechanistic basis and signal cascade, especially downstream of MMP-3 for this action, is unknown.

The monoclonal anti-α2 integrin antibody is known to potently suppress the expression of odontoblastic markers in these culture systems. We have previously confirmed that α2 integrin expression in ESCs triggered their differentiation into odontoblast-like cells (*12*). The proportion of α2 integrin-positive cells in the total population of differentiated odontoblast-like cells is a measure of the purity of the E14Tg2a-derived odontoblast-like cell preparation. Fluorescence-activated cell sorting analysis estimated the proportion of these cells to be 98.77 ± 2.24% (n = 3). In the present study, IL-1β-induced MMP-3 was found to stimulate the degradation of dentin matrix proteins, such as DMP-1, resulting in up-regulation of odontoblast-like cell proliferation by the degraded products. Interestingly, DMP-1 expression was dependent on IL-1β-induced MMP-3 in the odontoblast-like cells. It is therefore conceivable that compensatory increases in DMP-1 production by the odontoblast-like cells, as the counter partner, may occur in some stages during the progression of inflammation (within the microenvironment). Although it is unclear how IL-1β-induced MMP-3 regulates odontoblast-like cell proliferation and which molecular pathways in detail are involved in upregulation of MMP-3 upon exposure to IL-1β, we believe that the mechanism of IL-1β-induced cell proliferation is clearly different from intrinsic cell growth and DMP-1 production. This observation may represent a novel physiological function of MMP-3 and be physiologically relevant in counteracting the effects of local inflammation. Although DMP-1 has previously been reported to enhance cell attachment and migration (*32*), there are no reports on the effect of DMP-1 on cell proliferation, as shown in the current study.

In addition, we found a significant increase of IL-1β-induced MMP-3 in the cells. To extend and invade into dentin containing dentin matrix proteins, it is natural that odontoblasts have to secrete the destructive enzyme MMP-3. We demonstrated that IL-1β-induced MMP-3 could degrade DMP-1, but not the osteoblastic markers osteocalcin and osteopontin (Figure 2). Furthermore, the DMP-1 degradation products caused enhanced cell proliferation in odontoblasts, which may lead to the formation of dentin. We also confirmed that DMP-1 had no effect on cell proliferation in odontoblast-like cells (Figure 3). Although this mechanism is contradictory, an effective and novel autoregulation system for dentin metabolism within a closed microenvironment site, for example at sites of inflammation, is important for cell proliferation.

Our previous report demonstrates that this signaling cascade appears to be IL-1β→Wnt5→Lrp5/Fzd9→MMP-3, and is intimately involved in cell proliferation in stem cell-derived odontoblast-like cells (*33*). Combined with current evidence, we have demonstrated the signal cascade as follows: IL-1β→Wnt5→MMP-3→DMP-1→DMP-1 degradation products by MMP-3→cell proliferation (depicted in Figure 8). Odontoblasts produce and secrete dentin matrix proteins, including DMP-1, and are therefore surrounded by their products (*34*). DMP-1 is proteolytically processed into N- and C-terminal fragments in the dentin ECM and has been identified as a high-molecular-weight proteoglycan comprising the N-terminal DMP-1 fragment and chondroitin sulfate (*34*). Interestingly, because treatment with IL-1β results in the potent induction of DMP-1 protein, this production also may contribute to regeneration and wound healing. In addition to their dentin-secretory activity, odontoblasts play a role in defensive mechanisms and the stimulation of inflammatory responses against pathogen invasion through dentinal tubules (*34*). Although we identified a novel physiological function in mouse odontoblast-like cells in the current study, it remains to be elucidated whether a similar physiological function of human odontoblasts plays an important part against the inflammatory state. Because we have established conditions for the efficient conversion of human muscle stem cells to an odontoblast lineage (*35*), we will next examine these concerns.

Although we tried to identify the peptide sequences with proliferative action derived from DMP-1 by MMP-

3, we could not determine anything specific because of the numerous degradation products derived from this protein. We will therefore attempt to identify the peptide sequence(s) with proliferative action in the near future. When activated MMP-3 and recombinant DMP-1 were incubated at 37°C, mature DMP-1 (57 kDa) decreased time-dependently, while the degradation product of DMP-1 (27 kDa) appeared for up to 2 h. We therefore speculated that this degradation product of DMP-1 contributed to the cell proliferation of odontoblast-like cells (Figure 2B). Because DMP-1 belongs to the SIBLING family (*36*), it is speculated that the RGD sequence may be essential for cell proliferation. Dentin sialophosphoprotein (DSPP) and DMP-1 share many similarities in both their gene and protein structures, and it is now believed that DSPP arose from DMP-1 by a gene duplication event (*37*). DSPP and DMP-1 are both cleaved into two protein chains; the N-terminal regions are proteoglycans that contain chondroitin sulfate chains, and the C-terminal regions are highly phosphorylated (*38-40*). Because it is now obviously accepted that DSPP and DMP-1 play important roles in hard tissue development, DSPP and DMP-1 are positive regulators of hard tissue mineralization, with both acting on dentin. From preliminary studies, we have confirmed that IL-1β-induced DSPP elicits similar responses in odontoblast-like cells (data not shown), suggesting that the common mechanism between DMP-1 and DSPP may promote the proliferative effect on odontoblasts. The signal cascade, especially the downstream DMP-1 degradation products by MMP-3, remains to be elucidated.

A blocking experiment was carried out using polyclonal antibodies, which showed inhibition of cell proliferation (Figure 4). Because the polyclonal antibodies recognized every open region conformation and did not react with the closed region of DMP-1, one question that arises from this experiment is why intact DMP-1 had no proliferation activity (Figures 3C and 3D), which remains to be elucidated. Another concern of the present study is that IL-1β-induced MMPs, except for MMP-3, are required for cell proliferation. A peptide generated through the proteolytic processing of DMP-1 by MMP-2 can regulate the differentiation of mesenchymal cells during dentinogenesis and thus sustain reparative dentin formation in pathological situations, such as carious decay (*41*). However, we confirmed that there was no significant increase in MMP-2 mRNA in response to IL-1β-induced odontoblast-like cells derived from ESCs and KN-3 cells (data not shown).

In summary, increased MMP-3 activity may contribute not only as a primary initiating trigger for the destruction for bone matrix components, but also as a compensatory response owing to the degradation of dentin matrix protein, thus promoting cell proliferation, leading to formation of dentin. We have demonstrated that DMP-1 responds to IL-1β by up-regulating MMP-3 expression *via* the Wnt5 signaling pathway in mouse ESC-derived odontoblast-like cells. These results provide new insights into the role of MMP-3 in odontoblast cells, and may have relevance to our understanding of and ability to improve wound healing following dental pulp injury.

Acknowledgements

This work was supported by a Grant-in-Aid-for Scientific Research (A) (Grant No. 25253101; to SY), a Grant-in-Aid-for Scientific Research (C) (Grant No. 26462904; to NO) and a Grant-in-Aid-for Young Scientists (B) (Grant No. 15K20418; to NH) from the Ministry of Education, Culture, Sports, Science and Technology of Japan.

References

1. Paula-Silva FW, da Silva LA, Kapila YL. Matrix metalloproteinase expression in teeth with apical periodontitis is differentially modulated by the modality of root canal treatment. J Endod. 2010; 36:231-237.
2. Tseng WY, Huang YS, Chiang NY, Chou YP, Wu YJ, Luo SF, Kuo CF, Lin KM, Lin HH. Increased soluble CD4 in serum of rheumatoid arthritis patients is generated by matrix metalloproteinase (MMP)-like proteinases. PLoS One. 2013; 8:e63963.
3. Nagase H, Woessner JF, Jr. Matrix metalloproteinases. J Biol Chem. 1999; 274:21491-21494.
4. Westermarck J, Kahari VM. Regulation of matrix metalloproteinase expression in tumor invasion. FASEB J. 1999; 13:781-792.
5. Eba H, Murasawa Y, Iohara K, Isogai Z, Nakamura H, Nakamura H, Nakashima M. The anti-inflammatory effects of matrix metalloproteinase-3 on irreversible pulpitis of mature erupted teeth. PLoS One. 2012; 7:e52523.
6. Zheng L, Amano K, Iohara K, Ito M, Imabayashi K, Into T, Matsushita K, Nakamura H, Nakashima M. Matrix metalloproteinase-3 accelerates wound healing following dental pulp injury. Am J Pathol. 2009; 175:1905-1914.
7. Wisithphrom K, Windsor LJ. The effects of tumor necrosis factor-alpha, interleukin-1beta, interleukin-6, and transforming growth factor-beta1 on pulp fibroblast mediated collagen degradation. J Endod. 2006; 32:853-861.
8. Tani-Ishii N, Wang CY, Stashenko P. Immunolocalization of bone-resorptive cytokines in rat pulp and periapical lesions following surgical pulp exposure. Oral Microbiol Immunol. 1995; 10:213-219.
9. Hiyama T, Ozeki N, Mogi M, Yamaguchi H, Kawai R, Nakata K, Kondo A, Nakamura H. Matrix metalloproteinase-3 in odontoblastic cells derived from ips cells: Unique proliferation response as odontoblastic cells derived from ES cells. PLoS One. 2013; 8:e83563.
10. Ozeki N, Yamaguchi H, Kawai R, Hiyama T, Nakata K, Mogi M, Nakamura H. Cytokines induce MMP-3-regulated proliferation of embryonic stem cell-derived odontoblast-like cells. Oral Dis. 2014; 20:505-513.
11. Ozeki N, Mogi M, Kawai R, Yamaguchi H, Hiyama T, Nakata K, Nakamura H. Mouse-induced pluripotent

stem cells differentiate into odontoblast-like cells with induction of altered adhesive and migratory phenotype of integrin. PLoS One. 2013; 8:e80026.
12. Kawai R, Ozeki N, Yamaguchi H, Tanaka T, Nakata K, Mogi M, Nakamura H. Mouse ES cells have a potential to differentiate into odontoblast-like cells using hanging drop method. Oral Dis. 2014; 20:395-403.
13. Ozeki N, Yamaguchi H, Hiyama T, Kawai R, Nakata K, Mogi M, Nakamura H. IL-1beta-induced matrix metalloproteinase-3 regulates cell proliferation in rat dental pulp cells. Oral Dis. 2015; 21:97-105.
14. Yamaguchi H, Ozeki N, Kawai R, Tanaka T, Hiyama T, Nakata K, Mogi M, Nakamura H. Proinflammatory cytokines induce stromelysin-1-mediated cell proliferation in dental pulp fibroblast-like cells. J Endod. 2014; 40:89-94.
15. Koizumi Y, Kawashima N, Yamamoto M, Takimoto K, Zhou M, Suzuki N, Saito M, Harada H, Suda H. Wnt11 expression in rat dental pulp and promotional effects of Wnt signaling on odontoblast differentiation. Congenit Anom (Kyoto). 2013; 53:101-108.
16. Ozeki N, Hase N, Hiyama T, Yamaguchi H, Kawai R, Kondo A, Nakata K, Mogi M. IL-1beta-induced, matrix metalloproteinase-3-regulated proliferation of embryonic stem cell-derived odontoblastic cells is mediated by the Wnt5 signaling pathway. Exp Cell Res. 2014; 328:69-86.
17. Goldberg M, Kulkarni AB, Young M, Boskey A. Dentin: Structure, composition and mineralization. Front Biosci (Elite Ed). 2011; 3:711-735.
18. Kawasaki K, Weiss KM. SCPP gene evolution and the dental mineralization continuum. J Dent Res. 2008; 87:520-531.
19. Ravindran S, George A. Multifunctional ECM proteins in bone and teeth. Exp Cell Res. 2014; 325:148-154.
20. Narayanan K, Gajjeraman S, Ramachandran A, Hao J, George A. Dentin matrix protein 1 regulates dentin sialophosphoprotein gene transcription during early odontoblast differentiation. J Biol Chem. 2006; 281:19064-19071.
21. Narayanan K, Ramachandran A, Hao J, He G, Park KW, Cho M, George A. Dual functional roles of dentin matrix protein 1. Implications in biomineralization and gene transcription by activation of intracellular Ca2+ store. J Biol Chem. 2003; 278:17500-17508.
22. Hooper M, Hardy K, Handyside A, Hunter S, Monk M. HPRT-deficient (Lesch-Nyhan) mouse embryos derived from germline colonization by cultured cells. Nature. 1987; 326:292-295.
23. Kawaguchi J, Mee PJ, Smith AG. Osteogenic and chondrogenic differentiation of embryonic stem cells in response to specific growth factors. Bone. 2005; 36:758-769.
24. Noguchi F, Kitamura C, Nagayoshi M, Chen KK, Terashita M, Nishihara T. Ozonated water improves lipopolysaccharide-induced responses of an odontoblast-like cell line. J Endod. 2009; 35:668-672.
25. Mogi M, Togari A. Activation of caspases is required for osteoblastic differentiation. J Biol Chem. 2003; 278:47477-47482.
26. Ozeki N, Mogi M, Nakamura H, Togari A. Differential expression of the Fas-Fas ligand system on cytokine-induced apoptotic cell death in mouse osteoblastic cells. Arch Oral Biol. 2002; 47:511-517.
27. Koyama Y, Tanaka K. Endothelins stimulate the production of stromelysin-1 in cultured rat astrocytes. Biochem Biophys Res Commun. 2008; 371:659-663.
28. Candelario-Jalil E, Taheri S, Yang Y, Sood R, Grossetete M, Estrada EY, Fiebich BL, Rosenberg GA. Cyclooxygenase inhibition limits blood-brain barrier disruption following intracerebral injection of tumor necrosis factor-alpha in the rat. J Pharmacol Exp Ther. 2007; 323:488-498.
29. Ozeki N, Kawai R, Yamaguchi H, Hiyama T, Kinoshita K, Hase N, Nakata K, Kondo A, Mogi M, Nakamura H. IL-1beta-induced matrix metalloproteinase-13 is activated by a disintegrin and metalloprotease-28-regulated proliferation of human osteoblast-like cells. Exp Cell Res. 2014; 323:165-177.
30. Kessenbrock K, Dijkgraaf GJ, Lawson DA, Littlepage LE, Shahi P, Pieper U, Werb Z. A role for matrix metalloproteinases in regulating mammary stem cell function *via* the Wnt signaling pathway. Cell Stem Cell. 2013; 13:300-313.
31. Ma B, van Blitterswijk CA, Karperien M. A Wnt/beta-catenin negative feedback loop inhibits interleukin-1-induced matrix metalloproteinase expression in human articular chondrocytes. Arthritis Rheum. 2012; 64:2589-2600.
32. von Marschall Z, Fisher LW. Dentin matrix protein-1 isoforms promote differential cell attachment and migration. J Biol Chem. 2008; 283:32730-32740.
33. Ozeki N, Hase N, Hiyama T, Yamaguchi H, Kawai R, Kondo A, Nakata K, Mogi M. IL-1β-induced, matrix metalloproteinase-3-regulated proliferation of embryonic stem cell-derived odontoblastic cells is mediated by the Wnt5 signaling pathway. Exp Cell Res. 2014; 328:69-86.
34. Couve E, Osorio R, Schmachtenberg O. The amazing odontoblast: Activity, autophagy, and aging. J Dent Res. 2013; 92:765-772.
35. Ozeki N, Mogi M, Yamaguchi H, Hiyama T, Kawai R, Hase N, Nakata K, Nakamura H, Kramer RH. Differentiation of human skeletal muscle stem cells into odontoblasts is dependent on induction of alpha1 integrin expression. J Biol Chem. 2014; 289:14380-14391.
36. Fisher LW, Torchia DA, Fohr B, Young MF, Fedarko NS. Flexible structures of SIBLING proteins, bone sialoprotein, and osteopontin. Biochem Biophys Res Commun. 2001; 280:460-465.
37. Fisher LW. DMP1 and DSPP: Evidence for duplication and convergent evolution of two SIBLING proteins. Cells Tissues Organs. 2011; 194:113-118.
38. Butler WT, Bhown M, DiMuzio MT, Cothran WC, Linde A. Multiple forms of rat dentin phosphoproteins. Arch Biochem Biophys. 1983; 225:178-186.
39. Qin C, Huang B, Wygant JN, McIntyre BW, McDonald CH, Cook RG, Butler WT. A chondroitin sulfate chain attached to the bone dentin matrix protein 1 NH2-terminal fragment. J Biol Chem. 2006; 281:8034-8040.
40. Yamakoshi Y, Hu JC, Fukae M, Iwata T, Kim JW, Zhang H, Simmer JP. Porcine dentin sialoprotein is a proteoglycan with glycosaminoglycan chains containing chondroitin 6-sulfate. J Biol Chem. 2005; 280:1552-1560.
41. Chaussain C, Eapen AS, Huet E, Floris C, Ravindran S, Hao J, Menashi S, George A. MMP2-cleavage of DMP1 generates a bioactive peptide promoting differentiation of dental pulp stem/progenitor cell. Eur Cell Mater. 2009; 18:84-95.

(Received July 7, 2015; Revised August 8, 2015; Accepted August 9, 2015)

Original Article

DOI: 10.5582/bst.2015.01087

Protective effects on vascular endothelial cell in *N'*-nitro-*L*-arginine (*L*-NNA)-induced hypertensive rats from the combination of effective components of *Uncaria rhynchophylla* and *Semen Raphani*

Yunlun Li[1,*,], Wenqing Yang[2,*], Qingjun Zhu[2], Jinguo Yang[3], Zhen Wang[2]**

[1] *Affiliated Hospital of Shandong University of Traditional Chinese Medicine, Ji'nan, Shandong, China;*
[2] *Shandong University of Traditional Chinese Medicine, Ji'nan, Shandong, China;*
[3] *Shenzhen Longgang District Hospital of Traditional Chinese Medicine, Shenzhen, Guangdong, China.*

Summary **Endothelial dysfunction is closely associated with hypertension. Protection of vascular endothelial cell is the key to prevention and treatment of hypertension. *Uncaria rhynchophylla* total alkaloids and *Semen Raphani* soluble alkaloid, isolated from traditional Chinese medicine Uncaria rbyncbopbylla and *Semen Raphani* respectively, exhibit properties of anti-hypertension and protection of blood vessels. In the present study, we observed the protective effect of the combined use of *Uncaria rhynchophylla* total alkaloids and *Semen Raphani* soluble alkaloid to the vascular endothelial cell in *N'*-nitro-*L*-arginine-induced hypertensive rats and investigate the preliminary mechanism. Blood pressure was detected by non-invasive rats tail method to observe the anti-hypertension effect of drugs. Scanning electron microscopy was used to observe the integrity or shedding state of vascular endothelial cell. The amount of circulating endothelial cells and CD54 and CD62P expression on circulating endothelial cells were tested to evaluate the endothelium function. In this study, we found that the *Uncaria rhynchophylla* total alkaloids and *Semen Raphani* soluble alkaloid compatibility can effectively lower the blood pressure, improve the structural integrity of vascular endothelium, and significantly reduce the number of circulating endothelial cells. Furthermore, the mean fluorescence intensity of CD54 and CD62P expressed showed decrease after the intervention of *Uncaria rhynchophylla* total alkaloids and *Semen Raphani* soluble alkaloid compatibility. In conclusion, the combination of effective components of the *Uncaria rhynchophylla* total alkaloids and *Semen Raphani* soluble alkaloid demonstrated good antihypertension effect and vascular endothelium protective effect. The preliminary mechanism of the protective effect may attribute to relieve the overall low-grade inflammation.**

Keywords: *Uncaria rhynchophylla* total alkaloids, *Semen Raphani* soluble alkaloid, endothelial dysfunction, inflammation

1. Introduction

Hypertension is the most common cardiovascular risk factor and a major public health problem in the world. Development of hypertension was closely related to the vascular endothelial dysfunction. Endothelial dysfunction may contribute to increased systemic vascular resistance and lead to the development of hypertension. Endothelial dysfunction is commonly manifested as impaired endothelium dependent vasodilation due to an imbalance between vasoconstrictors and vasodilators (*1*). Thus, improving vascular endothelial dysfunction plays an important role in hypertension treatment.

In recent years, hypertension was considered to be a low-grade inflammatory disease (*2*), and vascular endothelial is the key part. When vascular endothelial damage, the activation of endothelial cells can secrete proinflammatory cytokines such as interleukin-6 (IL-6), interleukin-1 beta (IL-1β), and tumor necrosis factor

*These authors contributed equally to this works.
***Address correspondence to:*
Dr. Yunlun Li, Affiliated Hospital of Shandong University of Traditional Chinese Medicine, Ji'nan 250011, Shandong, China.
E-mail: yunlun.lee@hotmail.com

alpha (TNF-α) and also express the immunoglobulin superfamily cell adhesion molecules and selection family. These cytokines facilitate the adhesion of neutrophils and monocytes to endothelium affecting production of endothelium-derived nitric oxide (NO), impairing endothelial dependent vasodilation function, inducing inflammatory damage of vascular walls (*3*). Therefore, it is a key factor to lower blood pressure that secretion of inflammatory substances was regulate.

Although drugs and changing life styles have been widely promoted to control the hypertension, unfortunately, the prevention of the progression of vascular damage in hypertension patients remains pessimistic. Traditional Chinese medicine (TCM) provides a potential option to the treatment of hypertension. From the 1950s, Chinese physicians have been concentrating on effective prevention and cure for hypertension using TCM, and considerable progress has been achieved (*4*). Many TCMs and their active components have been reported to have anti-hypertension effects.

Syndrome differentiation is a diagnostic and treatment method used in TCM. It plays an important role in the therapeutic process and affects the therapeutic result of hypertension. Some scholars have found that yang hyperactivity was the most common excessive syndrome elements of hypertension (*5*). Hyperactivity of liver yang is characterized by vertigo, tinnitus, headache, flushing, red eyes, irritability, insomnia, lassitude in lion and legs, bitter mouth, red tongue, and wiry pulse. Our previous studies showed that hyperactivity of liver yang might be related to the fifteen compounds of the structure and metabolic pathways mainly including amino acids, free fatty acids, and sphingosine by high performance liquid chromatography coupled with time of flight mass spectrometry (HPLC-TOFMS) (*6*). Usually, calming the liver wind and liver Yang is an important treatment method.

Uncaria rhynchophylla Miq Jacks (Gouteng in Chinese) belongs to the family of Rubiaceae. Currently, *Uncaria rhynchophylla* is generally used to treat ailments in the cardiovascular and central nervous systems, such as lightheadedness, convulsions, numbness, and hypertension, *etc.* (*7,8*). The effective component of *Uncaria rhynchophylla* is *Uncaria rhynchophylla* total alkaloids. Our previous study had proved that *Uncaria rhynchophylla* total alkaloids had the pharmacological effects of lowering blood pressure, protecting vascular endothelium, inhibiting cell aging and improving the thoracic aorta wall reconstruction (*9-11*). *Semen Raphani* (Laifuzi in Chinese) belongs to the family of Brassicaceae and *Semen Raphani* soluble alkaloid is the main effective ingredient. Several researches indicated that *Semen Raphani* soluble alkaloid can had prominent function to lower the hypotension, improve the process of cardiovascular remodeling and protect target *via* antioxidation (*12,13*).

Uncaria rhynchophylla combined with *Semen Raphani* is widely used in clinics for hyperactivity of liver yang in hypertensive treatment in the Hospital of Shandong University of Traditional Chinese Medicine. The classical prescription can effectively reduce blood pressure in hypertensive patients. We speculate that *Uncaria rhynchophylla* combined with Semen Raphan should exhibit protective effects of vascular endothelial cells. Thus, in the present study, we investigated the protective effects of *Uncaria rhynchophylla* total alkaloids and *Semen Raphani* soluble alkaloid against vascular endothelial dysfunction in hypertensive rats induced by *N'*-nitro-*L*-arginine (*L*-NNA). Furthermore, the underlying mechanisms for *Uncaria rhynchophylla* total alkaloids and *Semen Raphani* soluble alkaloid-induced protective effects were investigated. Valsartan was purchased from Beijing Novartis Pharmaceutical Co., Ltd. (Beijing, China).

2. Materials and Methods

2.1. *Materials*

L-NNA was purchased from sigma (St. Louis, MO, USA). Anti-Rat CD54 PerCP-eFluor 710 and Anti-Rat CD3PE were purchased from eBioscience (San Diego, California, USA). CD31 FITC and rabbit monoclonal antibody to CD146 were purchased from Abcam (London, UK). CD62P PerCP was purchased from Santa Cruz Biotechnology (Santa Cruz, CA, USA). *Uncaria rhynchophylla* and *Semen Raphani* were purchased from Jianlian Traditional Chinese medicine Store (Jinan, China).

2.2. *Preparation of drugs*

Acid dyes staining method was utilized to determine the content of *Uncaria rhynchophylla* total alkaloids, and high performance liquid chromatography (HPLC) method was adopted to establish the fingerprint. The HPLC method was also applied to ensure that the contents of rhynchophylline accounted for more than 5.5% in *Uncaria rhynchophylla* total alkaloids and of sinapine cyanide sulfonate accounted for more than 40% in *Semen Raphani* soluble alkaloid. *Uncaria rhynchophylla* total alkaloids and *Semen Raphani* soluble alkaloid were provided by professor Honglei Zhou (Shandong University of Traditional Chinese Medicine). According to the result of multiple regression analysis and partial least-squares regression, we had proved that the optimal ratio of the two components in lowering blood pressure was 5/6 (*14*).

Then the mixture was dissolved in physiological saline and prepared into three suspensions, which contained the *Uncaria rhynchophylla* total alkaloids with concentration of 3.853mg/mL + the *Semen*

Raphani soluble alkaloid with concentration of 4.623 mg/mL, the *Uncaria rhynchophylla* total alkaloids with concentration of 3.853mg/mL and the *Semen Raphani* soluble alkaloid with concentration of 4.623 mg/mL. Valsartan dissolved in physiological saline to a concentration of 1.335 mg/mL and kept at 4°C. The suspensions were stored at 4°C before use.

2.3. *Modeling and grouping*

One hundred and twenty male Wistar Kyoto rats (WKY), SPF level, 5-week-old, 165-212 g, were purchased from Shandong Lukang Pharmaceutical Co., Ltd. (certificate: SCXL (Lu) 20080002). The animals were taken care under standard conditions (12 h light/dark cycle, ventilated, fixed temperature and humidity room). Rats were provided standard rat pellet food for nourishment and tap water as drinking water. All animal experiments were performed in accordance with the guidelines of Shandong University of Traditional Chinese Medicine for the care and use of laboratory animals and approved by the Animal Ethics Review Committee of Shandong University of Traditional Chinese Medicine.

One hundred and twenty rats were randomly divided into 2 groups, namely, the normal control group (n = 20), model group (n = 100). The modeling started after 7-day adaptive feeding. The model group was induced by intraperitoneal injection of *L*-NNA at a dose of 7.625 mg/kg·d, while the normal control group was injected the same volume of physiological saline. Blood pressure began to increase in the first modeling week. The injection lasted 2 weeks and formed stability hypertension, indicating successful modeling.

Rats proven to be hypertension (n = 100) were randomly assigned to five groups with 20 rats in each group: model group, valsartan group, *Uncaria rhynchophylla* total alkaloids group (U group), *Semen Raphani* soluble alkaloids (R group) and *Uncaria rhynchophylla* total alkaloids + *Semen Raphani* soluble alkaloid group (U-R group). And 20 Wistar Kyoto rats were recruited as the normal control group. Intragastric administration was performed once a day for each treatment group. The dosages of suspensions were calculated according to the body surface area of human and rat. The Valsartan was intragastrically administered at a dose of 2.67 mg/200g (prescription/body weight). The doses of *Uncaria rhynchophylla* total alkaloids, *Semen Raphani* soluble alkaloids and *Uncaria rhynchophylla* total alkaloids + *Semen Raphani* soluble alkaloid groups were 7.705 mg/200 g, 9.246 mg/200 g and (7.705 mg + 9.246 mg)/200 g (prescription/body weight) respectively. The normal control group and model group were intragastrically administrated by physiological saline at the equivalent dose. Every group was given suspensions for 6 days per week and 5 weeks in a row.

2.4. *Detection of blood pressure of tail artery*

Systolic blood pressure (SBP), diastolic blood pressure (DBP) and mean arterial blood pressure (MAP) were detected by a tail-cuff sphygmomanometer with an automated system photoelectric sensor (ALC-Non-Invasive Blood Pressure System, Shanghai Alcott Biotech Co., Ltd., Shanghai, China). Rats were heated to dilate rat-tail artery for blood pressure measurements. All rats were measured 3 times in parallel, and data was collected as a mean.

2.5. *Observation of rat vascular endothelial morphological*

Following 24 h fasting, rats were anesthetized by intraperitoneal injection of sodium pentobarbital (60 mg/kg). After drawing blood, the thoracic aorta, renal artery and mesenteric artery were gently separated as fast as possible, cleaned of connective tissue and flushed by saline. Samples were fixed in the 2.5% glutaraldehyde solution for 24 h. Scanning electron microscopy was used to observe the integrity or shedding state of vascular endothelial cell.

2.6. *Measurement of the number of circulating endothelial cells*

Peripheral blood was sampled at different time points: before modeling, the 1st, the 3rd and the 5th weekend after administration. The number of circulating endothelial cells (CECs) was measured by indirect FACS-fluorescence labeled antibody by flow cytometry (Shanghai, Chain). The percentage of mononuclear cells in white blood cells (WBC) (M1) was detected by flow cytometry. And then detected by flow cytometry the percentage of $CD3^-CD31^+CD62P^+$ cells in the mononuclear cells (M2). The results of M1 multiplied M2 were the circulating endothelial cells accounted leukocyte percentage (M). The absolute value of WBC was counted with hemocytometer under microscopy (N1). The results of M multiplied N1 were the circulating endothelial cell number (N = M × N1).

2.7. *Detection of circulating endothelial cells CD54 and CD62P expression*

FACS combined with fluorescently labeled antibodies indirect detection method was used to detect the mean fluorescence intensity of CD54 and CD62P on $CD3^-CD31^+$cell.

2.8. *Statistical analysis*

All the data was processed with SPSS 15.0 software (SPSS Inc., USA). The results were expressed as means ± SEM. The multi-group comparisons used one-way

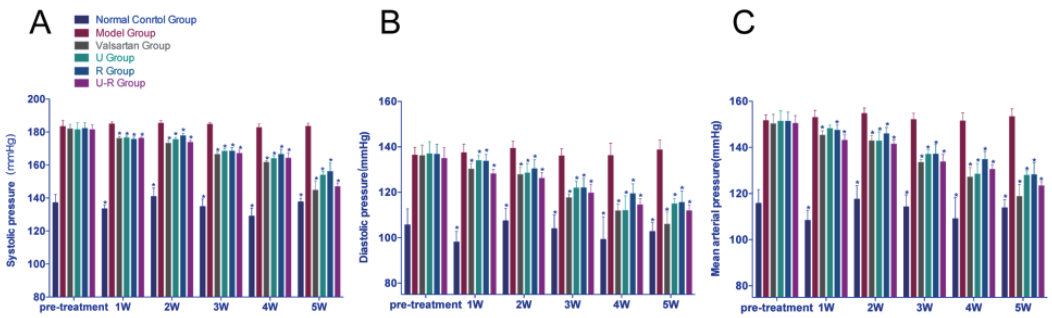

Figure 1. The changes of blood pressure in different groups. Systolic pressure **(A)**, diastolic pressure **(B)** and mean arterial pressure **(C)** of rats kept decreasing gradually during the 5-week-study in Valsartan group, *Uncaria rhynchophylla* total alkaloids group (U group), *Semen Raphani* soluble alkaloids group (R group), and *Uncaria rhynchophylla* total alkaloids + *Semen Raphani* soluble alkaloid group (U-R group), while model group have no significant changes. Significant difference ($p < 0.05$) due to comparing with model group is denoted by asterisk (*).

analysis of variance (ANOVA). A p value < 0.05 was considered statistically significant.

3. Results

3.1. *The changes of blood pressure in different groups*

Baseline SBP, DBP and MAP were similar in the six experimental groups ($p > 0.05$). The blood pressure of rats in the Valsartan group, U group, R group and U-R group were decreased significantly compared to the model group($p < 0.05$) (Figure 1A). DBP and MAP decreased in different extent after administration, but the effect was not as obvious as SBP (Figures 1B and 1C). From the perspective of lowering the blood pressure, the antihypertensive effect of *Uncaria rhynchophylla* total alkaloids and *Semen Raphani* soluble alkaloid compatibility was similar with that of valsartan ($p < 0.05$). When treated with *Uncaria rhynchophylla* total alkaloids, *Semen Raphani* soluble alkaloid and combination of the two, respectively, the blood pressure decreased at different degrees, however, the combination of the two demonstrated the most powerful effect on decreasing the blood pressure. This indicates the *Uncaria rhynchophylla* total alkaloids and *Semen Raphani* soluble alkaloid compatibility have an additive effect.

3.2. *Improve the morphology of vascular endothelial cells*

Endothelial morphology of thoracic aorta, renal artery and mesenteric artery were observed with scanning electron microscopy. The endothelial cells of rats in normal control group were showed neat cord blood vessels, completely connecting and mucosal smoothing endothelial cells, without significant fiber plaques adhesion on cell surface. In contrast, the model group had significantly shedding endothelial cells that gathered into a group. The disordered cable, loss of connections between cells that resulted in voids or

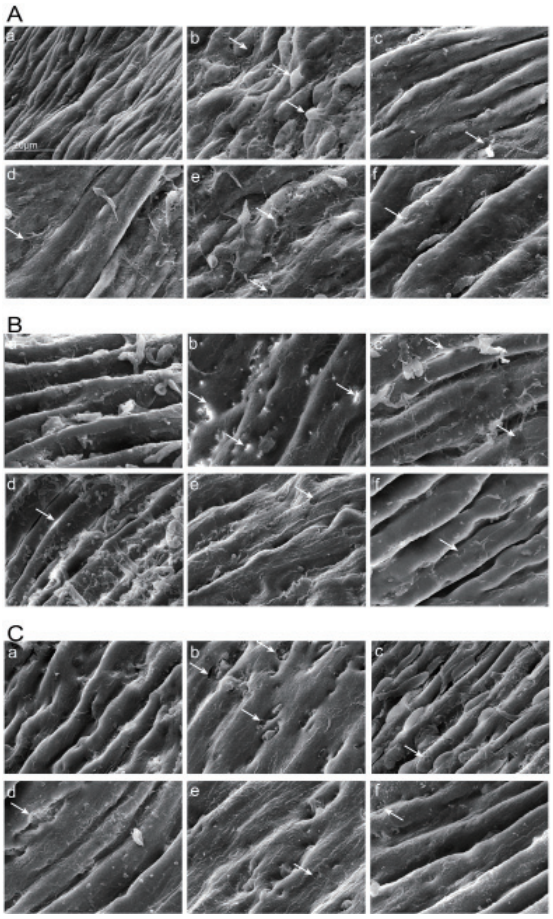

Figure 2. Endothelial morphology of thoracic aorta (A), renal artery (B) and mesenteric artery (C) were observed by scanning electron microscope after 5 weeks of drug treatment. a: normal control group; **b:** model group; **c:** valsartan group; **d:** U group; **e:** R group; **f:** U-R group. The arrows point to the endothelial damage and the change of endothelial morphology.

"honeycomb" shape endometrium was also observed by electron microscopy. Endometrial attachments were increased simultaneously. Injury of thoracic aorta was most, while mesenteric artery injury the degree lightest. After treatment, the rats endometrial integrity and shedding state of endothelial cells were significantly

improved which corresponded to the flow cytometry results. The improved effects of *Uncaria rhynchophylla* total alkaloids and *Semen Raphani* soluble alkaloid compatibility were better than single active fraction (Figure 2).

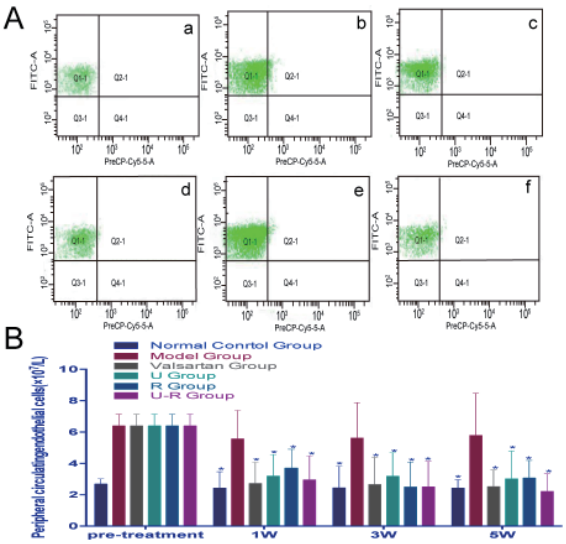

Figure 3. The number of CECs. $CD3^{-}CD31^{+}CD62P^{+}$ identifies the shedding number of circulating endothelial cells by flow cytometry. Figure 3A shows the CECs flow diagram of each group after 5 weeks of administration. Figure 3B shows the changes of CECs number in each group. Significant difference ($p < 0.05$) due to comparing with model group is denoted by asterisk (*). **a:** normal control group; **b:** model group; **c:** valsartan group; **d:** U group; **e:** R group; **f:** U-R group.

3.3. *The amount of CECs*

After treatment for 1, 3, 5 weeks, the number of CECs were detected. As shown in Figure 3, the number of CECs in model group was significantly increased compared to the control group ($p < 0.05$). While compared with the model group, the number of CECs in Valsartan group, U group, R group and U-R group have different extents of reduction in the administration of 1, 3, 5 weeks ($p < 0.05$). The number of CECs in U-R group was declined in early intervention and dropped 62% after administration for 5 weeks, which is better than U group and R group (decreased by 48% and 47% at 5 weeks end).

3.4. *The expression levels of CECs CD54 and CD62P*

Similar with the relationship of CECs number and blood pressure, the trend of mean fluorescence intensity of CD54 and CD62P was positively correlated with blood pressure. As shown in Figure 4, compared with the normal group, the mean fluorescence intensity of CD54 and CD62P in model group was significantly increased ($p < 0.05$). After treatment, with the reduction in blood pressure, the treatment group rats mean fluorescence intensity of CD54 and CD62P expressed with different degree of reduction ($p < 0.05$). We have observed CD62P expression on CECs continued to fall in U-R group (decreased by 30% at 5 week end), while the efficacy of U group and R group was not stable. Treated with drugs, CD54 expression on CECs has improved different degrees over the 5 weeks. U-R group showed

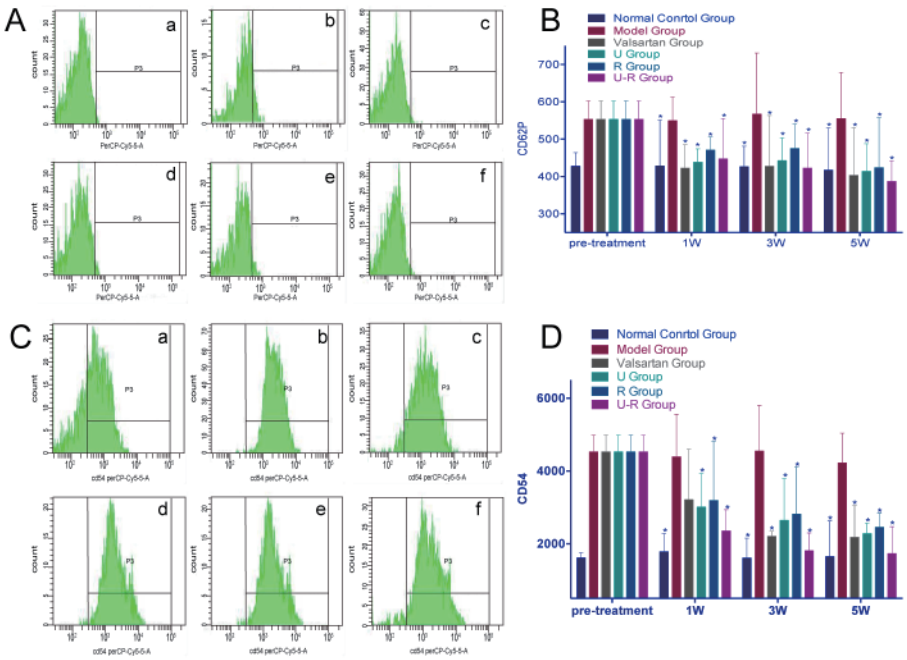

Figure 4. The expression levels of CECs CD54 and CD62P. 4A and **4C** show the CD54 and CD62P flow diagram of each group after 5 weeks of administration. **4B** and **4D** demonstrate the changes of the mean fluorescence intensity of CD54 and CD62P in each group. Significant difference ($p < 0.05$) due to comparing with model group is denoted by asterisk (*). **a:** normal control group; **b:** model group; **c:** valsartan group; **d:** U group; **e:** R group; **f:** U-R group.

the best efficacy, because of the decreased by 59% at the end 5 week.

4. Discussion

In this study, we have found that *Uncaria rhynchophylla* total alkaloids and *Semen Raphani* soluble alkaloid compatibility has efficacy on antihypertensive function and protection on vascular endothelial cells. Specifically, we have demonstrated protection vascular endothelial in three ways. First, the compatibility can significantly improve the endometrial integrity and shedding state of endothelial cells. Second, *Uncaria rhynchophylla* total alkaloids and *Semen Raphani* soluble alkaloid compatibility can reduce the number of CECs. Finally, the compatibility can decrease the expression of CD54 and CD62P on CECs.

The combination of *Uncaria rhynchophylla* and *Semen Raphani* contains complex chemical compositions and has the characteristics of multi-component, multi-level, multi-target and multi-metabolic pathways, resulting in difficulty to clarify the mechanism of action. In order to solve this problem, we use technology of composition compatibilities of traditional Chinese medicinals that persist syndrome differentiation and have the advantage of controllable compositions, clear targets and explicit mechanism. So, we extracted the effective components of *Uncaria rhynchophylla* and *Semen Raphani* (*Uncaria rhynchophylla* total alkaloids and *Semen Raphani* soluble alkaloid). *Uncaria rhynchophylla* total alkaloids contain multiple alkaloids, such as rhynchophyline, isorhychophyline and corynantheine *etc*. The rhynchophyline and isorhychophyline are the main active ingredient. The pharmacological studies indicated that the rhynchophyline and isorhychophyline showed antihypertensive activity, antiarrhythmic, inhibition of platelet aggregation and antithrombotic (*15*). The major active compounds in *Semen Raphani* are alkaloids, glucosinolates, brassinosteroids, flavonoids and so on. *Semen Raphani* soluble alkaloid demonstrated to have antihypertensive effects. Sinapine is the major bioactive alkaloid, existing in the form of sinapine thiocyanate in *Semen Raphani* (*16*). The pharmacological functions of sinapine include antihypertensive effect, antioxidative, and neuroprotective, *etc*. (*17*).

Vascular endothelial cells are the major regulator of vascular homeostasis. The endothelium is a single cell layer that lines the luminal surface of blood vessels and is involved in regulation of vascular tone and structure. They adjust the cardiovascular system by secreting a variety of active substances. In hypertensive pathological conditions due to blood flow shear stress and flow fluctuation is too strong, the structure and function of vascular endothelial cells are changed. This became one of the initial factors of endothelial cells dysfunction (*18*). On the other hand, injury of vascular endothelial cells undermined the self-regulating system balance, namely, increasing the synthesis of ET and decreasing the synthesis and release of NO, leading to vascular tension adjustment disorder and structural changes in the vascular wall, and ultimately triggering increased blood pressure (*19*).

CECs are a novel means of assessing endothelial dysfunction, meaning that mature cells are detached from the vascular intimal layer due to a great deal of insults (*20*). CECs are a stable and sensitive marker for endothelia damage, and may serve as a clinical marker in diagnosis, monitor and curative effect evaluation. Circulating levels of CECs are increased in hypertension associated with endothelial dysfunction (*21,22*). Research suggested significantly higher CECs counts among seven patients with hypertension, when compared with 22 matched, healthy control subjects (*23*). However, the precise surface antigen(s) used to identify CECs has not been established; CD31, CD54, CD106, CD141, CD146, *etc*. have all been used to identify cells of endothelial origin (*22*). These markers were not specific to vascular endothelial cells, and actually there is no such a standard yet. CD31 is a constitutive marker expressed on endothelial cells. CD62P can be used as a molecular marker of endothelial dysfunction (*24*). Referring to the most commonly used CD molecules and considering two positive markers are highly recommended, we chosed, in this experiment, CD3-PE, CD31-FITC and CD62P-PerCP to mark CECs.

In our study, the amount of CECs of model group was much higher than that of normal group. During the 5-week study, the CECs count of each treatment group kept decreasing, especially in valsartan and U-R groups. This showed that *Uncaria rhynchophylla* total alkaloids and *Semen Raphani* soluble alkaloid compatibility could protect the vascular endothelial cells effectively and prevent vascular endothelial cells falling off.

Vascular wall inflammation reaction exists in hypertension patients, and inflammation is involved in the pathophysiological process (*25*). In the hypertensive state, vascular endothelial cells could induce secretion of a variety of inflammation-related substances, such as the immunoglobulin superfamily cell adhesion molecule-1 (ICAM-1; CD54), vascular cell adhesion molecule-1 (VCAM-1) and selectin family of P-selectin (CD62P). CD54 is the important adhesion molecule and plays an important role in both innate and adaptive immune responses. It is involved in the trans-endothelial migration of leukocytes to sites of inflammation (*26*). CD62P is also an important adhesion molecule and is stored in the α granules of platelets and the Weibel-Palade bodies of endothelial cells. CD62P mainly mediated leukocytes adhesion and activated endothelial cells, which was a direct result of adhesion between cells and matrix. Inflammation-related substances would further damage and activate endothelial cells.

The vicious cycle is created, which is prompting the development of hypertension. Therefore, improving endothelial function and inhibiting the expression of inflammation-related substances in the wall is not only the basic strategy of vascular endothelial protection, but also an important goal of antihypertensive.

In our experiment, we observed that the model group rats increased expression of CD54 and CD62P. The changes above verified elevated blood pressure could indeed increase various inflammatory substances secretion and expression. After treatment, the number of vascular endothelial cell adhesion molecule expression was significantly decreased. And *Uncaria rhynchophylla* total alkaloids and *Semen Raphani* soluble alkaloid compatibility exhibited the best efficiency, which suggested that these two components can protect vascular endothelial cells by reducing adhesion molecule expression, inhibiting leukocyte and endothelial cell adhesion and suppressing vascular wall inflammation.

5. Conclusion

The effective components of the combination of *Uncaria rhynchophylla* and *Semen Raphani* (*Uncaria rhynchophylla* total alkaloids and *Semen Raphani* soluble alkaloid) demonstrated good anti-hypertension effect and vascular endothelium protective effect. The preliminary mechanism may attribute to relieving the overall low-grade inflammation. The results also proved that composition compatibilities of traditional Chinese medicinals show potential in analysis of multi-target and multi-pathway mechanism of Chinese herbs.

Acknowledgements

This work was funded by Natural Science Foundation of China # 81072794.

References

1. Chrissobolis S, Faraci FM. The role of oxidative stress and NADPH oxidase in cerebrovascular disease. Trends Mol Med. 2008; 14:495-502.
2. Varpula M, Pulkki K, Karlsson S, Ruokonen E, Pettilä V; FINNSEPSIS Study Group. Predictive value of N-terminal pro-brain natriuretic peptide in severe sepsis and septic shock. Critical Care Medicine. 2007; 35:1277-1283.
3. Polovina MM, Potpara TS. Endothelial dysfunction in metabolic and vascular disorders. Postgrad Med. 2014; 126:38-53.
4. Xiong X, Yang X, Liu W, Chu F, Wang P, Wang J. Trends in the treatment of hypertension from the perspective of traditional chinese medicine. Evid Based Complement Alternat Med. 2013;2013:275279.
5. Wang J, Xiong XJ, Liu W. Traditional Chinese Medicine syndromes for essential hypertension: a literature analysis of 13,272 patients. Evid Based Complement Alternat Med. 2014;2014:418206.
6. Jiang HQ, Li YL, Xie J. Urine metabonomic study on hypertension patients of ascendant hyperactivity of gan yang syndrome by high performance liquid chromatography coupled with time of flight mass spectrometry. Zhongguo Zhong Xi Yi Jie He Za Zhi. 2012; 32:333-337. (in Chinese)
7. Lee JS, Kim J, Kim BY, Lee HS, Ahn JS, Chang YS. Inhibition of phospholipase cgamma1 and cancer cell proliferation by triterpene esters from *Uncaria rhynchophylla*. J Nat Prod. 2000; 63:753-756.
8. Shi JS, Yu JX, Chen XP, Xu RX. Pharmacological actions of Uncaria alkaloids, rhynchophylline and isorhynchophylline. Acta Pharmacol Sin. 2003; 24:97-101.
9. Zhang YH, Li YL, Zhao J, Hou Q. The Effect of Total Alkaloids in Rhynchophylla on β-galactosidase and Telomerase in Vascular Endothelial Cell in Spontaneous Hypertensive Rat. Shan Xi Zhong Yi. 2011; 27:44-50. (in Chinese)
10. Jiang YH, Li YL, Zhao J, Hou Q. Uncaria Alkaloids-Intervention on the Aged Endothelial Cell Induced by D Galactose. Zhongguo Dong Mai Ying Hua Za Zhi. 2011; 19:474-478. (in Chinese)
11. Sun JC, Qi DM, Zhou HL, Li YL. The influence of gouteng alkaloid on SHR aorta smooth muscle cell apoptosis and proliferation. Zhongguo Yao Li Xue Tong Bao. 2011; 27:925-928. (in Chinese)
12. Li BG, Li TY, Zhang HX, *et al*. Experimental Study of Hypotensive Effect of Soluble *Semen Raphani* Alkaloids in Spontaneous Hypertensive Rats. Changchun Zhong Yi Yao Da Xue Xue Bao. 2007; 23:7-8. (in Chinese)
13. Li TY, Li TG, Zhang GX, *et al*. Experimental Study of Hypotensive Effect of Soluble *Semen Raphani*. Shi Jie Zhong Xi Yi Jie He Za Zhi. 2007; 2:25-28. (in Chinese)
14. Jiang HQ, Nie L, Zhou HL, Li, YL. Optimization for compatibility of RamulusUncariae cum Uncie total alkaloids and *Semen Raphani* total alkaloids based on partial least-squares regression analysis. Zhong Cao Yao. 2013; 44:2531-2536. (in Chinese)
15. Ndagijimana A, Wang X, Pan G, Zhang F, Feng H, Olaleye O. A review on indole alkaloids isolated from *Uncaria rhynchophylla* and their pharmacological studies. Fitoterapia. 2013; 86:35-47.
16. Xing J, Yuan YX, Feng BM. Extraction and high performance liquid chromatographic determination of sinapine in five cruciferous plants. Journal Home of Analytical Science. 2012; 28:523-526.
17. Sham TT, Yuen ACY, Ng YF, Chan CO. Mok DKW, Chan SW. A review of the phytochemistry and pharmacological activities of raphani semen. Evid Based Complement Alternat Med. 2013;2013:636194.
18. Ercan E, Tengiz I, Ercan HE, Nalbantgil I. Left ventricular hypertrophy and endothelial functions in patients with essential hypertension. Coron Artery Dis. 2003 Dec;14:541-544.
19. Wallace SM, Yasmin, McEniery CM, Mäki-Petäjä KM, Booth AD, Cockcroft JR, Wilkinson IB. Isolated systolic hypertension is characterized by increased aortic stiffness and endothelial dysfunction. Hypertension. 2007; 50:228-233.
20. Karthikeyan VJ, Lip GY. Endothelial damage/dysfunction and hypertension in pregnancy. Frontiers in Front Biosci (Elite Ed). 2011; 3:1100-1108.
21. Boos CJ, Lane DA, Karpha M, Beevers DG, Haynes R,

Lip GY. Circulating endothelial cells, arterial stiffness, and cardiovascular risk stratification in hypertension. Chest. 2007; 132:1540-1547.
22. Burger D, Touyz RM. Cellular biomarkers of endothelial health: microparticles, endothelial progenitor cells, and circulating endothelial cells. J Am Soc Hypertens. 2012; 6:85-99.
23. Koc M, Bihorac A, Segal MS. Circulating endothelial cells as potential markers of the state of the endothelium in hemodialysis patients. Am J Kidney Dis. 2003; 42:704-712.
24. Blake GJ, Ridker PM. Novel clinical markers of vascular wall inflammation. Circ Res. 2001; 89:763-771.
25. Vardas P, Marketou M. CRP in non-dippers: new perspectives and old queries. J Hum Hypertens. 2008; 22:447-449.
26. Lawson C, Wolf S. ICAM-1 signaling in endothelial cells. PPharmacol Rep. 2009; 61:22-32.

(Received June 22, 2015; Revised August 23, 2015; Accepted August 24, 2015)

Original Article

DOI: 10.5582/bst.2015.01088

Dual regulating effect of Ningdong granule on extracellular dopamine content of two kinds of Tourette's syndrome rat models

Lin Zhao[1,*], Fanghua Qi[1,*], Feng Zhang[1], Zhixue Wang[1], Linmao Mu[1], Yuan Wang[1], Qi En[1], Jijun Li[2], Yifeng Du[3,], Anyuan Li[1,**]**

[1] *Department of Traditional Chinese Medicine, Provincial Hospital affiliated to Shandong University, Ji'nan, China;*
[2] *Shanghai Children's Medical Center affiliated to Shanghai Jiaotong University School of Medicine, Shanghai, China;*
[3] *Department of Neurology, Provincial Hospital affiliated to Shandong University, Ji'nan, China.*

Summary **Tourette's syndrome (TS) is an inherited chronic neuropsychiatric disorder characterized by involuntary stereotyped motor and phonic behaviors called tics. Its pathogenesis is still unclear and its treatment remains limited. Our previous basic and clinical studies have shown that traditional Chinese medicine (TCM) preparation Ningdong granule (NDG) is effective for the treatment of TS with little side effects. In the current study, two TS rat models (Apomorphine (Apo)- and 3,3'-iminodipropionitrile (IDPN)-induced) were used to explore the dual regulating effects and mechanisms of NDG on extracellular DA concentration. We found that NDG could regulate the extracellular DA concentration dually: it could make a gradual recovery in extracellular DA content from both an up-regulated level in Apo-induced rats and down-regulated level in IDPN-induced rats measured by high-performance liquid chromatography (HPLC). The protein expression of DA transporter (DAT) was measured by Western blot and the result showed that NDG could elevate DAT expression when DA release was up-regulated and could decrease DAT expression when extracellular DA concentration was down-regulated. The main mechanism of the dual regulating effect of NDG on extracellular DA release might be related to DAT protein expression in TS, through which the released DA is re-uptaken into nerve terminals. Taken together, compared with conventional single-target anti-tics drugs such as haloperidol (Hal), NDG with the dual regulating effect would be more significant for TS treatment.**

Keywords: Tourette's syndrome (TS), dual regulating effect, Ningdong granule (NDG), dopamine hypothesis, dopamine transporter

1. Introduction

Tourette's syndrome (TS) is an inherited chronic neuropsychiatric disorder characterized by involuntary stereotyped motor and phonic behaviors called tics. Initial symptoms of TS usually start in childhood with a peak age between 7 to 15 years old (*1*). The prevalence of this syndrome is estimated to be four to six per 1,000 children and adolescents with an incidence in males 3-9 times higher than in females (*2*). TS can cause lifelong impairment and about 5% of TS patients have life-threatening symptoms including mild self-injurious behaviors and borderline personality disorders (*3*).

Currently, the detailed etiological and pathophysiological mechanism of TS is still unclear. It is widely believed that abnormalities of dopamine (DA) neurotransmission play a primary role in the pathophysiology of TS (*4*). DA content in postmortem striatum of neurologically normal subjects increased two to three fold from birth to 9 years of age, and then gradually declined from a probable peak in late adolescence (*5*), which is concordant with the natural history of TS. DA is a

Released online in J-STAGE as advance publication August 4, 2015.

*These authors contributed equally to this works.
***Address correspondence to:*
Dr. Anyuan Li, Department of Traditional Chinese Medicine, Provincial Hospital affiliated to Shandong University, No. 324, Jingwuweiqi Road, Ji'nan 250021, Shandong, China.
E-mail: sdslyy999@163.com

Dr. Yifeng Du, Department of Neurology, Provincial Hospital affiliated to Shandong University, No. 324, Jingwuweiqi Road, Ji'nan 250021, Shandong, China.
E-mail: yifengdu5757@126.com

key monoamine neurotransmitter released by nerve terminals originating from midbrain neurons. It plays an important role in the regulation of motor and limbic functions through stimulation of DA receptors, such as movement, learning, moods, neurobehavioral abilities, problem solving, and so on (*6,7*). TS is reported to be correlated with the content and activity of DA, and the density and sensitivity of DA receptors in striatum. However, the relationship between the pathophysiology of TS and DA is far from been clearly elucidated. Interestingly, in some pathological and functional imaging studies the increased DA release in TS patients has been confirmed, while other investigations of the striatal DA content have either failed to find differences between normal controls and TS patients or have yielded contradictory results (*8-10*). Furthermore, the available dopaminergic system related TS agents, including the classical neuroleptics with D2 receptors antagonistic activity, are all considered as decreasing "the effects of DA release" in striatum, while a number of DA agonists (*e.g.*, levodopa) with the effect of promoting DA release have been shown to suppress tics (*8,11,12*). These seemingly conflicting findings suggest that, DA release, either in an increased or decreased manner, would play a role in the generation of TS (*8*).

Dopamine transporter (DAT) is a high-affinity glycoprotein localized exclusively at the presynaptic membrane of DA neurons. It is responsible for modulating extracellular DA concentration by re-uptaking the released DA into nerve terminals (*4*). In recent years, some findings using molecular, pharmacological and genetic techniques have established the importance of DAT in the maintenance of DA homeostasis, which might be an essential role for the control of normal brain function (*8*). Furthermore, the activity of DAT in regulation of DA homeostasis might underlie subsequent pathological states in TS (*4,13*). All these might provide us a new way for TS management.

Haloperidol (Hal) is approved by the Food and Drug Administration (USA) for treating TS. It can effectively inhibit the excitability of the cortical motor area through restraining the activity of DA receptors (*14*). However, a very high proportion of patients eventually refused further therapy with Hal because of the side effects including sedation, weight gain, extrapyramidal symptoms, and QT prolongation (*7*). Therefore, development of novel drugs for treatment of TS is urgently needed.

Traditional Chinese medicine (TCM) has been widely used in the treatment of various diseases such as nervous system disease, infectious diseases, and cancer, in China, Japan, South Korea and other Asian countries for thousands of years (*13,15*). Ningdong granule (NDG), a TCM preparation dedicated to treating TS with the guidance of therapeutic principles of TCM, has been used as an anti-tic agent in clinics in China for several years (*16-18*). Our previous studies showed that NDG has had a total effective rate of 73.3-83.3% in TS patients with few apparent side or toxic effects (*16,18*). Our previous studies also showed that NDG could regulate the disturbance of DA, DRD2, 5-TH and so on in animals and patients with TS (*7,14*). However, the possible pharmacological mechanism of NDG for treating TS is still unclear. Thus, in the current study, two TS rat models (Apomorphine (Apo)- and 3,3'-iminodipropionitrile (IDPN)-induced) were used to explore the regulating effects and possible mechanisms of NDG on extracellular DA concentration.

2. Materials and Methods

2.1. *Reagents*

Apomorphine (Apo), 3,3-iminodipropionitrile (IDPN) and bovine serum albumin (BSA) was purchased from Sigma-Aldrich Co. Ltd. (USA), and Haloperidol (Hal) was purchased from Shanghai Pharmaceutical Group Co. Ltd. (Shanghai, China). Primary antibody against DAT was bought from Abcam (Cambridge, MA, USA). Enhanced chemiluminescence agents (ECL) were bought from Millipore Co. (Billerica, MA, USA). Peroxidase-conjugated affini-pure goat anti-rabbit antibody IgG and anti β-actin antibody were purchased from ZSGB-BIO Inc. (Peking, China).

2.2. *NDG Preparation*

NDG was provided by 999 Modern Chinese Medicine Co. Ltd. (999 Co. Ltd., Shenzhen, China). NDG formulation includes main components (*18*): Rhizoma Gastrodiae, Codonopsis pilosula, Dwarf lilyturf tuber, Radix Paeoniae Alba, Fossil fragments, Oyster shell, and Pheretima asiatica. The proportions of these eight components in NDG granule were 2:3:2:4:5:5:2:2. After being mixed in proportion, all of them were macerated with distilled water for 1 h at room temperature, and the whole mixture was decocted twice for 30min each time. The filtrates were mixed and condensed and then dried by vacuum-drier at 60°C. The yield granule was stored at 4°C.

2.3. *Experimental Animals*

Seventy male Wistar rats (4 weeks old, 100 ± 20 g) were bought from Shandong Experimental Animal Center (Jinan, China), and were housed in an air-conditioned animal room with 12 h light/dark cycle, temperature of 22 ± 2°C and humidity of 50 ± 10%. Rats were constantly provided with a laboratory diet and water *ad libitum*.

After a week, the rats were randomly divided into control group (n = 10), Apo-induced TS model group (n = 30) and IDPN-induced TS model group (n = 30).

Rats in the Apo-induced TS model group and IDPN-induced TS model group were intraperitoneally injected (*i.p.*) with Apo (2mg/kg) and IDPN (150mg/kg, *i.p.*) respectively, while the control group received normal saline (NS) (5 mL/kg, *i.p.*). Both Apo-induced and IDPN-induced TS model groups were further divided into 3 groups, that is Apo + NS group (n = 10), Apo + NDG group (n = 10), Apo + Hal group (n = 10); IDPN + NS group (n = 10), IDPN + NDG group (n = 10), IDPN + Hal group (n = 10), and the rats were administered normal saline by gastric perfusion (0.9%) at 10 mL/kg (Control group, Apo + NS group and IDPN + NS group), NDG at 370 mg/kg (Apo + NDG group and IDPN + NDG group), and Hal at 1.0 mg/kg (Apo + Hal group and IDPN + Hal group) respectively once a day for 8 weeks (*8,14*).

All animal experimental protocols were handled in accordance with the Code of Ethics of the World Medical Association, and all research procedures were approved by medical ethics committee of Provincial Hospital Affiliated to Shandong University.

2.4. *Behavior recordings*

Stereotypy actions of rats were recorded according to the evaluating standards of stereotypic actions (*19*) (Table 1). These were conducted once a week by trained observers who were blind to the group condition. Each animal was observed for one min of every 5 min for a total of 6 observation periods. One or more episodes recorded with the grades received the corresponding score. The average scores were calculated on the basis of results from observers as the objective indicator of behavioral changes.

2.5. *Intracranial surgery*

The procedure of current section was conducted according to our previous study (*8*). In brief, for surgical implantations, the rats were anesthetized with chloral hydrate (400 mg/kg, *i.p.*) and fixed in a stereotaxic instrument. A guide cannula was implanted in striatum (AP: 0.0, ML: +2.0, DV: -7.0mm from bregma) and secured with two stainless steel skull screws and dental cement. Rats were then singly housed and allowed to recover for one day before microdialysis.

On the day of microdialysis, a polyarylene-ether-sulfone MAB/6 probe (4 mm in length, 15 kDa molecular weight cut off) was slowly lowered into the position of striatum as mentioned above and perfused at 2 μL/min using 0.9% normal saline. Before experimental sampling began, the rats were perfused with saline for 2 h to maintain equilibrium of fluid exchange. Subsequently, the dialyzate samples (20 μL) were collected every 20 min. The microdialysis samples were stored at -80°C until analyzed.

2.6. *HPLC analysis*

The dialyzate samples from the striatum were analyzed by high-performance liquid chromatography with electrochemical detection (HPLC-ECD) according to the previous reported methods (*8*). The levels of extracellular DA and HVA content in striatum were detected use this method. Compound separation was achieved on a C18 reverse-phase analytical column (50 mm × 2.1 mm, 1.9 μm particle size) with a mobile phase consisting of 150 mM citric acid, 150 mM trisodium citrate dihydrate, 100 mM ethylenediamine tetraacetic acid disodium salt (EDTA • 2Na), 1 mM sodium 1-heptanesulfonate and 10% methanol (v/v). The mobile phase was passed through the system at 0.2 mL/min, while the column was maintained at 28°C and the potential of the electrochemical detector was set at 0.8 V.

2.7. *Western blot analysis*

After the intracranial microdialysis, rats were sacrificed and striatum tissues were dissected and quickly homogenized on ice in RIPA lysis buffer (50 mM Tris-Hcl (PH 7.4), 150 mM NaCl, 1% NP-40, 0.1% sodium dodecyl sulfate (SDS)) with protease inhibitors (PMSF) and centrifuged at 12,000 rpm for 15min at 4°C. After determination by BCA protocol, the Protein amounts in the supernatant were diluted in 5× loading buffer and then boiled at 100°C for 5 min. SDS polyacrylamide gel (SDS-PAGE) electrophoresis was carried out on 10% Tris-glycine gels. The separated proteins were then electrophoretically transferred to PVDF membranes (0.45 μm) that were treated previously with methanol, and blocked with 1% BSA in TBS-T (Tris-buffered saline containing 0.1% Tween 20) for 1 hour at room

Table 1. Scales for stereotypic behaviors

Score	Stereotypic behaviors
0	Asleep, resting in place or normal activity in place
1	Increased sniffing and head raising
2	Discontinuous increased sniffing with body raising
3	Discontinuous increased sniffing, licking with head and body raising primarily in one place, with occasional rapid burst of locomotor activity (2-5 steps)
4	Continuous sniffing, biting, head bobbing and repetitive body raising/wall climbing in place
5	Continuous sniffing, biting, licking, head bobbing, and continuous body raising/wall climbing wherein forepaws do not touch cage floor

temperature. After washing in TBS-T, the membranes were incubated with primary antibody against DAT (1:1,000) overnight at 4°C, and then were further incubated with peroxidase-conjugated affini-pure goat anti-rabbit antibody IgG (1:10,000) for 1 h at room temperature. Blots were developed with enhanced chemiluminescence agents before exposure to X-ray film. To confirm equivalent loading of samples, the same membranes were incubated with anti β-actin antibody (1:1,000) and visualized *via* enhanced chemiluminescence as mentioned earlier.

2.8. *Statistical analysis*

Data were expressed as mean ± S.D. and statistical differences between groups were determined by one-way analysis of variance (ANOVA). Repeated-measure analysis of variance was used to analyze the differences of the stereotypic scores of the rats. The data were analyzed using the SPSS® statistical package, version 16.0 (SPSS Inc., Chicago, IL, USA) for Windows®. A two-tailed significance level of $p < 0.05$ was used for all statistical analyses.

3. Results

3.1. *Assessment of stereotypic behaviors*

Administrations of both Apo and IDPN could produce significant stereotypic multiple behaviors in rats ($p < 0.01$). After being treated with NDG and Hal respectively, the dyskinetic-hyperkinetic syndromes in Apo-induced rats were dramatically improved, and there were no remarkable differences between the two treatments ($p > 0.05$). Moreover, in the IDPN-induced rats, which received the same therapies as Apo-induced rats, the general tendency of stereotypic behavioral improvements in the NDG groups showed no differences compared with the Apo groups. In conclusion, both NDG and Hal could make significant improvements in stereotypic abnormalities of rats with no distinctive differences between these two treatments (Figures 1A and 1B).

3.2. *Levels of extracellular DA content in striatum*

The two pharmacological manipulations used to induce stereotypic behaviors of rats caused completely opposite effects on extracellular DA content in the striatum of the rats. There was a dramatic increase in extracellular DA content in Apo + NS group ($p < 0.01$), while in IDPN + NS group the extracellular concentration of DA was found decreased significantly ($p < 0.01$), when both were compared with the control group. Furthermore, the dual regulating effect of NDG on extracellular DA content in striatum was found in the current study. It could down-regulate elevated DA content in Apo-induced rats (Apo + NDG group) ($p < 0.05$ *vs*. Apo + NS group) while up-regulate decreased DA content in IDPN-induced rats (IDPN + NDG group) ($p < 0.01$ *vs*. IDPN + NS group) by moving them towards a normal extracellular DA level. However, in the Hal treated groups, no significant differences were found in the concentration of extracellular DA after the treatment (Apo + Hal group *vs*. Apo + NS group, $p > 0.05$; IDPN + Hal group *vs*. IDPN + NS group, $p > 0.05$) (Figures 2A and 2B).

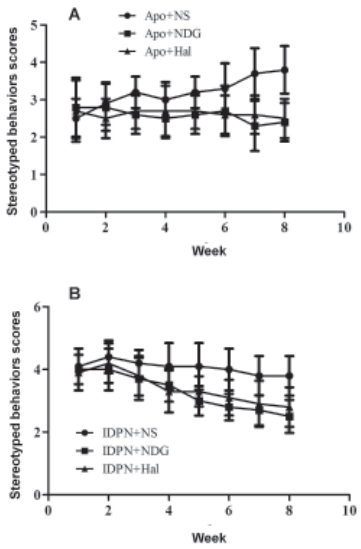

Figure 1. Stereotypic behavior of rats in the three experimental groups during an 8-week period. The data represent mean ± S.D. ($n = 10$). Administration of both Apo **(A)** and IDPN **(B)** could produce significant stereotypic multiple behaviors in rats ($p < 0.01$). The stereotypic behavior scores at baseline showed no differences among groups ($p > 0.05$). After being treated respectively with NDG and Hal, both dyskinetic-hyperkinetic syndrome scores in Apo-induced and IDPN-induced rats decreased significantly ($p < 0.01$).

3.3. *Levels of extracellular HVA content in striatum*

The effects of DNG on the extracellular HVA concentration in striatum of the rats are shown in Figure 3. Compared to the control group, neither NDG nor Hal caused any conspicuous changes in extracellular HVA content in Apo-induced rats ($p > 0.05$) (Figure 3A). Furthermore, in IDPN-induced rat groups, no significant differences were found in extracellular HVA content either, whether they were treated by NDG or by Hal ($p > 0.05$) (Figure 3B).

3.4. *DAT protein expression in striatum*

The effects of NDG on DAT protein expression in striatum of the rats were detected by *Western blot* as shown in Figure 4. Both of the pharmacological manipulations, Apo and IDPN, could significantly increase DAT protein expression in striatum compared with the control group. The treatment of NDG caused totally opposite effects on DAT protein expression in striatum: there was a dramatic decrease in DAT protein

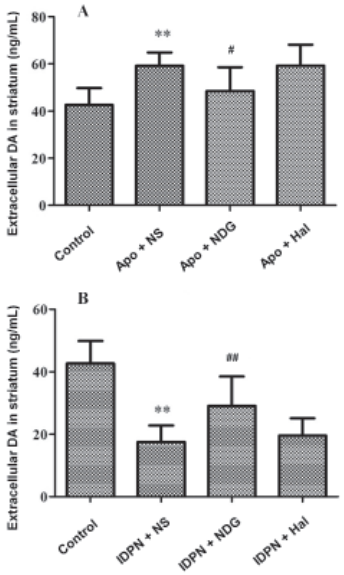

Figure 2. Levels of extracellular DA content in striatum. The data represent mean ± S.D. (n = 10). **(A)** Effects of NDG on extracellular DA content in the striatum of the Apo-induced rats. There was dramatic increase in extracellular DA content in Apo + NS group (**p < 0.01 *vs*. control group). After being treated with NDG, the content of extracellular DA decreased (#p < 0.05 *vs*. Apo + NS group). **(B)** Effects of NDG on extracellular DA content in the striatum of the IDPN-induced rats. There was a dramatic decrease in extracellular DA content in IDPN + NS group (**p < 0.01 *vs*. control group). After being treated with NDG, the content of extracellular DA increased significantly (##p < 0.01 *vs*. IDPN + NS group).

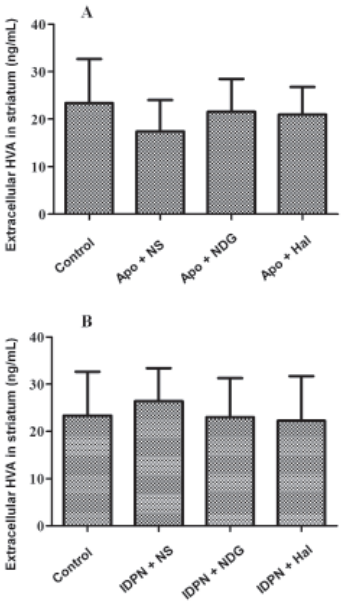

Figure 3. Levels of extracellular HVA content in striatum. The data represent mean ± S.D. (n = 10). Compared with the control group, neither NDG nor Hal made any conspicuous changes in extracellular HVA content of Apo-induced and IDPN-induced rats (p > 0.05).

expression in Apo + NDG group (p < 0.01), while in IDPN + NDG group, DAT protein expression was found elevated significantly (p < 0.01). However, in the Hal treated groups, no significant difference was found in the concentration of DAT after the treatment (Apo + Hal group *vs*. Apo + NS group, p > 0.05; IDPN + Hal group *vs*. IDPN + NS group, p > 0.05) (Figures 4A and 4B).

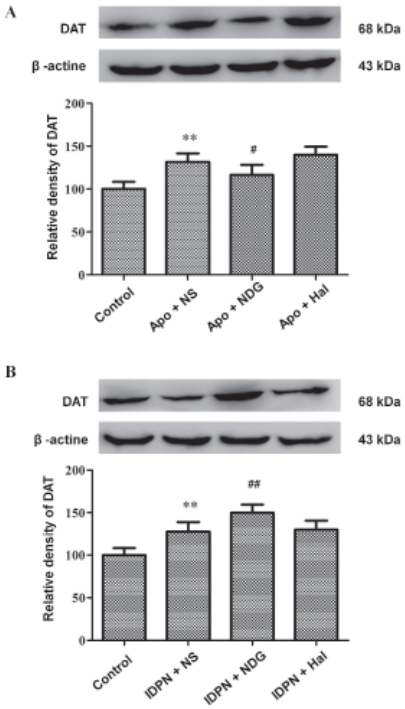

Figure 4. DAT protein expression in striatum. Both of the pharmacological manipulations, Apo and IDPN, could significantly increase DAT protein expression in striatum (**p < 0.01 *vs*. control group). The treatment of NDG caused totally opposite effects on DAT protein expression in striatum: there was a dramatic decrease in DAT protein expression in Apo + NDG group (#p < 0.05 *vs*. Apo + NS group), while in IDPN + NDG group, DAT protein expression was found elevated significantly (##p < 0.01 *vs*. IDPN + NS group). Hal made no conspicuous changes in DAT protein expression in striatum of Apo-induced and IDPN-induced rats.

4. Discussion

The TCM preparation NDG has been used as an anti-tic agent for several years in clinics in China, which mainly includes 8 Chinese herbal medicines as described in the previous section. According to TCM theory, NDG is well known to have effects on nourishing heart, soothing liver, and relieving convulsion and spasm (*16,17*). Pharmacological studies have found that NDG contains a number of active substances such as saponin (*e.g.*, gastrodin and paeoniflorin), steroid saponin, carbohydrates and their glycosides, alkaloids, organic acids, and flavonoids, which have been proved to have positive antioxidant, protect brain neurons, tranquilize and allay excitement effects (*20*). Gastrodin, as one of the main active ingredients of NDG, was previously found to have the effect of regulation of extracellular DA concentration dually in TS rats: it could make a gradual recovery in extracellular DA content from both up-regulated and down-regulated levels (*8*). We wondered if NDG also possesses a dual regulating effect on extracellular DA content in TS. Thus, in the current study, the regulating effects and possible mechanisms of

NDG on extracellular DA concentration was explored.

As is well known, TS is correlated with the content and activity of DA and the density and sensitivity of postsynaptic receptors in striatum. However, the relationship between the pathophysiology of TS and DA system has far from been clearly elucidated. Apo, a dopamine receptor D1/D2 agonist, could produce similar stereotypic behaviors including biting, licking and sniffing on rodents (*21*). IDPN has been widely used as a tool for neuropathological studies and can induce a series of neurobehavioral disturbances such as dyskinesia and repetitive motor-defects similar to the characteristics of TS (*22,23*). IDPN is also known to interfere with a range of neurotransmitters including DA (*23*). Currently, Apo and IDPN are two manipulations that are commonly used to develop TS models (*14,23,24*). Accumulating evidence suggested that both Apo and IDPN manipulated dyskinesia of TS models exhibited marked alterations in DA: rats exposed to Apo showed significantly increased DA content (*14*) while rats exposed to IDPN showed significantly decreased DA content (*23*). The TS models with different alterations in DA make it possible to investigate multiple therapeutic values of drugs on the neurotransmitter. Thus, in the current study, to investigate the regulating effect of NDG on extracellular DA content in TS, we selected these two pharmacological manipulations, Apo and IDPN, to imitate both of these pathogenic forms of the DA hypothesis.

DA is a key monoamine neurotransmitter in the brain with a regulatory role for motor and limbic functions (*7*). Lots of evidence gave us a signal that dopamine is the final common neurobiological pathway for the expression of TS symptoms (*25,26*). It is transported across the pre-synaptic neuron membranes by DAT. After reuptake by DAT, DA was transformed into HVA in neurons and released into the blood. In the present study, we found that NDG similar to Hal could effectively improve stereotypic behaviors including continuous sniffing, biting, licking, head bobbing, body climbing and so on in both Apo and IDPN induced TS rat models. We also found that NDG could help make a gradual recovery of the abnormal striatal DA content from both increased and decreased levels, while Hal caused no significant alternation of extracellular DA level in either TS rat model. These findings indicated that NDG could regulate striatal DA concentration dually in these two TS rat models, which made quite distinct effects on striatal DA content compared to Hal.

Since the pathogenesis of TS is complicated, the dual regulating effect of NDG might have superiority compared to the Hal with a single-target pharmacological mechanism. Because of the highly heterogeneous nature of the human body, such as age, gender, states, and comorbidities, there could be large differences in real pathological changes among TS patients, even though the anatomical structures and physiological functions of their bodies are nearly the same. The chief pathological alterations of some TS patients, who respond well to Hal, might be the up-regulated density and/or sensitivity of D2 receptors. However, in some other TS patients, the elevated striatal DA release might be a main aspect for the occurrence of the disorder. In this case, the ideal effect of Hal on them must be hard to achieve. Thus, with the displayed properties in normalizing the dopaminergic dysfunction caused by more than one mechanism, NDG might have a positive effect in either of them.

To further uncover the probable mechanism of the dual regulating effect of NDG on extracellular DA release, extracellular HVA content and DAT protein expression were measured. HVA is generally regarded as a main metabolite of DA in the central nervous system. DAT is a high-affinity glycoprotein localized exclusively at the presynaptic membrane of DA neurons. It plays an important role for maintaining sufficient DA levels for release into the synaptic cleft in the striatum, in other words, it is responsible for modulating extracellular DA concentration by uptake of the released DA into nerve terminals (*27,28*). Furthermore, recent studies have highlighted the primary role of DAT, not only in the regulation of the extracellular concentration of DA, but also in the homeostatic maintenance of presynaptic function (*29*). Our findings indicate that NDG could elevate DAT expression when DA release was up-regulated and decrease DAT expression when extracellular DA concentration was down-regulated, while in the extracellular concentration of HVA, the NDG treatment caused no remarkable changes. It could therefore be speculated that the main mechanism of the dual regulating effect of NDG on extracellular DA release might be related to DAT protein expression in TS. The DAT-mediated re-uptake system controls the intensity as well as the duration of dopamine actions at synaptic receptors. In addition, since the NDG treatment made no remarkable changes in the extracellular HVA content, it could therefore be speculated that the dual regulating effect of NDG on extracellular DA release might not be through the metabolic pathways. In all, DAT might be critically involved in the dopaminergic dysfunction associated with TS and might be an essential factor for the management of TS.

In conclusion, to make a significant improvement in stereotypic behavioral abnormalities of TS rats Hal is given and NDG could regulate the extracellular DA concentration dually: it could make a gradual recovery in extracellular DA content from both up-regulated and down-regulated levels, while Hal showed no conspicuous effect on the same neurotransmitter. The main mechanism of the dual regulating effect of NDG on extracellular DA release might be related to DAT protein expression in TS, through which the released DA is re-uptaken into nerve terminals. Taken together, compared with conventional single-target anti-tics drugs such as Hal, NDG with the dual regulating effect would

be more significant for the treatment of TS. The unique therapeutic property of NDG might be meaningful for the treatment of TS.

Acknowledgements

The article was supported by the National Natural Science Foundation of China (81273798), the Natural Science Foundation of Shandong province (ZR2012HM030, BS2015YY030), the Development Project of Science and Technology of Traditional Chinese Medicine of Shandong Province (2013ZDZK-085), the Development Projects of Shandong Province Science and Technology (2011GSF11903), the Postdoctoral Science Foundation of China (2014M551924) and the National Natural Science Foundation of China (81202724).

References

1. Hallett M. Tourette Syndrome: Update. Brain Dev. 2015. pii:S0387-7604(14)00266-6. (doi:10.1016/j.braindev)
2. Bloch MH, Leckman JF. Clinical course of Tourette's syndrome. J Psychosom Res. 2009; 67:497-501.
3. Zhang F, Li A. Dual ameliorative effects of Ningdong granule on dopamine in rat models of Tourette's syndrome. Sci Rep. 2015; 5:7731. (doi:10.1038/srep07731)
4. Wong DF, Brasić JR, Singer HS, Schretlen DJ, Kuwabara H, Zhou Y, Nandi A, Maris MA, Alexander M, Ye W, Rousset O, Kumar A, Szabo Z, Gjedde A, Grace AA. Mechanisms of dopaminergic and serotonergic neurotransmission in Tourette syndrome: Clues from an in vivo neurochemistry study with PET. Neuropsychopharmacology. 2008; 33:1239-1251.
5. Haycock JW, Becker L, Ang L, Furukawa Y, Hornykiewicz O, Kish SJ. Marked disparity between age-related changes in dopamine and other presynaptic dopaminergic markers in human striatum. J. Neurochem. 2003; 87:574-585.
6. Wise RA. Dopamine, learning and motivation. Nat Rev Neurosci. 2004; 5:483-494.
7. Wang S, Qi F, Li J, Zhao L, Li A. Effects of Chinese herbal medicine Ningdong granule on regulating dopamine (DA)/serotonin (5-TH) and gamma-amino butyric acid (GABA) in patients with Tourette syndrome. Biosci Trends. 2012; 6:212-218.
8. Zhang F, Li A. Dual regulating effects of gastrodin on extracellular dopamine concentration in rats models of Tourette's syndrome. Int J Neurosci. 2014; [Epub ahead of print].
9. Steeves TD, Ko JH, Kideckel DM, Rusjan P, Houle S, Sandor P, Lang AE, Strafella AP. Extrastriatal dopaminergic dysfunction in tourette syndrome. Ann Neurol. 2010; 67:170-181.
10. Stamenkovic M, Schindler SD, Asenbaum S, Neumeister A, Willeit M, Willinger U, de Zwaan M, Riederer F, Aschauer HN, Kasper S. No change in striatal dopamine re-uptake site density in psychotropic drug naive and in currently treated Tourette's disorder patients: A [(123)I]-beta-CIT SPECt-study. Eur Neuropsychopharmacol. 2001; 11:69-74.
11. Steeves TD, Fox SH. Neurobiological basis of serotonin-dopamine antagonists in the treatment of Gilles de la Tourette syndrome. Prog Brain Res. 2008; 172:495-513.
12. Black KJ, Mink JW. Response to levodopa challenge in Tourette syndrome. Mov Disord. 2000; 15:1194-1198.
13. Wang DH, Li W, Liu XF, Zhang JM, Wang SM. Chinese medicine formula "Jian-Pi-Zhi-Dong Decoction" attenuates Tourette syndrome *via* downregulating the expression of dopamine transporter in mice. Evid Based Complement Alternat Med. 2013; 2013:385685.
14. Lv H, Li A, Ma H, Liu F, Xu H. Effects of Ningdong granule on the dopamine system of Tourette's syndrome rat models. J Ethnopharmacol. 2009; 124:488-492.
15. Qi F, Zhao L, Zhou A, Zhang B, Li A, Wang Z, Han J. The advantages of using traditional Chinese medicine as an adjunctive therapy in the whole course of cancer treatment instead of only terminal stage of cancer. Biosci Trends. 2015; 9:16-34.
16. Li AY, Lv H, Sun R, Lv LL, Zhang XL, Wang P. Study on the pharmacodynamics of Ningdong granule for Tourette syndrome. J Chin Pediatr Integr Tradit West Med. 2009; 1:48-50. (in Chinese)
17. Li AY, Cong S, Lv H, Li JJ, Zhao L. Clinical observation on treatment of Tourette syndrome by integrative medicine. Chin J Integr Med. 2009; 15:261-265.
18. Zhao L, Li AY, Lv,H., Liu FY, Qi FH. Traditional Chinese medicine Ningdong granule: The beneficial effects in Tourette's disorder. J Int Med Res. 2010; 38:169-175.
19. Napier TC, Istre ED. Methamphetamine-induced sensitization includes a functional up-regulation of ventral pallidal 5-HT2A/2C receptors. Synapse. 2008; 62:14-21.
20. Zhao L. The clinical and molecular biological mechanism study of Ningdong granule on Tourette's syndrome [D]. Jinan: Medical College of Shandong University. 2010; PP. 22-24
21. Bronfeld M, Israelashvili M, Bar-Gad I. Pharmacological animal models of Tourette syndrome. Neurosci Biobehav Rev. 2013; 37:1101-1119.
22. Diamond BI, Reyes MG, Borison R. A new animal model for Tourette syndrome. Adv Neurol. 1982; 35:221-225.
23. Wakata N, Araki Y, Sugimoto H, Iguchi H, Kinoshita M. IDPN-induced monoamine and hydroxyl radical changes in the rat brain. Neurochem Res. 1999; 25:401-404.
24. Cadet JL, BraunT, Freed WJ. Clonidine and prazosin block the iminodipropionitrile (IDPN) induced spasmodic dyskinetic syndrome in mice. Pharmacol. Biochem Behav. 1987; 26:791-795.
25. Albin RL, Mink JW. Recent advances in Tourette syndrome research. Trends Neurosci. 2006; 29:175-182.
26. Seo D, Patrick CJ, Kennealy PJ. Role of serotonin and dopamine system interactions in the neurobiology of impulsive aggression and its comorbidity with other clinical disorders. Aggress Violent Behav. 2008; 13:383-395.
27. Stayte S, Rentsch P, Li KM, Vissel B. Activin a protects midbrain neurons in the 6-hydroxydopamine mouse model of Parkinson's disease. PLoS One. 2015; 10:e0124325.
28. Leckman JF. Tourette's syndrome. Lancet. 2002; 360:1577-1586.
29. Torres GE, Gainetdinov RR, Caron MG. Plasma membrane monoamine transporters: Structure, regulation and function. Nat Rev Neurosci. 2003; 4:13-25.

(Received May 21, 2015; Revised June 26, 2015; Accepted June 29, 2015)

Original Article

DOI: 10.5582/bst.2015.01080

The diagnostic value of contrast-enhanced ultrasound in differentiating small renal carcinoma and angiomyolipoma

Lin Chen[1,*], Ling Wang[2,*], Xuehong Diao[1], Weiqing Qian[3], Liang Fang[1], Yun Pang[1], Jia Zhan[1,], Yue Chen[1,**]**

[1] *Department of Ultrasound, Huadong Hospital, Fudan University, Shanghai, China;*
[2] *Department of Reproductive Immunology, Obstetrics and Gynecology Hospital, Fudan University, Shanghai, China;*
[3] *Department of Urology, Huadong Hospital, Fudan University, Shanghai, China.*

Summary **The aim of this study was to explore the value of contrast-enhanced ultrasound (CEUS) in differentiating small renal masses. A total of 102 small renal masses (≤ 3 cm) in 99 patients were examined using conventional ultrasound (CUS) and CEUS, and the findings were reviewed and evaluated in comparison to pathology. Significant differences between renal cell carcinomas (RCCs) and angiomyolipomas (AMLs) were noted in terms of the orientation and echogenicity on CUS ($p < 0.05$ for both), but the location, shape, margins, homogeneity, and blood flow signals of RCCs on color Doppler flow imaging (CDFI) were similar to those of AMLs ($p > 0.05$ for all). On CEUS, however, the enhancement intensity, washout in the late phase, and perilesional rim-like enhancement differed significantly for RCCs and AMLs ($p = 0.000$ for all). Significant differences between CEUS and CUS in terms of sensitivity (88.9% *vs*. 55.6%), the negative predictive value (68.0% *vs*. 29.5%), the false negative rate (9.9% *vs*. 44.5%), and accuracy (88.3% *vs*. 58.9%) were noted ($p < 0.05$ for all). CEUS, with its unique features, has value in diagnosing small RCCs and AMLs and outperforms CUS in differentiation of small RCCs and AMLs.**

Keywords: Ultrasonography, contrast agent, renal cell carcinoma, angiomyolipomas

1. Introduction

Renal cell carcinoma (RCC), the most common malignancy involving the kidney, originates in the renal tubular epithelium of the urinary system. Its incidence in China is 2% to 3% in adults, making it second only to bladder cancer (*1*), but its mortality is the highest of all tumors in the urinary system (*2*). Fortunately, the high incidence of small renal masses (SRMs) over the past few decades can be partly attributed to increased sensitivity and widespread use of imaging modalities such as computed tomography (CT), ultrasonography (US), and magnetic resonance imaging (MRI) (*3*). Detection and treatment in the earliest possible stage is key to reducing mortality. Conventional ultrasound (CUS) is a readily available, inexpensive, non-invasive, and non-ionizing imaging modality to detect renal masses, but it has limited use when attempting to differentiate between RCC and renal angiomyolipoma (AML). A safe and accurate imaging modality is needed to differentiate between RCC and AML, and contrast-enhanced ultrasound (CEUS) using microbubble-based contrast agents has garnered increasing attention in this regard (*4,5*).

Dynamic observation of enhancement features on CEUS provides an accurate characterization of lesions, and this helps to determine other examinations that are needed for a faster and more precise diagnosis. Some studies have reported that CEUS is useful in detecting and diagnosing RCC (*6-7*), but there is a dearth of literature investigating its value in the differential diagnosis of SRMs.

The aim of this study was to evaluate the characteristics of SRMs on CEUS and to determine

Released online in J-STAGE as advance publication August 11, 2015.

*These authors contributed equally to this work.
***Address correspondence to:*
Dr. Jia Zhan and Dr Yue Chen, Department of Ultrasound, Huadong Hospital, Fudan University, 211 West Yan'an Rd, Shanghai 200040, China.
E-mail: 13764433262@163.com (Zhan J)
ultrasound_chen@126.com (Chen Y)

whether CEUS is better than US at diagnosing small RCC.

2. Materials and Methods

2.1. *Patient selection*

Between September 2011 and March 2015, a total of 268 renal masses in 261 consecutive patients were examined with CEUS after detection with baseline CUS. Of 268 renal masses, 166 (in 162 patients) were excluded either because they were large in size (> 3 cm) or because subsequent pathology results were unavailable. Patients with a pathologic diagnosis of a simple cyst, oncocytoma, a metastatic tumor, an adenoma, or and a *Wilm's* tumor were also excluded. Thus, this study examined 102 masses in 99 patients, 79 patients with RCC (ages ranging from 25-87, mean 56.6 ± 16.5 years), and 20 patients with AML (ages ranging from 25-87, mean 56.6 ± 16.5 years). An open or laparoscopic partial nephrectomy was performed for all of the masses that were studied. Table 1 shows the baseline characteristics of patients.

This study was approved and supervised by this Hospital's institutional review board, and informed consent was obtained from each patient.

2.2. *CUS*

CUS was performed using an Acuson S2000 ultrasound system (Siemens Medical Solutions, Mountain View, CA, USA) with a 4C1 convex transducer (frequency range: 1.0-4.0 MHz). All examinations were performed by a single radiologist (C.L.) with 13 years of experience in abdominal US and 9 years in CEUS. The long-axis view of the kidney was obtained by placing the probe over the lower back with the patient in the lateral position. Imaging settings such as time gain compensation (TGC), total gain, depth, and focal zone were optimized to ensure adequate image quality. CUS, both gray-scale ultrasound and color Doppler flow imaging (CDFI), was performed to detect and reveal renal masses. After CUS, all patients underwent CEUS.

2.3. *CEUS*

CEUS was performed using contrast pulse sequencing (CPS) technology integrated in the Acuson S2000 unit at a mechanical index of 0.05-0.07. CEUS was performed by the same radiologist who performed CUS (C.L.). CPS allows continuous low-mechanical-index (MI) imaging with a high microbubble tissue ratio. The depth of focus was 7 to 10 cm at the bottom of the lesion. The US contrast agent used in this study was SonoVue (Bracco, Milan, Italy), which consists of sulfur hexafluoride (SF_6) -filled microbubbles stabilized with phospholipids. Before use, an ampoule of 5 mg of SonoVue was shaken with 5 ml of normal saline to serve as a microbubble suspension. A bolus of 1.2 ml of SonoVue suspension was injected intravenously followed by a 5-ml saline flush. A timer and video recorder were activated at the same time the contrast agent was administered. The tumor and renal cortex were observed continuously for at least 3 min., and the images and video clips for each detected mass were saved to a local hard drive for subsequent analysis.

2.4. *Image review and data evaluation*

Two radiologists (D.X.H. and F.L.), both blinded to the pathologic diagnosis, independently reviewed all renal images and video clips of CUS and CEUS saved on the local hard drive. The two radiologists, one with 7 and the other with 9 years of experience in abdominal US, had over 4 years of experience in reading CEUS images. The CUS characteristics that were documented and described included location, shape, orientation, margins, echogenicity, homogeneity, and vascularity. Characteristic changes in enhancement on CEUS were evaluated and recorded, including the initial enhancement time, the extent and pattern of enhancement, and dynamic changes in enhancement. The echotexture or signal intensity from the tumor was identified as hyperechoic, isoechoic, or hypoechoic in

Table 1. Baseline characteristics of patients

Characteristics	Description	RCC (n = 81)	AML (n = 21)	χ^2	p
Gender	Male	56 (69.1)	12 (57.1)	1.079	0.299
	Female	25 (30.9)	9 (42.9)		
Laterality	Left kidney	45 (55.6)	10 (47.6)	0.123	0.516
	Right kidney	36 (44.4)	11 (52.4)		
Tumor location	Upper pole	17 (22.2)	6 (28.6)	0.551	0.759
	Middle part	43 (49.4)	10 (47.6)		
	Lower pole	21 (28.4)	5 (23.8)		
Surgical methods	Open PN	28 (34.6)	5 (23.8)	0.882	0.343
	Laparoscopic PN	53 (65.4)	16 (76.2)		

AML, angiomyolipoma; RCC, renal cell carcinoma; PN, partial nephrectomy. Values are presented as the number (%).

comparison to the adjacent renal cortex, and the pattern was identified as homogeneous and inhomogeneous. CEUS was divided into a wash-in phase (7-15 s to 35-40 s after contrast injection) and a wash-out phase (41-46 s to 180 s) in conjunction with vascular perfusion of the renal cortex. The wash-in and wash-out of contrast in renal masses were described as faster than, slower than, or in sync with perfusion of the adjacent renal cortex. "Pseudocapsule enhancement" around the tumor on CEUS was defined as rim-like enhancement that became more distinct in the late phase. Masses were classified as malignant or benign depending on the image characteristics and the radiologists' experience. On CUS, masses with hypoechogenicity or iso-echogenicity and that were oriented outward from the renal capsule were defined as RCC, and those with hyperechogenicity or iso-echogenicity and that were oriented inward at the renal capsule were defined as AML. On CEUS, masses with hyperenhancement or iso-enhancement and with fast wash-in and/or fast wash-out or rim-like enhancement were defined as RCC, and those with hypoenhancement, iso-enhancement, or synchronous enhancement in the wash-in phase and wash-out phase were defined as AML.

The two radiologists made independent diagnoses and conclusions. In the event their conclusions differed, they consulted to reach a mutually acceptable final conclusion.

2.5. *Statistical analysis*

Continuous data were expressed as a percent or mean ± standard deviation (SD). An *Independent-Sample t* test was used to compare the size of the RCCs and AMLs. A *chi-square* test was performed to compare the image characteristics of RCCs and AMLs and to analyze the sensitivity, specificity, positive predictive value, negative predictive value, and accuracy of CUS and CEUS. $P < 0.05$ was considered significant. Statistical analysis was performed using SPSS software version 13.0 (SPSS Inc., Chicago, IL, USA).

3. Results

3.1. *Pathologic findings*

A pathologic diagnosis was obtained for all masses *via* a laparoscopic or open partial nephrectomy. One single nodule was detected in 77 patients with RCC and 19 patients with AML, and multiple nodules were detected in the remaining 3 patients. Of the patients with multiple nodules, 2 had RCC; 1 had 2 masses (1 in each kidney) and 1 had 2 nodules in the left kidney. One patient had AML with 2 nodules in the right kidney. Of the 102 renal masses, 81 (79.4%) were RCCs and 21 (20.6%) were AMLs. The 81 RCCs were clear cell carcinoma (68, 84.0%), papillary carcinoma (8, 9.9%), chromophobe carcinoma (4, 4.9%), or collecting duct carcinoma (1, 1.2%).

3.2. *CUS features of small RCCs and AMLs*

The mean maximum diameter of the renal masses, obtained from CUS, was 1.81 ± 0.59 cm (1.0 to 3.0 cm) for RCCs and 1.77 ± 0.52 cm (1.2 to 3.0 cm) for AMLs ($p > 0.05$). Significant differences between RCCs and AMLs in terms of the orientation and echogenicity on CUS were noted ($\chi^2 = 4.646$, 20.560; $p = 0.031$, 0.000, respectively). However, there were no significant differences between RCCs and AMLs in terms of location ($\chi^2 = 0.424$; $p = 0.809$), shape ($\chi^2 = 0.981$; $p = 0.322$), margins ($\chi^2 = 0.293$; $p = 0.588$), homogeneity ($\chi^2 = 0.036$; $p = 0.850$) and blood flow signals in CDFI (χ^2

Table 2. Characteristics of small RCC and AML in CUS

Lexicon	Description of lesions	RCC (n = 81)	AML (n = 21)	χ^2	p
Shape	Round/Oval	75 (92.6)	18 (85.7)	0.981	0.322
	Irregular	6 (7.4)	3 (14.3)		
Margins	Circumscribed	76 (93.8)	19 (90.5)	0.293	0.588
	Indistinct	5 (6.2)	2 (9.5)		
Orientation	Inward at the renal parenchyma	54 (66.7)	19 (90.5)	4.646	0.031
	Outward from the renal capsule	27 (33.3)	2 (9.5)		
Echogenicity	Hypoechoic	41 (50.6)	2 (9.5)	20.560	0.000
	Iso-echoic	25 (30.9)	5 (23.8)		
	Hyperechoic	15 (18.5)	14 (66.7)		
Homogeneity	Homogeneous	67 (82.7)	17 (81.0)	0.036	0.850
	Heterogeneous	14 (17.3)	4 (19.0)		
Blood flow signals in CDFI	With	18 (48.1)	4 (23.8)	0.099	0.753
	Without	63 (51.9)	17 (76.2)		

AML, angiomyolipoma; RCC, renal cell carcinoma. Values are presented as the number (%).

Table 3. Characteristics of small RCC and AML in CEUS

Enhancement pattern	Enhancement of lesions	RCC (n = 81)	AML (n = 21)	χ^2	p
Intensity	Hyperenhancement	64 (79.0)	3 (14.3)	32.062	0.000
	Iso-enhancement	10 (12.3)	13 (61.9)		
	Hypoenhancement	7 (8.7)	5 (23.8)		
Homogeneity	Heterogeneous	27 (33.3%)	3 (14.3)	2.914	0.088
	Homogeneous	54 (66.7%)	18 (85.7)		
Wash-in phase	Faster	37 (45.7)	3 (14.3)	7.917	0.019
	Synchronous	32 (39.5)	11 (52.4)		
	Slower	12 (14.8)	7 (33.3)		
Wash-out phase	Faster	63 (77.8)	2 (9.5)	37.227	0.000
	Synchronous	13 (16.0)	9 (42.9)		
	Slower	5 (6.2)	10 (47.6)		
Rim-like enhancement	Without	36 (44.4)	19 (90.5)	8.700	0.003
	With	45 (55.6)	2 (9.5)		

AML, angiomyolipoma; RCC, renal cell carcinoma. Values are presented as the number (%).

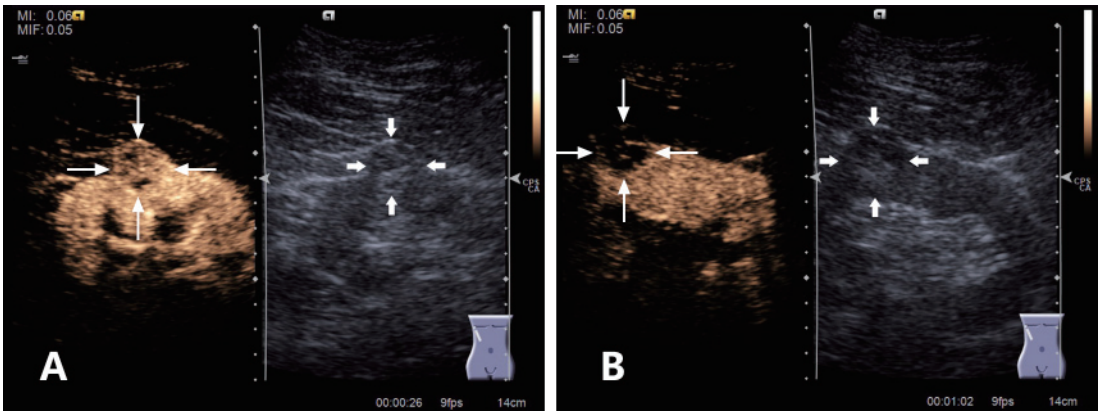

Figure 1. A 57-year-old man with clear cell renal carcinoma. CUS revealed a hypoechoic small renal mass located in the middle of the right kidney (short arrows). **(A)** CEUS imaging in the early phase revealed heterogeneous hyperenhancement. Peritumoral rim-like enhancement was observed (long arrows); **(B)** CEUS imaging in the late phase indicated that the region of the tumor was washed out with heterogeneous hypoechogenicity (long arrows).

= 0.099; p = 0.753). Table 2 details the image features of RCC and AML on CUS.

3.3. *CEUS features of RCCs and AMLs*

RCCs and AMLs differed significantly in enhancement intensity, wash-out in the late phase, and perilesional rim-like enhancement (p = 0.000 for all), but there were no significant differences in homogeneity and wash-in in the early phase (p > 0.05 for both) (Table 3). The typical characteristics of RCCs were hyperenhancement (64/81, 79.0%), homogeneous enhancement (54/81, 66.7%), wash-out of contrast earlier than that in the peripheral cortex in the late phase (63/81, 77.8%), and peripheral rim-like enhancement (45/81, 55.6%) (Figure 1), whereas the dominant features of AMLs were iso-enhancement (13/21, 61.9%), homogeneous enhancement (18/21, 85.7%), wash-in of contrast in sync with perfusion of the peripheral cortex in the early phase (11/21, 52.4%) and wash-out of contrast later than that in the peripheral cortex in the late phase (10/21, 47.6%) (Figure 2).

3.4. *Comparison of the diagnostic value of CUS and CUES*

Of the 102 masses, 51 were diagnosed as malignant and 51 were diagnosed as benign based on CUS, while 77 masses were diagnosed as malignant and 25 were diagnosed as benign based on CEUS. CEUS significantly outperformed CUS in differentiating SRMs (Table 4). Although CEUS and CUS were similar in terms of their specificity (80.9% *vs*. 71.4%), positive predictive value (94.8% *vs*. 88.3%), and false positive rate (19.1% *vs*. 28.6%) (p > 0.05 for all), they differed significantly in terms of their sensitivity (88.9% *vs*. 55.6%), negative predictive value (68.0% *vs*. 29.5%), false negative rate (9.9% *vs*. 44.5%), and accuracy (88.3% *vs*. 58.9%) (p < 0.05 for all).

4. Discussion

RCC is a malignant neoplasm that requires total or partial nephrectomy, and thus definite differentiation

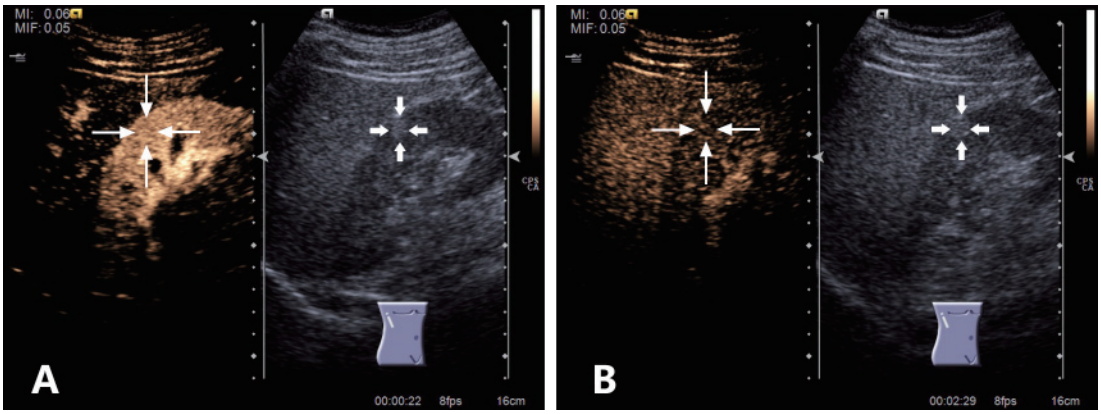

Figure 2. A 65-year-old man with angiomyolipoma. CUS revealed a hyperechoic small renal mass located in the middle of the right kidney (short arrows). **(A)** CEUS imaging in the early phase revealed homogeneous hyperenhancement similar to the peritumoral renal cortex (long arrows). There was no distinct boundary between the mass and the renal cortex; **(B)** CEUS imaging in the late phase showed that the region of the tumor was washed out in sync with perfusion of the peritumoral renal cortex (long arrows).

Table 4. Diagnostic performance of CUS and CEUS in comparison to pathology results

Modality	Sensitivity	Specificity	PPV	NPV	FPR	FNR	Accuracy
CUS	45/81(55.6)	15/21(71.4)	45/51(88.3)	15/51(29.5)	6/21(28.6)	36/81(44.5)	60/102(58.9)
CEUS	73/81(88.9)	17/21(80.9)	73/77(94.8)	17/25(68.0)	4/21(19.1)	8/81 (9.9)	90/102(88.3)
χ^2	3.883	0.071	0.075	3.878	0.324	14.276	7.080
p	0.049	0.790	0.784	0.049	0.569	0.000	0.008

CUS, conventional ultrasound; CEUS, contrast-enhanced ultrasound; PPV, positive predictive value; NPV, negative predictive value; FPR, false positive rate; FNR, false negative rate. Values are presented as the number (%).

between RCCs and benign masses is essential. Imaging studies such as CT, MRI, and US are essential to surgery to treat renal carcinomas. Among these modalities, CUS is usually the first choice for the diagnosis of RCC in China because it is readily accessible, inexpensive, noninvasive, and provides images in real time. However, CUS may be limited because of its lower accuracy in the characterization of some renal masses, and particularly small masses. The current study showed that, among all of the characteristics on CUS, only orientation and echogenicity allowed the differentiation of RCCs and AMLs. To the extent known, hypoechoic renal masses are mostly considered to be malignant while hyperechoic and iso-echoic renal masses are often referred to as benign. However, RCCs that were hyperechoic were noted in 15 masses (18.5%) and RCCs that were iso-echoic were noted in 25 masses (30.9%). Two AMLs (9.5%) were hypoechoic on gray-scale US in this study. Forman *et al*. (*8*) reported that approximately 30% of small RCCs appear as hyperechoic, which is how small benign renal masses similarly appear. In the current study, 6% of the benign renal masses were atypically iso-echoic and 29% of those masses were slightly hyperechoic. Moreover, small RCCs were similar to small AMLs in shape, margins, and homogeneity; both were mostly round/oval, circumscribed, and homogeneous in the present study. Just as US echogenicity is unreliable in differentiating solid renal masses, conventional color Doppler US may have limited ability to detect intra-tumoral vascularity in RCCs, with a sensitivity of 41% according to one source (*9*). The present study found that CDFI was not effective in the differentiation of the SRMs because of its low sensitivity. Therefore, further imaging studies are needed for patients with uncharacterized SRMs.

As a result of the recent development of microbubble contrast media and imaging techniques, CEUS has been actively used in the detection and differentiation of lesions in parenchymatous organs. Microbubble contrast agents, with a diameter ranging from 1-10 μm (median 2 μm), cannot be filtered by the lungs or enter interstitial fluid. Therefore, they are considered to be pure blood pool agents (*10*). Under US, microbubbles alternately contract and expand with the same resonance frequency as US waves by amplifying the ultrasound signal. Advantages of CEUS imaging include the ability to detect microvasculature that can be overlooked by CDFI. In addition, CEUS allows continuous dynamic imaging after injection as opposed to the intermittent static acquisitions possible with CECT and MR. SonoVue has been used to successfully detect and characterize focal liver lesions and their vascularity (*11*). SonoVue microbubbles consist of a sulphur hexafluoride gas with a phospholipid shell. This contrast agent is metabolized by the liver, and the sulphur hexafluoride gas is exhaled *via* the lungs. Therefore, it is relatively harmless with a lower incidence of adverse reactions,

such as nephrotoxicity (*12*). In addition, CEUS has advantages over CT and MRI including unmatched temporal resolution due to continuous real-time imaging and potential cost savings (*13*). Moreover, CEUS is suitable for patients with a metal implant who cannot undergo MRI. Updated in 2011, the guidelines of the European Federation of Societies for Ultrasound in Medicine and Biology (EFSUMB) recommend kidney CEUS for patients with renal artery stenosis, renal ischemia, and focal renal lesions, for the differentiation of solid renal masses and pseudotumors, and for the characterization of complex cystic masses and renal infections (*14*). Previous studies have found that CEUS is useful in differentiating malignant renal masses from benign ones (*6,7*). However, few studies have focused on the usefulness of CEUS in differentiating SRMs. The purpose of the present study, therefore, was to investigate the value of CEUS in the differential diagnosis of small RCCs and AMLs.

This study showed that CEUS outperformed CUS in the diagnosis of small renal tumors, as is evident in Table 4. The current findings were consistent with the results of previous studies. In a prospective study of 49 lesions (38 RCCs and 11 AMLs), Oh *et al*. (*15*) reported that CEUS had a sensitivity of 86.8%, a specificity of 63.6%, an accuracy of 81.6%, a positive predictive value of 89.2% and a negative predictive value of 58.3%. In a study of 137 lesions (117 RCCs and 20 AMLs), Ignee *et al*. (*6*) reported that CEUS had a sensitivity of 97%, a specificity of 45%, an accuracy of 90%, a positive predictive value of 91%, and a negative predictive value of 75%. The high diagnostic accuracy of CEUS can be ascribed to its performance in assessing vascular morphology and its enhancement patterns that allow evaluation of the micro- and macro-circulation of tumors.

Dynamic observation of blood perfusion with CEUS can provide more useful diagnostic information for the differentiation of RCCs and AMLs. The present study noted rapid accumulation of contrast media in the form of hyperenhancement in the early phase (64/81, 79%), followed by early washout in the late phase for most RCCs (63/81, 77.8%). In contrast, most AMLs (13/21, 61.9%) mainly had slow accumulation of contrast agents in the form of iso-enhancement, followed by a slow wash-out (10/21, 47.6%). Such findings may be related to the pathologic changes produced by RCCs and AMLs. RCC is characterized by numerous immature thin-walled blood vessels with widespread arterio-venous fistulas (*16*), whereas AML is a mesenchymal tumor consisting of a variable proportion of fat tissue, spindle and epithelioid smooth muscle cells, and abnormally thick-walled blood vessels (*17*).

Previous studies reported that RCCs often demonstrated heterogeneous enhancement on CEUS, which can be attributed to the fast growth of those malignant tumors. When the blood supply to the RCC cannot satisfy the growth of the tumor, intratumoral necrosis may result (*18*). AML, a benign tumor with slow growth, is unlikely to develop necrosis and it displays inhomogeneous enhancement. In the present study, there were no significant differences between RCCs and AMLs in terms of the frequency of homogeneous enhancement (66.7% *vs*. 85.7%; $p > 0.05$). This might be explained by the fact that the masses included in this study were smaller than those in previous studies and that there is a relatively low incidence of necrosis in small masses. Lu *et al*. (*19*) reported that CEUS resulted in homogeneous enhancement for all AMLs ($n = 18$) and for 34.3% of RCCs ($n = 105$). However, the maximal diameter of the masses ranged from 1.0 cm to 11.5 cm (mean 4.3 ± 2.1 cm). Jiang *et al*. (20) analyzed CEUS features of clear cell renal cell carcinoma in relation to tumor size, and they found that tumors ≤ 3 cm (72%) had a significantly higher frequency of homogeneity than did tumors > 3cm (9%) ($p < 0.05$).

Rim-like enhancement around the tumor might represent the tumoral pseudocapsule resulting from compression, ischemia, and necrosis produced by tumor growth in the adjacent normal parenchyma, with subsequent deposition of fibrous tissue (*21*). The present study noted significant differences between the rim-like enhancement of RCCs and AMLs ($p = 0.000$). However, rim-like enhancement was observed in only 55.6% (45/81) of RCCs, which is similar to the figure (56.7%, 34/60) reported by Jiang *et al*. (*20*) in clear cell RCCs ≤ 3 cm. However, this figure is significantly lower than that in other studies. Xu *et al*. (*22*) reported noting rim-like enhancement in 79.6% (74/93) of RCCs. This difference may be due to the small size of the masses in the current study and the study by Jiang *et al*. (*20*). The current study found that 2 (9.5%) AMLs displayed incomplete rim-like enhancement. This might be related to the distribution of blood vessels in AMLs. Rim-like enhancement of AMLs needs to be investigated further.

The current study has several limitations. First, this study examined fewer AMLs than RCCs, so a larger sample size is needed for further evaluation. Second, this study included few papillary RCCs, chromophobe RCCs, or chromophobe RCCs. A larger set of samples is needed to further confirm the enhancement features of these RCCs. Finally, CEUS has limited ability to image the kidneys because of the interference of bowel gas, the ribs, and large body habitus (obesity), and CEUS can be influenced by the lesion location, as is true of CUS. In such instances, CECT can provide additional information.

Based on the present findings, the unique features of CEUS are useful in evaluating SRMs with a higher level of accuracy than CUS. CEUS may serve as a promising modality in the differential diagnosis of small RCCs and AMLs.

Acknowledgements

This work was supported by grants for a 2013 Science and Technology Project to Guide Medicine (project no. 134119a9200, Chen L) and a 2015 Science and Technology Project to Guide Medicine (project no. 15401932200, Wang L) of the Shanghai Municipal Science and Technology Commission, a 2008 grant (P08471) from the JSPS Postdoctoral Fellowship for Foreign Researchers (Wang L), a grant from the National Natural Science Foundation of China (No. 30801502, Wang L), and a grant from the Shanghai Pujiang Program (No. 11PJ1401900, Wang L).

References

1. Motzer RJ, Jonasch E, Agarwal N, *et al*. Kidney cancer, version 3.2015. J Natl Compr Canc Netw. 2015; 13:151-159.
2. Jemal A, Bray F, Center MM, Ferlay J, Ward E, Forman D. Global cancer statistics. CA Cancer J Clin. 2011; 61:69-90.
3. Jamis-Dow CA, Choyke PL, Jennings SB, Linehan WM, Thakore KN, Walther MM. Small (< or = 3-cm) renal masses: Detection with CT versus US and pathologic correlation. Radiology. 1996; 198:785-788.
4. Nicolau C, Ripollés T. Contrast-enhanced ultrasound in abdominal imaging. Abdom Imaging. 2012; 37:1-19.
5. Barozzi L, Capannelli D, Imbriani M. Contrast enhanced ultrasound in the assessment of urogenital pathology. Arch Ital Urol Androl. 2014; 86:319-324.
6. Ignee A, Straub B, Brix D, Schuessler G, Ott M, Dietrich CF. The value of contrast enhanced ultrasound (CECU) in the characterisation of patients with renal masses. Clin Hemorheol Microcirc. 2010; 46:275-290.
7. Houtzager S, Wijkstra H, de la Rosette JJ, Laguna MP. Evaluation of renal masses with contrast- enhanced ultrasound. Curr Urol Rep. 2013; 14:116-123.
8. Forman HP, Middleton WD, Melson GL, McClennan BL. Hyperechoic renal cell carcinomas: Increase in detection at US. Radiology. 1993; 188:431-434.
9. Xu ZF, Xu HX, Xie XY, Liu GJ, Zheng YL, Liang JY, Lu MD. Renal cell carcinoma: Real-time contrast-enhanced ultrasound findings. Abdom Imaging. 2010; 35:750-756.
10. Li X, Liang P, Guo M, Yu J, Yu X, Cheng Z, Han Z. Real-time contrast-enhanced ultrasound in diagnosis of solid renal lesions. Discov Med. 2013; 16:15-25.
11. Sporea I, Badea R, Popescu A, *et al*. Contrast- enhanced ultrasound (CEUS) for the evaluation of focal liver lesions - a prospective multicenter study of its usefulness in clinical practice. Ultraschall Med. 2014; 35:259-266.
12. Cokkinos DD, Antypa EG, Skilakaki M, Kriketou D, Tavernaraki E, Piperopoulos PN. Contrast enhanced ultrasound of the kidneys: What is it capable of? Biomed Res Int. 2013; 2013:595873.
13. Gulati M, King KG, Gill IS, Pham V, Grant E, Duddalwar VA. Contrast-enhanced ultrasound (CEUS) of cystic and solid renal lesions: A review. Abdom Imaging. 2015; (Epub ahead of print).
14. Piscaglia F, Nolsoe C, Dietrich CF, *et al.* The EFSUMB guidelines and recommendations on the clinical practice of contrast enhanced ultrasound (CEUS): Update 2011 on non-hepatic applications. Ultraschall Med. 2012; 33:33-59.
15. Oh TH, Lee YH, Seo IY. Diagnostic efficacy of contrast-enhanced ultrasound for small renal masses. Korean J Urol. 2014; 55:587-592.
16. Ljungberg B, Cowan NC, Hanbury DC, Hora M, Kuczyk MA, Merseburger AS, Patard JJ, Mulders PF, Sinescu IC; European Association of Urology guideline group. EAU guidelines on renal cell carcinoma: The 2010 update. Eur Urol. 2010; 58:398-406.
17. Esheba Gel S, Esheba Nel S. Angiomyolipoma of the kidney: Clinicopathological and immunohistochemical study. J Egypt Natl Canc Inst. 2013; 25:125-134.
18. Reese JH. Renal cell carcinoma. Curr Opin Oncol. 1992; 4:427-434.
19. Lu Q, Wang W, Huang B, Li C, Li C. Minimal fat renal angiomyolipoma: The initial study with contrast-enhanced ultrasonography. Ultrasound Med Biol. 2012; 38:1896-1901.
20. Jiang J, Chen Y, Zhou Y, Zhang H. Clear cell renal cell carcinoma: Contrast-enhanced ultrasound features relation to tumor size. Eur J Radiol. 2010; 73:162-167.
21. Pickhardt PJ, Lonergan GJ, Davis CJ Jr, Kashitani N, Wagner BJ. From the archives of the AFIP. Infiltrative renal lesions: Radiologic-pathologic correlation. Armed Forces Institute of Pathology. Radiographics. 2000; 20:215-243.
22. Xu ZF, Xu HX, Xie XY, Liu GJ, Zheng YL, Lu MD. Renal cell carcinoma and renal angiomyolipoma: Differential diagnosis with real-time contrast-enhanced ultrasonography. J Ultrasound Med. 2010; 29:709-717.

(Received June 7, 2015; Revised July 22, 2015; Accepted July 24, 2015)

Original Article

DOI: 10.5582/bst.2015.01111

The Chinese version of monitoring and evaluation system strengthening tool for human immunodeficiency virus (HIV) capacity building: Development and evaluation

Ran Zhao[1,*], Ren Chen[1,*], Bing Zhang[2], Ying Ma[1], Xia Qin[1,], Zhi Hu[1,**]**

[1] *School of Health Services Management, Anhui Medical University, Hefei, Anhui, China;*
[2] *Anhui Provincial Hospital, Hefei, Anhui, China.*

Summary **Monitoring and evaluation (M&E) for human immunodeficiency virus (HIV) capacity building has become a significant step for HIV prevention and control. The M&E system strengthening tool published by the United Nations Joint Programme on HIV/AIDS (UNAIDS) was intended to be the most authoritative assessment tool internationally. Facing the fact that the M&E system in China did not function at an optimum level, we considered taking the international standards for reference. By linguistic validating and different stages' discussions and revisions, we came up with the Chinese version of the capacity diagnosis tool with at least 12 components and tested its validity and reliability. The tool turned out to have a sufficiently linguistic validation and proved to be a scientific and feasible instrument which was suitable for China's national conditions.**

Keywords: Monitoring and evaluation, capacity building, reliability and validity, HIV/AIDS, China

1. Introduction

The human immunodeficiency virus (HIV) epidemic remains a major public health challenge globally (*1,2*). Case reporting data show that there were a reported 437,000 people living with HIV and a reported 136,000 deaths at the end of 2013 in China (*3*). With the rapid scale-up of resources investment, M&E has become a significant step for HIV prevention and control. In China, the government had already developed a national framework and an operational manual in 2007 and 2008 which symbolized that China had entered a new phase with more scientific and standardized management for HIV M&E system (*4,5*).

However, the following midterm evaluation of the "China Action Plan for HIV Prevention and Control (2006-2010)" showed that the framework did not function at an optimum level (*6,7*). The barriers have seriously hindered the progress of China's national HIV M&E system. China has to rearrange the relevant information as a whole and use the international standards for reference.

The "Organizing Framework for a Functional National HIV/AIDS M&E System" was published by UNAIDS in 2008 (*8*). It described 12 main components of a multi-sectoral HIV M&E system, formed the basis for M&E system assessments, and guided capacity development for M&E systems (*9-12*). The following "12 Components M&E System Strengthening Tool" provided further clarification about the individual questions in the 12 components (*13*).

The M&E system strengthening tool consists of 12 components for 3 domains. The first part is composed of 6 components, which are "A multi-sectoral HIV M&E system including organizational structures with HIV M&E functions", "Human capacity for HIV M&E", "Partnerships to plan, coordinate and manage the M&E System", "National, multi-sectoral HIV M&E Plan", "Annual, costed, national HIV M&E work plan", "Communication, advocacy and culture for HIV M&E". It is the outer ring which includes individuals, organizations, functions/actions, and the organizational culture that are fundamental to improve and sustain M&E system performance. The second part is composed of 5 components, which are "Routine HIV

*These authors contributed equally to this works.
***Address correspondence to:*
Dr. Zhi Hu and Dr. Xia Qin, School of Health Services Management, Anhui Medical University, No. 81, Meishan Road, Hefei 230032, Anhui, China.
E-mail: aywghz@126.com (Hu Z); aywgqinxia@sina.com (Qin X)

programme monitoring", "Surveys and surveillance", "National and sub-national HIV databases", "Supportive supervision and data auditing", "HIV evaluation and research agenda". It is the middle ring that focuses on the mechanisms through which data are collected, verified and analyzed. The third part is the component "Data dissemination and use" and it is the center which represents the primary purpose of the M&E system, *i.e.*, using data for decision-making (*12*).

This tool was the product of a comprehensive review and consolidation of existing assessment tools. It could not only provide a comprehensive assessment of the 12 components of a national HIV M&E system, but also replace the multiple assessment tools with the same intent, thereby reducing redundancy and standardizing the assessment for independent departments (*12,14*). It had been endorsed by the global M&E Reference Group (MERG) and intended to be the most authoritative assessment tool internationally for HIV M&E system to enhance their performance (*14*). Until now, no Chinese version has been put forward or tested in the current research.

In order to make an accurate and appropriate assessment of relevant research, an attempt was made in this study to perform a linguistic validation of the tool, to develop the Chinese version of M&E system strengthening tool and to examine the reliability and validity according to China's HIV epidemic situation, prevention and control environment as well as the M&E operating mechanism. We hope to provide measuring tool and theoretical reference for China's national HIV M&E system and to ensure effective and specific strategies for HIV M&E capacity building.

2. Materials and Methods

2.1. *Linguistic validation*

A well-established 3-phase linguistic validation procedure was used after obtaining approval for translation from UNAIDS.

Phase 1: Two bilingual Chinese translators, both of whom understood the content and purpose of the tool perfectly, collaborated to translate the original UNAIDS version from English into Chinese and avoided errors in the forward translation. An agreement on the forward-translated version of the tool in Chinese was reached during a committee between the two translators and another bilingual Chinese who had prior experience of linguistic and health policy (*15*).

Phase 2: Followed the suggestions of Diane *et al.* (*16,17*), this first translation was sent separately to two bilingual native-English-speaking translators who were specialists in health policy and had not seen the original tool. Once the two back-translations were completed, another meeting was held with the same committee members to discuss the discrepancies among the forward-translated version (Chinese), the back-translated version (English) and the original UNAIDS version.

Phase 3: We invited 5 experts to comment on the questionnaire items and instructions. Revisions were made accordingly to ensure the translation did not differ conceptually from the original UNAIDS version.

After the 3-phase linguistic validation procedure, we obtained the first version of the tool.

The research group, at the same time, determined 12 agencies/departments for our study at different levels preliminarily. Specifically, there were HIV working committee office, member units, Centers for Disease Control (CDC) and social organizations at the provincial level, HIV working committee office, CDC, medical institutions, social organizations at the municipal level, HIV working committee office, CDC, community health service institutions and social organizations at the district level.

2.2. *Focus group interviews*

The interviews were divided into 3 rounds with 15 experts in each group and facilitated by the principal researcher in our study group who had rich host experience and had participated in group interviews before. During the interviews, experts discussed the objects, the components and the questionnaires according to their working experience. These 45 experts, chosen from national, provincial, municipal and district levels, were specialists on HIV prevention and treatment system in theory and practice, which guaranteed the credibility and objectivity of the research. We got the second version of the tool after further adjustments and revisions with the experts.

2.3. *Pilot study*

To identify potentially misleading words or questions and to verify that the tool would be perfectly understood, a pilot study was conducted using the second version of the tool. We chose Fuyang city in Anhui province conveniently because the AIDS epidemic of the city is relatively serious throughout the province (*18*) and their AIDS prevention and treatment agencies kept good relationships with our research group. We selected 2 key informants respectively in HIV working committee office, CDC, social organizations and 4 key informants in the member units. During the implementation of this pilot study, any possible doubts were answered and recorded. Then we had further modification about the questionnaire and obtained the final version of the tool.

2.4. *Field trial study*

We numbered all the 31 provinces of mainland China and randomly selected one province in the lower-level epidemics and one province in the higher-level epidemics

according to the lower and higher level epidemics distribution in China (*19,20*). Then we numbered all the cities in the two provinces and randomly selected one city in each province. After that, we selected one district in each city randomly based on the same method (*21,22*). After rigorous sample selection, we chose Anhui and Hunan province, and selected Hefei city and its Luyang district, Hengyang city and its Zhuhui district as our study sites. On the principle of convenience sampling, we then selected 2 key informants in HIV working committee office, CDC, social organizations and 4 key informants in the member units at each level. From December 2012 to February 2013, we sent questionnaires to all the 72 participants and 70 questionnaires were collected. 66 of them were valid questionnaires and the effective recovery rate was 91.7%. There were several invalid questionnaires because of incomplete filling or option leakage.

2.5. *Analysis*

All data were input using the EpiData (version 3.0) with double entry verification and statistical analyses were performed through the SPSS statistical package (Windows version 11.5, SPSS Inc., Chicago, Illinois, USA). Construct validity was established by principal component analysis with a varimax orthogonal rotation. Beforehand, Kaiser-Meyer-Olkin (KMO) and Bartlett tests were performed as measures of sampling adequacy. Criteria used to determine the components were minimum eigenvalues > 1.00 or cumulative variance > 70% (*23*). Internal reliability was calculated through examination of Cronbach's Alpha. Reliability would be considered good if Cronbach's Alpha ranged between 0.7 and 0.9 (*24,25*).

3. Results

3.1. *Development of the final Chinese version of the tool*

After different stages' discussions and revisions, we came up with the final Chinese version of the tool. Table 1 showed revisions in different versions and the process of changing we have been through. During the linguistic validation, 12 components with 127 questions for 12 different agencies/departments formed the first version of the tool. After the focus group interviews, we deleted medical institutions and community health service institutions and added member units at municipal and district levels as our assessment. We also cut several components and questions for some agencies/departments and got the second version comprised of 12 components with 97 questions for 12 different agencies/departments. The following pilot study gave us a further modification about the questionnaires. We deleted 4 questions that were repetitive or expressed the same meaning and deleted the "Not at all" option in 5-point scale and "Not Applicable" option in 3-point scale. After revisions about the answering formats, we developed the final Chinese version of the tool.

Table 1. Revisions in different versions of the tool

Revisions	The Original Version	The First Version	The Second Version	The Final Version
Assessment Agency				
National Level	National AIDS coordinating authority; Ministry of health AIDS control programme, *etc.*	/	/	/
Sub-National Level	Local government authority/ AIDS coordinating authorities; Health facilities; Other implement of HIV services	Provincial level: HIV working committee office, CDC, member units and social organizations; Municipal level: HIV working committee office, CDC, medical institutions, social organizations; District level: HIV working committee office, CDC, community health service institutions, social organizations	HIV working committee office, CDC, member units and social organizations at provincial level, municipal level and district level separately.	HIV working committee office, CDC, member units and social organizations at provincial level, municipal level and district level separately.
Components	12 for all the agencie	12 for all the agencie	12, but different agencies contained different components	12, but different agencies contained different components
Numbers of Questions	127	127	97	93
Response Formats	A 5-point scale; A 3-point scale; Numerical responses	A 5-point scale; A 3-point scale; Numerical responses	A 5-point scale; A 3-point scale; Numerical responses	A 4-point scale; A 2-point scale; Numerical responses

Table 2. Components and contents in the final Chinese version of the tool

No.	Component	Content
1	A multi-sectoral HIV M&E system including organizational structures with HIV M&E functions	There is an M&E unit/professional within the entity. The number of full-time and part-time M&E posts, *etc*.
2	Human capacity for HIV M&E	There are written plans to support capacity building. M&E capacity is being built through on-the-job training and routine examination, *etc*.
3	Partnerships to plan, coordinate and manage the M&E system	There are clearly responsibility descriptions for M&E technical working group. Multi-sectors are well coordinated with M&E institutions/departments, *etc*.
4	National, multi-sectoral HIV M&E plan	There are entity-specific and timely-update M&E framework and plans. The feasibility of the M&E plans has been well tested, *etc*.
5	Annual, costed, national HIV M&E work plan	There are annual working plans and cost budgeting for M&E programmes. There are clearly time schedules for planning implementation, *etc*.
6	Communication, advocacy and culture for HIV M&E	There are advocacy activities to support M&E within the agency/organization, *etc*.
7	Routine HIV programme monitoring	Guidelines and related databases are well performed for M&E. Mechanisms/ procedures are in place to provide data reports and systematic feedback, *etc*.
8	Surveys and surveillance	There are survey and surveillance conducted for M&E, *etc*.
9	National and sub-national HIV databases	There is a functional integrated database for data capturing and storing. IT equipment, supplies and human resources are available for maintaining the database, *etc*.
10	Supportive supervision and data auditing	There are guidelines, tools and plans for supportive supervision. Supportive supervision results have been recorded and feedback are provided to supervises, *etc*.
11	HIV evaluation and research agenda	There are demand survey, program planning, financial planning for HIV evaluation. There are joint HIV program reviews during annual reporting, *etc*.
12	Data dissemination and use	HIV stakeholder information needs have been assessed.There are guidelines to support the analysis, presentation and use of data, *etc*.

In the final version, the assessment agencies were HIV working committee office, CDC, member units and social organizations at the provincial, municipal and district levels. The assessment participants were key informants in the HIV prevention and treatment system. The response formats were 4-point scale, 2-point scale and numerical responses. There were 12 components with at least 93 questions and the specific component and its contents were shown in Table 2.

In the meantime, different agencies/departments involved with different numbers of components and questions were shown in Table 3. For example, all the 12 components were contained for HIV working committee office at provincial level. Social organizations and member units at district level, however, deleted component 3, 4, 6, 7, 10, 11 and contained only 6 components.

3.2. *Field trial results*

3.2.1. *Sample description*

66 respondents' age mainly ranged from 30 to 50 years old, and most of them had bachelor degree (Table 4). Participants distributed averagely at the provincial, municipal and district levels. Most participants' technical post levels were middle-level or advanced-level. Besides, the number of part-time professionals was more than the full-time ones. A full description summary of the respondents was provided in Table 4.

3.2.2. *Internal reliability*

Examination of internal reliability results revealed a Cronbach Alpha reliability coefficient of 0.826 and the results of each component at provincial, municipal and district level varied from 0.631 to 0.924.

3.2.3. *Construct validity*

In this study, the KMO value of the variables was 0.918, which was much higher than the acceptable threshold of 0.5 (*26*). The Bartlett's test of sphericity result was high enough (χ^2 = 19714.718) with significance $p < 0.01$ (*27-29*). The results confirmed that the data were acceptable for factor analysis. Then we used the criteria of cumulative variance > 70% and 3 common factors were extracted by principal component analysis, explaining 71.808% of the total variance. Rotated component matrix was revealed in Table 5. Specifically, factor 1 comprised components 1, 2, 3, 5, 6, 10 and could be defined as the layer of basic conditions. Factor 2 comprised components 4, 7, 8, 9 and could be defined as the layer of basic function. Factor 3 comprised components 11, 12

Table 3. Numbers of components and questions in different agencies/departments

Assessment Agency	Numbers of Components Involved	Deleted Components' No.	Numbers of Questions
Provincial Level			
HIV working committee office	12	/	93
CDC	10	3, 4	77
Member units and social organizations	7	3, 4, 6, 7, 10	49
Municipal Level			
HIV working committee office	10	3, 10	75
CDC	9	3, 4, 10	67
Member units and social organizations	7	3, 4, 6, 7, 10	49
District Level			
HIV working committee office	9	3, 10, 11	66
CDC	8	3, 4, 10, 11	58
Member units and social organizations	6	3, 4, 6, 7, 10, 11	42

Table 4. Characteristics of the study participants (*n* = 66)

Variables	No. (%)	Variables	No. (%)
Age Group		Agency	
20-29 years	2 (0.030)	HIV working committee office	11 (0.167)
30-39 years	**24 (0.364)**	CDC	12 (0.182)
40-49 years	**24 (0.364)**	Member units	22 (0.333)
≥ 50 years	16 (0.242)	Social organizations	21 (0.318)
Education Level		Technical Post	
High school or under	4 (0.061)	Advanced	**16 (0.242)**
Junior college	8 (0.121)	Middle	**16 (0.242)**
Undergraduates	**42 (0.636)**	Primary	6 (0.091)
Graduates or above	12 (0.182	Others	28 (0.424)
Agency Level		Nature of Work	
Provincial	22 (0.333)	Full-time	24 (0.364)
Municipal	24 (0.364)	Part-time	**42 (0.636)**
District	20 (0.303)		

Table 5.Rotated component matrix

No.	Items	Component		
		1	2	3
1	A multi-sectoral HIV M&E system including organizational structures with HIV M&E functions	**0.798**	0.059	0.056
2	Human capacity for HIV M&E	**0.689**	0.251	0.132
3	Partnerships to plan, coordinate and manage the M&E system	**0.735**	0.392	0.274
4	National, multi-sectoral HIV M&E plan	0.033	**0.807**	0.348
5	Annual, costed, national HIV M&E work plan	**0.772**	0.095	0.249
6	Communication, advocacy and culture for HIV M&E	**0.788**	0.218	0.102
7	Routine HIV programme monitoring	0.315	**0.756**	0.102
8	Surveys and surveillance	0.082	**0.605**	0.042
9	National and sub-national HIV databases	0.339	**0.603**	0.189
10	Supportive supervision and data auditing	**0.818**	0.313	0.328
11	HIV evaluation and research agenda	0.155	0.318	**0.511**
12	Data dissemination and use	0.228	0.135	**0.609**

and could be defined as the layer of core purpose.

4. Discussion

Although it was the first attempt to translate the M&E system strengthening tool invented by UNAIDS into Chinese and to use it to gather data from M&E professionals in China, it showed great scientificity during the process of its development.

During the linguistic validation, we chose the provincial, municipal and district levels as our study sites rather than the national level because the Chinese version of the tool was special for sub-national evaluation in China. And the assessment agencies/departments we

chose were the current key positions for AIDS prevention and control system in China. Specifically, HIV working committee office was the chief mechanism for each site's coordination while member units helped build the multi-sectoral HIV M&E system. CDC provided business and technical guidance for different departments, and social organizations gave assistance for resources integration. Besides, medical institutions and community health service institutions were the specific service providers.

In order to make sure the tool was more suitable for the national conditions and specific HIV situation, we conducted focus group interviews. In this stage, experts helped us get a deeper and better understanding of HIV M&E system.

Firstly, we deleted medical institutions and community health service institutions because they were not familiar with M&E system and only responsible for antiviral therapy for AIDS patients. We also added member units at municipal and district levels at the same time because they could also provide sectoral assistance for M&E.

Secondly, unlike the UNAIDS version choosing all the components for all the agencies/departments, we selected the components and questions that were suitable for each agency/department and deleted the immeasurable ones because some agencies/departments did not contain all human and technical resources. For example, we deleted component 3 and 10 at both municipal and district levels because they were only responsible for data submitting and knowledge publicity and did not contain enough human and technical resources for the AIDS prevention and control system.

Thirdly, the number of questions was far less than the original UNAIDS version. On the one hand, we deleted some questions that were only suitable for national conditions because the original version partly developed for national level's evaluation. For example, one question in component 3 is "International development partners actively participate in the National M&E Committee coordinated by National AIDS Coordinating Authority (NACA)", which was not applicable at the provincial, municipal and district levels we assessed. On the other hand, we deleted some questions that were not fit for China's specific situation. For example, one question in component 2 is "M&E human capacity relative to the M&E system is being built through colleges, universities or technical schools". There were no majors or related courses specialized for students or colleges currently and we offered on-the-job training for capacity building in China.

In the stage of pilot study, we deleted 4 questions that were repetitive or expressed the same meaning to make the tool more readable and deleted the "Not at all" option in 5-point scale and "Not Applicable" option in 3-point scale because we found that all the questions could get corresponding answers during pilot study stage.

In the field trial study stage, we tested the validity and reliability to find out whether these adjustments above were reasonable for the tool. All the Cronbach's Alpha reliability coefficients met the requirements of surveying and demonstrated good internal reliability of the questionnaire (*30*). Construct validity results also illustrated balance of resolution for each common factor. The three layers we defined were close to the UNAIDS version's expression. Specifically, the layer of basic conditions was corresponding to the outer ring which provided fundamental to improve and sustain M&E system performance, while the layer of basic function was corresponding to middle ring which guaranteed data collecting and analyzing. And the layer of core purpose was corresponding to the center domain which represented the purpose of the M&E system (*8,12*).

This study has some limitations that should be mentioned. Firstly, the sample size was not large enough owing to limitations of time and funds which would seriously affect the stability and reliability of the results to some extent. Secondly, during the field trial study, we selected only 12 agencies/departments which might also limit the representation of the samples. We need larger sample size and better revisions about the tool considering the changes of the AIDS epidemic trends and practical application situations in the following researches.

In summary, this study was the first attempt to translate and develop the national HIV M&E capacity diagnosis tool in China. After multi-stage's discussion and modification, we selected some key components and questions to monitor and evaluate different agencies/departments. Based on our findings, it reflected great scientificity and feasibility during the process of its development and was found to be a reliable and valid tool. However, HIV M&E turned out to be a systematic project and the development of the diagnose tool was just a basic step. We should therefore consider the assessment time, the assessment subject, the operating methods as well as the data analysis and feedback as a whole in the follow-up studies to ensure effective and specific guidance for HIV M&E capacity building in China.

Acknowledgements

This project was granted by the National Natural Science Foundation of China (Grant No. 71173002).

References

1. Ekouevi DK, Karcher S, Coffiea PA. Strengthening health systems through HIV monitoring and evaluation in Sub-Saharan Africa. Curr Opin HIV AIDS. 2011; 6:245-250.
2. UNAIDS. Global report: UNAIDS report on the global AIDS epidemic 2013. *http://www.unaids.org/en/media/unaids/contentassets/documents/epidemiology/2013/gr2013/UNAIDS_Global_Report_2013_en.pdf* (accessed Nov 31, 2012).
3. National Health and Family Planning Commission of

China. 2014 China AIDS response progress report. *http://www.unaids.org.cn/en/index/topic.asp?id=1030&classname=Statements%20 and%20Updates&class=2* (accessed Mar 4, 2015).
4. State Council AIDS Working Office of China. A framework of monitoring and evaluating HIV prevention and control programmes for China (trial). People's Medical Publishing House, Beijing, China, 2000; pp. 3-15. (in Chinese)
5. Han MJ, Hu Z. The instruction manual of monitoring and evaluating HIV prevention and control programmes for China (trial). People's Medical Publishing House, Beijing, China, 2008; pp. 1-8. (in Chinese)
6. Lv K, Chen R, Ma Y, Hu H, Ma YP, Qin X, Hu Z. Analysis on the development of national HIV/ AIDS monitoring and evaluation system. Zhongguo Ji Bing Kong Zhi Za Zhi. 2012; 16:54-56. (in Chinese)
7. Hu Z, Qin X, Tang ZR, Zhu MZ, Ma SS, Li JX. Current situation evaluation of monitoring and evaluating HIV prevention and control programmes for China. The 14th National Skin Venereal Academic Convention for Chinese Medical Association. Nanjing, China, 2008. (in Chinese)
8. UNAIDS. Guidance on capacity building for HIV monitoring and evaluation. *http://www.unaids.org/en/media/unaids/contentassets/documents/document/2010/5_4_MERG_Guidance_HIV_ME_Capacity_Buidling.pdf* (accessed May 4, 2010).
9. Görgens M, Kusek JZ. Making monitoring and evaluation systems work: A capacity development toolkit. *http://www-wds.worldbank.org/external/default/WDSContentServer/WDSP/IB/2010/03/05/000333037_20100305004732/Rendered/PDF/533030PUB0moni101Official0Use0Only1.pdf* (accessed Mar 5, 2010).
10. Porter LE, Bouey PD, Curtis S, Hochgesang M, Idele P, Jefferson B, Lemma W, Myrick R, Nuwagaba-Biribonwoha H, Prybylski D, Souteyrand Y, Tulli T. Beyond indicators: Advances in global HIV monitoring and evaluation during the PEPFAR era. J Acquir Immune Defic Syndr. 2012; 60:120-126.
11. UNAIDS. Organizing framework for a functional national HIV monitoring and evaluation system. *http://www.unaids.org/en/media/unaids/contentassets/documents/document/2010/20080430_JC1769_Organizing_Framework_Functional_v2_en.pdf* (accessed Apr 30, 2008).
12. UNAIDS. Twelve components monitoring & evaluation system assessment. *http://www.unaids.org/en/media/unaids/contentassets/documents/document/2010/1_MERG_Assessment_12_Components_ME_System.pdf* (accessed Jan 10, 2010).
13. UNAIDS. Twelve components monitoring and evaluation system strengthening tool. *http://www.unaids.org/en/media/unaids/contentassets/documents/document/2010/2_MERG_Strengthening_Tool_12_Components_ME_System.pdf* (accessed Jan 10, 2010).
14. UNAIDS. Indicator standards: Operational guidelines for selecting indicators for the HIV response. *http://www.unaids.org/en/media/unaids/contentassets/documents/document/2010/4_3_MERG_Indicator_Standards.pdf* (accessed Apr 3, 2010).
15. Liu W, Watson R, Lou F. The Edinburgh Feeding Evaluation in Dementia scale (EdFED): cross-cultural validation of the simplified Chinese version in mainland China. J Clin Nurs. 2014; 23:45-53.
16. Wild D, Grove A, Martin M, Eremenco S, McElroy S, Verjee-Lorenz A, Erikson P; ISPOR Task Force for Translation and Cultural Adaptation. Principles of Good Practice for the Translation and Cultural Adaptation Process for Patient-Reported Outcomes (PRO) Measures: Report of the ISPOR Task Force for Translation and Cultural Adaptation. Value Health. 2005; 8:94-104.
17. Medrano Sánchez EM, Suárez Serrano CM, De la Casa Almeida M, Díaz Mohedo E, Chillón Martínez R. Spanish version of the broome pelvic muscle self-efficacy scale: Validity and reliability. Phys Ther. 2013; 93:1696-1706.
18. Ministry of Health of the People's Republic of China, UNAIDS, WHO. 2012 China AIDS response progress report. Chinese Journal of AIDS & STD. 2012; 1:8-11.
19. UNAIDS. A framework for monitoring and evaluating HIV prevention programmes for Most-At-Risk populations. *http://www.unaids.org/en/media/unaids/contentassets/documents/document/2010/17_Framework_ME_Prevention_Prog_MARP_E.pdf* (accessed Apr 1, 2008).
20. Center For Disease Control In Hunan Province of China. Information notification of the prevention and control programmes in Hunan, China. http://www.54md.com/news/n1/83413.html (accessed Dec 12, 2008).
21. Ma LJ. Research on Capacity Evaluation of HIV Monitoring and Evaluation System in China. Anhui Medical University, Anhui, China, 2013; pp.15-28. (in Chinese)
22. Provincial AIDS Working Committee Office in Anhui of China. Press release of the prevention and control programmes in Anhui, China, 2012. *http://www.ahwst. gov.cn/chn200909261718343/article.jsp?articleId=62321798* (accessed Nov 30, 2012).
23. Stephan A, Mayer H, Renom Guiteras A, Meyer G. Validity, reliability, and feasibility of the German version of the Caregiver Reaction Assessment scale (G-CRA): A validation study. Int Psychogeriatr. 2013; 25:1621-1628.
24. Nijboer C, Triemstra M, Tempelaar R, Sanderman R, van den Bos GA. Measuring both negative and positive reactions to giving care to cancer patients: Psychometric qualities of the Caregiver Reaction Assessment (CRA). Soc Sci Med. 1999; 48:1259-1269.
25. Fang JQ. The measuring method and application of quality of life. Unionsverlag of Peking University Health Science Center and Chinese Peking Union Medical College, Beijing, China, 2000; pp. 90-105. (in Chinese)
26. Chan CTW. The principal factors affecting construction project overhead expenses: An exploratory factor analysis approach. Construction Management and Economics. 2012; 30:903-914.
27. George D, Mallery P. SPSS for Windows Step by Step: A Simple Guide and Reference 18.0 Update. Prentice Hall, Upper Saddle River, New Jersey, USA, 2010; pp. 12-40.
28. Lattin J, Carroll JD, Green PE. Principal components analysis and exploratory factor analysis, in Analyzing Multivariate Data. Pacific Grove, CA, USA, 2003; pp. 108-165.
29. Gorsuch RL. Factor Analysis, 2nd ed., Lawrence Erlbaum Associates. Hillsdale, New Jersey, USA, 1983; pp. 1-20.
30. Wu ML. Questionnaire statistical Analysis Practice: Operation and Application of SPSS. Chongqing University Press, Chongqing, China, 2010; pp. 194-263. (in Chinese)

(Received May 15, 2015; Revised August 21, 2015; Accepted August 22, 2015)

Brief Report

DOI: 10.5582/bst.2015.01109

Toad skin extract cinobufatini inhibits migration of human breast carcinoma MDA-MB-231 cells into a model stromal tissue

Munehiro Nakata[1,*], Shuya Mori[1], Yo Kamoshida[1], Shota Kawaguchi[1], Yoko Fujita-Yamaguchi[1,2], Bo Gao[3], Wei Tang[4]

[1] *Department of Applied Biochemistry, Tokai University, Hiratsuka, Kanagawa, Japan;*
[2] *Beckman Research Institute of City of Hope, Duarte, CA 91010, USA;*
[3] *Anhui Jinchan Biochemical Co., Ltd., Anhui, China;*
[4] *Hepato-Biliary-Pancreatic Surgery Division, Department of Surgery, Graduate School of Medicine, The University of Tokyo, Tokyo, Japan.*

Summary **Toad skin extract cinobufatini study has been focused on anticancer activity, especially apoptosis-inducing activity by bufosteroids. The present study examined effect of the toad skin extract on cancer cell migration into model stromal tissues. Human breast carcinoma cell line MDA-MB-231 was incubated in the presence or absence of toad skin extract on a surface of reconstituted type I collagen gel as a model stromal tissue allowing the cells to migrate into the gel. Frozen sections were microscopically observed after azan staining. Data showed a decrease of cell number in a microscopic field and shortening of cell migration into the model stromal tissue in a dose dependent manner. This suggests that toad skin extract may possess migration-preventing activity in addition to cell toxicity such as apoptosis-inducing activity. The multifaceted effects including apoptosis-inducing and cancer cell migration-preventing activities would improve usefulness of toad skin extract cinobufatini as an anticancer medicine.**

Keywords: Toad skin extract cinobufatini, cell migration, type I collagen, cancer

1. Introduction

An aqueous extract from the skin of toad *Bufo bufo* gargarizans Cantor is used as a source of the Chinese traditional medicine cinobufacini (*1*). The toad skin extract has been found to possess anticancer activity (*2-4*). Although the detailed nature of the ingredients contained in the extract remains unknown, recent studies have revealed that a series of bufosteroids such as bufalin, cinobufagin, and regibufogenin shows apoptosis-inducing activity against cancer cells *via* some cell signaling pathways (*2,5-7*).

Carcinoma cells that begin in epithelial tissues first destroy basement membranes and start to infiltrate and invade into stromal tissues (*8,9*). In this process, various types of metalloproteinases are involved in degradation of matrix proteins such as collagens (*10,11*). Since cell infiltration and invasion is the first step of metastasis, it should be important to inhibit this step to control cancer.

Our previous study reported a method for assessment of cancer cell invasion into reconstituted a type I collagen gel as a model stromal tissue that includes processes of freeze sectioning and azan staining (*12*). The method permits us to observe the distribution of the cells migrating into the collagen gels from the gel surface and to evaluate invading ability of cancer cells and inhibiting activity of compounds of interest against cancer cell invasion. The present study applied this method to analyze the effect of toad skin extract on cell migration into the model stromal tissue. We describe that toad skin extract may possess cancer cell migration-preventing activity in addition to cell toxicity such as apoptosis-inducing activity.

2. Materials and Methods

2.1. *Reagents*

Toad skin extract cinobufatini was kindly provided by

**Address correspondence to:*
Dr. Munehiro Nakata, Department of Applied Biochemistry, Tokai University, Hiratsuka, Kanagawa 259-1292, Japan.
E-mail: nak@tsc.u-tokai.ac.jp

Anhui Jinchan Biochemical Co., Ltd., Anhui, China. Bovine skin collagen type I was purchased from (Koken, Tokyo, Japan) and diluted to 1 mg/mL in 0.05 M acetic acid before use. Reconstitution buffer used to prepare reconstituted type I collagen gels was 1 M Hepes buffer, pH 7.4, containing 10 M $NaHCO_3$. All the chemicals used were of analytical grade.

2.2. *Cells*

Human breast carcinoma cell line MDA-MB-231 was obtained from American Type Culture Collection (ATCC; Rockville, MD, USA). The cells were maintained in high-glucose Dulbecco's modified Eagle's medium (DMEM; Invitrogen, Carlsbad, CA, USA) containing 10% fetal calf serum (FCS) supplemented with penicillin-streptomycin and 2 mM glutamine at 37°C in a 5% CO_2 atmosphere. The cells were harvested after preincubation in serum-free medium for 24 h at 37°C and subjected to experiments.

2.3. *Bilayer reconstituted type I collagen gel*

Bilayer reconstituted type I collagen gels were prepared in wells of an 8-well chamber slide (Nalge Nunc, Naperville, IL, USA) as described previously (*12*) with minor modifications. Briefly, lower gels were prepared by mixing 100 µL of 0.1% collagen solution with 10% FCS, DMEM, and reconstitution buffer (8:1:1, v/v) in an 8-well chamber slide. Two-hundred µL of type I collagen solution without FCS was mixed with or without 1 µL of toad skin extract diluent and incubated on the lower gel at 37°C to form the upper gel.

2.4. *Histochemical observation of cell distribution in the gel*

Cell suspensions (10^5 cells/mL) were preincubated in the presence or absence of toad skin extract diluent for 30 min at 37°C. The suspension (250 µL each) was loaded onto the reconstituted type I collagen gel in a chamber slide and incubated for 3 h at 37°C in a 5% CO_2 atmosphere. After incubation, the gel surface was rinsed twice with 250 µL of phosphate-buffered saline and then DMEM containing 0.1% BSA to remove unbound cells. The gel was subsequently incubated for 15 h at 37°C in a 5% CO_2 atmosphere to allow the cells to migrate into the gel.

After removing the medium on the gel surface, the gel was then mounted using an embedding compound (Tissue-Tek O.C.T. Compound; Sakura Finetechnical, Tokyo, Japan) and frozen at –80°C. The frozen gel was sliced perpendicularly to the gel surface with a cryostat at a 50 µm thickness and the section was placed on a glass slide.

Frozen sections of reconstituted type I collagen gel into which cells were allowed to migrate were stained by the azan staining method as described previously (*12*). The sections stained were observed under a microscope (×200; BX-51, Olympus, Tokyo, Japan).

2.5. *Data analysis*

Migration distance of each cell from the gel surface was measured using at least 5 photographs of microscopic visual fields (× 200) or at least 150 cells. The Mann–Whitney *U* test was conducted with StatMate III software (ATMS, Tokyo, Japan) and a p value less than 0.05 was considered significant.

3. Results and Discussion

Figures 1A and 1B show typical microphotographs of frozen sections of reconstituted collagen gels after incubating cells in the absence or presence of toad skin extract, respectively. Histochemical observation of MDA-MB-231 cells in type I collagen gels showed that some cells remained on the gel surface and the others migrated into the gel with a wide range of distribution from the gel surface (Figure 1A). In contrast, at a glance, the number of cells observed in a microscopic field was decreased in the presence of toad skin extract (Figure 1B). The decrease in the number of cells depended on the concentration of toad skin extract when undiluted and ×100-diluted extract was added in the cell suspensions (Table 1).

Toad skin extract has been known to have potent anticancer activity (*2-4,13,14*). Some reports have suggested that apoptosis of cancer cell lines was induced by bufosteroids, unique steroid compounds contained in toad skin extract and toad venom, such as bufalin and cinobufagin (*15-19*). Decrease in MDA-MB-231 cell numbers observed in our experiments may

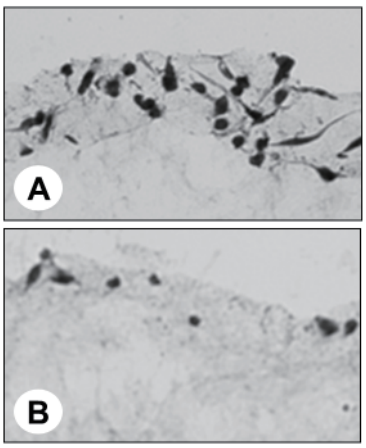

Figure 1. Typical histochemical observations of type I collagen gels where cells were allowed to migrate into the gels. MDA-MB-231 cells were allowed to migrate into type I collagen gels in the absence **(A)** or presence **(B)** of toad skin extract. The frozen sections were stained with azan and observed under a microscope. Original magnification: ×200.

Table 1. Decrease in the numbers of cells observed in microscopic fields by toad skin extract treatment

Treatments	% (means ± SD)[a]
Control	100
Toad skin extract	
×100-Diluted	35.5 ± 7.6
Undiluted	19.8 ± 5.3

[a] MDA-MB-231 cells treated with or without toad skin extract diluents were allowed to migrate into type I collagen gels. The frozen sections were stained with azan as described in Materials and Methods. Cell numbers observed in microscopic fields were counted and compared with untreated control.

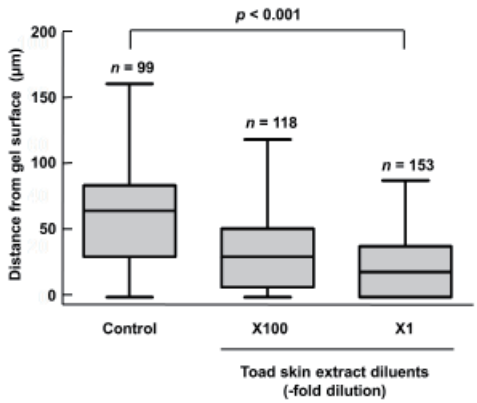

Figure 2. Effect of toad skin extract on cancer cell migration into type I collagen gels. MDA-MB-231 cells were treated with toad skin extract diluents as indicated in the figure and allowed to migrate into type I collagen gels with or without toad skin extract diluents. The frozen sections were stained with azan and then the distance from the gel surface was measured for each cell in microscopic fields.

be due to apoptosis of the cells in the presence of toad skin extract.

Figure 2 shows the distribution of the distance that cells migrated from the gel surface for untreated control cells and cells treated with various concentrations of toad skin extract. Some cells migrated a relatively long distance in the presence of toad skin extract but the median distance that cells migrated from the gel surface was significantly shorter depending on the concentration of toad skin extract (Figure 2).

Cancer cell migration and invasion are promoted by a degradation of matrix collagen by metalloproteinases (*20-22*). In our previous paper, we reported suppression of MDA-MB-231 cell migration into type I collagen gels in the presence of galardin which is known as an MMP inhibitor (*12*). Our present data suggest that toad skin extract may contain unknown compounds possessing MMP inhibitor activity. Actually, a preliminary study using metalloproteinase activity of FCS and a synthetic peptide analog as a substrate showed that the enzyme activity was inhibited by diluents of toad skin extract but not by bufosteroids such as bufalin, cinobufagin, and regibufogenin (unpublished data). This suggests that unknown compounds other than bufosteroids might participate in inhibiting metalloproteinase activity and result in suppressing cancer cell migration in the collagen gels. Further investigation to clarify the nature of the compounds is needed.

4. Conclusion

Toad skin extract cinobufatini study has been focused on anticancer activity, especially apoptosis-inducing activity by bufosteroids. Recently, cinobufatini has been clinically applied to patients with cancer (*23-25*). The present study suggests that the toad skin extract has an additional anticancer activity because it prevents cancer cell migration in model stromal tissues. Multifaceted effects such as apoptosis-inducing and migration-preventing activities should improve the usefulness of cinobufatini as an anticancer medicine.

References

1. Lu CX, Nan KJ, Lei Y. Agents from amphibians with anticancer properties. Anticancer Drugs. 2008; 19:931-939.
2. Qi F, Li A, Inagaki Y, Kokudo N, Tamura S, Nakata M, Tang W. Antitumor activity of extracts and compounds from the skin of the toad *Bufo bufo* gargarizans Cantor. Int Immunopharmacol. 2011; 11:342-349.
3. Man S, Gao W, Wei C, Liu C. Anticancer drugs from traditional toxic Chinese medicines. Phytother Res. 2012; 26:1449-1465.
4. Qi J, Tan CK, Hashimi SM, Zulfiker AH, Good D, Wei MQ. Toad glandular secretions and skin extractions as anti-inflammatory and anticancer agents. Evid Based Complement Alternat Med. 2014; 2014:312684.
5. Qi FH, Li AY, Lv H, Zhao L, Li JJ, Gao B, Tang W. Apoptosis-inducing effect of cinobufacini, *Bufo bufo* gargarizans Cantor skin extract, on human hepatoma cell line BEL-7402. Drug Discov Ther. 2008; 2:339-343.
6. Wang JY, Chen L, Zheng Z, Wang Q, Guo J, Xu L. Cinobufocini inhibits NF-κB and COX-2 activation induced by TNF-α in lung adenocarcinoma cells. Oncol Rep. 2012; 27:1619-1624.
7. Wang D, Bi Z. Bufalin inhibited the growth of human osteosarcoma MG-63 cells *via* down-regulation of Bcl-2/Bax and triggering of the mitochondrial pathway. Tumour Biol. 2014; 35:4885-4890.
8. Hagedorn EJ, Sherwood DR. Cell invasion through basement membrane: the anchor cell breaches the barrier. Curr Opin Cell Biol. 2011; 23:589-596.
9. Valastyan S, Weinberg RA. Tumor metastasis: molecular insights and evolving paradigms. Cell. 2011; 147:275-292.
10. Liotta LA, Thorgeirsson UP, Garbisa S. Role of collagenases in tumor cell invasion. Cancer Metastasis Rev. 1982; 1:277-288.
11. Ennis BW, Matrisian LM. Matrix degrading metalloproteinases. J Neurooncol. 1994; 18:105-109.
12. Fukuda K, Kamoshida Y, Kurokawa T, Yoshida M, Fujita-Yamaguchi Y, Nakata M. Migration of breast cancer cells into reconstituted type I collagen gels assessed *via* a combination of frozen sectioning and azan staining. Biosci Trends. 2014; 8:212-216.

13. Qi F, Li A, Zhao L, Xu H, Inagaki Y, Wang D, Cui X, Gao B, Kokudo N, Nakata M, Tang W. Cinobufacini, an aqueous extract from *Bufo bufo* gargarizans Cantor, induces apoptosis through a mitochondria-mediated pathway in human hepatocellular carcinoma cells. J Ethnopharmacol. 2010; 128:654-661.
14. Qi F, Li A, Inagaki Y, Xu H, Wang D, Cui X, Zhang L, Kokudo N, Du G, Tang W. Induction of apoptosis by cinobufacini preparation through mitochondria- and Fas-mediated caspase-dependent pathways in human hepatocellular carcinoma cells. Food Chem Toxicol. 2012; 50:295-302.
15. Wang DL, Qi FH, Xu HL, Inagaki Y, Orihara Y, Sekimizu K, Kokudo N, Wang FS, Tang W. Apoptosis-inducing activity of compounds screened and characterized from cinobufacini by bioassay-guided isolation. Mol Med Rep. 2010; 3:717-722.
16. Qi F, Inagaki Y, Gao B, Cui X, Xu H, Kokudo N, Li A, Tang W. Bufalin and cinobufagin induce apoptosis of human hepatocellular carcinoma cells *via* Fas- and mitochondria-mediated pathways. Cancer Sci. 2011; 102:951-958.
17. Jiang L, Zhao MN, Liu TY, Wu XS, Weng H, Ding Q, Shu YJ, Bao RF, Li ML, Mu JS, Wu WG, Ding QC, Cao Y, Hu YP, Shen BY, Tan ZJ, Liu YB. Bufalin induces cell cycle arrest and apoptosis in gallbladder carcinoma cells. Tumour Biol. 2014; 35:10931-10941.
18. Zhao H, Zhao D, Tan G, Liu Y, Zhuang L, Liu T. Bufalin promotes apoptosis of gastric cancer by down-regulation of miR-298 targeting bax. Int J Clin Exp Med. 2015; 8:3420-3428.
19. Baek SH, Kim C, Lee JH, Nam D, Lee J, Lee SG, Chung WS, Jang HJ, Kim SH, Ahn KS. Cinobufagin exerts anti-proliferative and pro-apoptotic effects through the modulation ROS-mediated MAPKs signaling pathway. Immunopharmacol Immunotoxicol. 2015; 37:265-273.
20. Zhang J, Li X, Zhu HW, Wang Q, Feng JH, Mou JJ, Li YG, Fang H, Xu WF. Design, synthesis, and primary activity evaluation of pyrrolidine derivatives as matrix metalloproteinase inhibitors. Drug Discov Ther. 2010; 4:5-12.
21. Tauro M, McGuire J, Lynch CC. New approaches to selectively target cancer-associated matrix metalloproteinase activity. Cancer Metastasis Rev. 2014; 33:1043-1057
22. Davies KJ. The complex interaction of matrix metalloproteinases in the migration of cancer cells through breast tissue stroma. Int J Breast Cancer. 2014; 2014:839094.
23. Qin TJ, Zhao XH, Yun J, Zhang LX, Ruan ZP, Pan BR. Efficacy and safety of gemcitabine-oxaliplatin combined with huachansu in patients with advanced gallbladder carcinoma. World J Gastroenterol. 2008; 14:5210-5216.
24. Meng Z, Yang P, Shen Y, Bei W, Zhang Y, Ge Y, Newman RA, Cohen L, Liu L, Thornton B, Chang DZ, Liao Z, Kurzrock R. Pilot study of huachansu in patients with hepatocellular carcinoma, nonsmall-cell lung cancer, or pancreatic cancer. Cancer. 2009; 115:5309-5318.
25. Sun T, Zhang Y, Shen Y, Hu K, Zuo M. A case of advanced lung cancer with malignant pericardial effusion treated by intrapericardial Cinobufacini injection instillation. Biosci Trends. 2014 Jul 20.

(Received August 2, 2015; Accepted August 12, 2015)

Brief Report

DOI: 10.5582/bst.2015.01059

Diseases that precede disability among latter-stage elderly individuals in Japan

Takashi Naruse*, Mahiro Sakai, Hiroshige Matsumoto, Satoko Nagata

Department of Community Health Nursing, Graduate School of Medicine, The University of Tokyo, Tokyo, Japan.

Summary **Understanding causes of disability among elderly individuals is an important public health issue, particularly because of the increasing rate of disabled elderly individuals and the social costs in a rapidly aging society. Accordingly, we aimed to describe the diseases that precede disability and investigate the types of diseases that are related to severe disability among Japanese elderly individuals aged over 75 years. Using claim data from the latter-stage elderly healthcare system and long-term care insurance system, we identified 76,265 elderly individuals over 75 years old who did not qualify as disabled on April 1, 2011. Among them, 3,715 elderly individuals who had been newly qualified as disabled between April 1, 2011 and March 31, 2012 were selected. Disease codes from the medical claim data in the 6 months prior to disability were collected. All descriptions were developed separately for six groups divided by gender and disability level (low, middle, and high). The results of the ordinal logistic analysis including sex and age revealed that men tended to have significantly higher levels of disability ($\beta = 0.417$, $p < 0.001$) than women. Cerebrovascular disorder (CVD) was the most common disease in almost all age and disability level groups. In low-level disability groups, cancer in men (12.8%) and arthropathy and fracture in women (11.9% and 13.5%, respectively) were as common as cerebrovascular disorder (12.2% and 9.7%, in men and women, respectively). Stroke was the most common disease for all genders and disability levels. The diseases preceding low-level disability differed by gender. This study demonstrated the need to consider arthropathy and fracture as well as CVD in order to prevent disability.**

Keywords: Disability, disease, potential risk factors for disability, aging, long-term care

1. Introduction

Understanding the cause of disability and factors that precede it among elderly individuals is important to ensure both prevention of disability and cost saving in care for disabled persons. In Japan, disabled elderly individuals are supported by the long-term care insurance system (*1*), which covers long-term care services including home visits and institutional care service. In March 2014, about 53% of disabled persons who received long-term care services were mildly disabled (care levels 1-3 in the Japanese long-term care insurance system), while 47% were severely disabled (care level 4 or 5).

Cerebrovascular disorder (CVD), including stroke, has been reported as the most common disease among disabled persons. Adamson and colleagues found that the effect of CVD on disability was greater than that of other chronic diseases among UK adults (*2*). In the US, stroke is a leading cause of disability (*3*). Further, in a nationwide self-reported survey, over 33.0% of disabled people recognized that the direct cause of their disability was CVD (*4*).

However, in Newman and Brach's (*5*) review, arthritis was reported as the greatest cause of disability among elderly individuals because it limits their everyday activities. While the impact of arthritis on disability severity might be smaller than that of CVD, from a public health perspective, the benefit of preventing mild disability among elderly individuals might be comparable

**Address correspondence to:*
Dr. Takashi Naruse, Department of Community Health nursing, Graduate School of Medicine, the University of Tokyo, 7-3-1, Hongo, Bunkyo-ku, Tokyo 113-0033, Japan.
E-mail: takanaruse-tky@umin.ac.jp

to that related to preventing CVD.

Objective data collection instruments are preferred in measuring disability; however, the majority of studies rely on self-report measures of disability (*5*). This might lead to problems of reliability in measuring disability and detecting disabled elderly individuals. In Japan, claim data from the long-term care insurance system can provide objective information on who is disabled among elderly individuals, when s/he became disabled, and how severely s/he is disabled. Further, other claim data from the healthcare system (latter-stage elderly healthcare system) can provide objective information about disease among disabled elderly individuals. If we merge the two types of claim data, we can determine the diagnosed disease that preceded disability. This study aimed to describe the kinds of diseases that preceded disability and investigate the types of diseases that are related to severe disability among Japanese elderly individuals. Because of data availability, we targeted individuals aged at least 75 years.

2. Methods

2.1. *Definition of disability*

We referred to the qualification of the long-term care insurance system for service use as a disability index. It ranged in terms of support level from care level 1 to 5, which indicate increasing difficulty and need for assistance with activities of daily living. Care level 1 indicates "having difficulty in independent walking or daily activity, but not chair bound," care levels 2 and 3 mean "almost chair bound, but not bedridden," and care levels 4 and 5 indicate "almost or completely bedridden." For ease of understanding, care levels 1, 2/3, and 4/5 were categorized as low, middle, and high disability, respectively.

The certification was based on the clients' or their families' proposal to local governments, and the certification level was determined based on two perspectives: the standardized statistical algorithm for estimating the amount of care requirements and a local committee of specialists (*i.e.* physicians, public health nurses, social workers, and so on).

Elderly individuals were considered "newly disabled" when they had not been certified for more than 2 months, and then certification was detected in the next month based on receipt data. In the Japanese certification system, disabled individuals rarely distinguish their certification in 1 month due to any systematic errors. We consulted with two specialists on a local committee, and this algorithm was considered valid to detect disabled elderly individuals.

2.2. *Design and data collection*

We used claim data from the latter-stage elderly healthcare system and the long-term care insurance system in Fukui prefecture, Japan. The data from the latter-stage elderly healthcare system was provided by the Fukui Latter-Stage Elderly Healthcare System Association, and the data from the long-term care insurance system was provided by the Fukui National Health Insurance Organization. Two types of claim data were managed by the different organizations; however, we can merge them and identify the same individuals with a common ID. Using the merged data, we can determine each person's medical and long-term care insurance service consumption volume, disability level, disease code, and region for each month.

This study was conducted under a large collaborative study called the Fukui Gerontology Study of Fukui prefecture and Institute of Gerontology, The University of Tokyo. In this study, Fukui prefecture, the Fukui National Health Insurance Organization, the Fukui Latter-Stage Elderly Healthcare System Association, and the University of Tokyo collaborated from April 2011 to March 2015. All data were provided for researchers in the form of anonymous electric data. The Ethics Committee of the Graduate School of Medicine at the University of Tokyo approved this study.

2.3. *Subjects*

First, elderly individuals aged 75 years or older who were insured by the Fukui latter-stage elderly healthcare system from April 1, 2011 through March 31, 2012 were detected. On April 1, 102,450 elderly individuals were observed. Between April 1 and March 31, 1,627 elderly individuals (1.6%) dropped out after moving or for other unknown reasons, and 6,411 (6.4%) had deceased. We excluded 1,627 individuals who dropped out, leaving a total of 100,823 elderly individuals. Among them, 24,558 were already disabled with low- (5,920; 24.1%), middle- (10,166; 41.4%), and high-level disabilities (8,392; 34.1%), and 80 (0.3%) had been certified as low- or middle-level disability in February or March, but not in April 2011. Thus, there were 76,265 elderly individuals that remained non-disabled on April 1, 2011. We followed up their claim data and detected newly disabled persons between April 2011 and March 2012 (n = 3,715), whose data were then analyzed.

2.4. *Definition of the disease preceding disability*

For newly disabled elderly individuals, we observed the disease code in the latter-stage elderly healthcare system claim data over the 6 months preceding disability. The latter-stage elderly healthcare system claim data includes five separate types of medical consumption data for elderly individuals: admission to hospital, outpatient, dentistry, pharmacy, and home-visiting nursing. We included all types of data and investigated

the diseases that were coded in the 6 months preceding disability.

We focused on nine types of diseases as predisposing factors for disability: (1) cancer (C00-97 in ICD-10); (2) CVD (I60, 61, 63, 69.0, 69.1, 69.3); (3) arthropathy (M15-19); (4) fracture (S02, S12, S22, S32, S42, S52, S62, S72, S82, S92 T02, T08, T10, T12); (5) pneumonia J12-18); (6) chronic obstructive pulmonary disease (COPD, J41-44); (7) dementia (F01, F03, G30); (8) psychiatric disorder (F20-48); and (9) neurological disorder (G00-29, G31-99). If one or more corresponding code for each of these nine diseases was detected in 6 months, the person was considered to have the disease. Other types of individual information, including age at certified month and sex, were collected from receipt data.

2.5. *Analysis*

First, a *t*-test compared the mean age of certified month between men and women. Second, we separately summarized percentages of each disease according to sex and disability level (low, middle, high). To determine the age-adjusted differences of disability level among men and women, multivariate ordinal logistic analysis for disability level (1 = low, 2 = middle, 3 = high) was conducted. Lastly, in order to investigate the types of diseases associated with severe disability, multivariate ordinal logistic regression analysis for disability level was conducted for men and women separately, with age and nine types of diseases included as independent variables. SPSS version 22.0 for Windows was used for all analysis, and $p < 0.05$ was defined as significant.

3. Results and Discussion

The mean age of certified month was 84.2 years (standard deviation (SD) = 5.1; range: 75-103). Men were younger at first certified age (83.5 (SD = 4.8) in men and 84.8 (SD = 5.1) in women, $p < 0.001$). In Table 1, among all newly disabled elderly individuals, low-level disability was present in 1,705 (45.9%) participants, and high-level disability was present in 681 (18.3%). These percentages were quite different from the cross-sectional prevalence of disability level in April 2011: 24.1%, 41.4%, and 34.1% for low-, middle-, and high-level disability, respectively. This difference suggests that about half of latter-stage elderly individuals have low-level disabilities initially, but then ultimately progress to higher stages of disability.

For men, there were 617 (39.8%) individuals with low-level disability and 327 (21.1%) with high-level disability. For women, 1,088 (50.2%) individuals had low-level disability, and 354 (16.3%) had high-level disability. The results of the ordinal logistic analysis including sex and age revealed that men tended to have significantly higher levels of disability ($\beta = 0.417$, $p < 0.001$) than women. These results can be understood from two perspectives. First, men tend to be disabled more severely initially, or second, men tend to avoid filing their qualification for long-term care insurance until their disability worsens. The former is supported by the disease distribution presented in Table 2. Ordinal logistic analysis including age and disease showed that there were no sex differences in the relationship between disease and disability severity. In both men and women, cancer, CVD, fracture, pneumonia significantly related to higher levels of disability, and arthropathy and dementia significantly related to lower levels of disability. In men, CVD and cancer are the most common diseases at all disease levels (12.2%, 15.9%, and 27.8% for CVD and 12.8%, 18.8%, 16.8% for cancer for low, middle, and high levels, respectively). On the other hand, arthropathy and fracture were more common in low- and middle-level disabled women than they were in men (11.9% *vs*. 7.1% and 10.9% *vs*. 6.0% for arthropathy among low- and middle-level disability, respectively; 8.2% *vs*. 4.7% and 17.2% *vs*. 6.3% for fracture among low- and middle-level disability, respectively). With regard to diseases that precede disability, these results imply that men tend to have a higher number of diseases that are associated with severe disability, than women. This may be because of the age-specific rate of stroke is higher in men generally (*6*), and thus, men could be considered to have a greater risk for more severe disability.

Table 1. Frequency of disease and disability level (*n* = 3,715)

Items	Total	Low	Middle	High
Total	3,715 (100.0%)	1,705 (45.9%)	1,329 (35.8%)	681 (18.3%)
Cancer	410 (11.0%)	138 (8.1%)	179 (13.5%)	93 (13.7%)
CVD	507 (13.6%)	180 (10.6%)	159 (12.0%)	168 (24.7%)
Arthropathy	306 (8.2%)	174 (10.2%)	102 (7.7%)	30 (4.4%)
Fracture	343 (9.2%)	118 (6.9%)	142 (10.7%)	83 (12.2%)
Pneumonia	111 (3.0%)	31 (1.8%)	51 (3.8%)	29 (4.3%)
COPD	68 (1.8%)	28 (1.6%)	28 (2.1%)	12 (1.8%)
Dementia	284 (7.6%)	207 (12.1%)	63 (4.7%)	14 (2.1%)
Psychiatric	158 (4.3%)	92 (5.4%)	49 (3.7%)	17 (2.5%)
Neurological disorder	208 (5.6%)	103 (6.0%)	76 (5.7%)	29 (4.3%)

Values are presented as *n* (%); CVD, cerebral vascular disorder; COPD, chronic obstructive pulmonary disease.

Table 2. Frequency of disease and disability level by sex (*n* = 3,715)

Items	Total	Low	Middle	High	B*	*p*
Men	1,549 (100.0%)	617 (39.8%)	605 (39.1%)	327 (21.1%)		
Cancer	248 (16.0%)	79 (12.8%)	114 (18.8%)	55 (16.8%)	0.286	0.029
CVD	262 (16.9%)	75 (12.2%)	96 (15.9%)	91 (27.8%)	0.766	< 0.001
Arthropathy	90 (5.8%)	44 (7.1%)	36 (6.0%)	10 (3.1%)	- 0.512	0.015
Fracture	96 (6.2%)	29 (4.7%)	38 (6.3%)	29 (8.9%)	0.561	0.004
Pneumonia	73 (4.7%)	19 (3.1%)	36 (6.0%)	18 (5.5%)	0.470	0.036
COPD	55 (3.6%)	20 (3.2%)	23 (3.8%)	12 (3.7%)	0.159	0.538
Dementia	98 (6.3%)	60 (9.7%)	32 (5.3%)	6 (1.8%)	- 0.951	< 0.001
Psychiatric	55 (3.6%)	28 (4.5%)	19 (3.1%)	8 (2.4%)	- 0.410	0.125
Neurological disorder	91 (5.9%)	37 (6.0%)	38 (6.3%)	16 (4.9%)	- 0.106	0.607
Women	2,166 (100.0%)	1,088 (50.2%)	724 (33.4%)	354 (16.3%)		
Cancer	162 (7.5%)	59 (5.4%)	65 (10.7%)	38 (11.6%)	0.626	< 0.001
CVD	245 (11.3%)	105 (9.7%)	63 (10.4%)	77 (23.5%)	0.645	< 0.001
Arthropathy	216 (10.0%)	130 (11.9%)	66 (10.9%)	20 (6.1%)	- 0.428	0.003
Fracture	247 (11.4%)	89 (8.2%)	104 (17.2%)	54 (16.5%)	0.588	< 0.001
Pneumonia	38 (1.8%)	12 (1.1%)	15 (2.5%)	11 (3.4%)	0.727	0.017
COPD	13 (0.6%)	8 (0.7%)	5 (0.8%)	0 (0.0%)	- 0.581	0.332
Dementia	186 (8.6%)	147 (13.5%)	31 (5.1%)	8 (2.4%)	- 1.284	< 0.001
Psychiatric	103 (4.8%)	64 (5.9%)	30 (5.0%)	9 (2.8%)	- 0.381	0.070
Neurological disorder	117 (5.4%)	66 (6.1%)	38 (6.3%)	13 (4.0%)	- 0.288	0.130

Values are presented as *n* (%); CVD, cerebral vascular disorder; COPD, chronic obstructive pulmonary disease; *B, partial regression coefficient in the ordinal regression analysis for disability level (1 = low, 2 = middle, 3 = high), adjusted with age.

The latter perspective is supported by previous studies regarding underuse of services. Elderly individuals and their caregivers have been reported to underuse long-term care services until informal care arrangements become unmanageable (*7*). In Japan, the most common primary caregivers are cohabitant spouses (26.2% in 2013) and women (68.7%) (*4*). Because healthy life expectancy is longer in women than it is in men (*8*), men might be able to depend on their wives for caregiving. On the other hand, women might not be able to depend on their husbands. In addition to a shorter healthy life expectancy, male caregivers require more formal help (*9*). The difference in intention to recruit outside support might relate to differences in disability level among newly qualified elderly individuals differently by gender.

For the total sample, the most frequent disease was CVD (13.6% of all newly disabled elderly individuals). The association between stroke and disability has been examined in several reviews. In the Global Burden of Disease Study, Murray and Lopez (*10*) estimated that, in developed regions, the leading causes of loss of disability-adjusted life years include CVD. In the Japanese nationwide survey "Comprehensive Survey of Living Conditions," participants living with disabled persons were asked about the direct cause of disability, and the most common disease among highly disabled persons is CVD (about 30–35% of participants) (*4*). Because these were the results of caregiver self-reports, under-reporting or over-reporting is a possibility. Our findings show the same trend for CVD, supporting the suggestion that CVD is the most common disease directly preceding disability in elderly individuals.

Our results further provide evidence for the effect of arthropathy, fracture, and dementia on incidence of disability. For women, these diseases accounted for about 10% of low-level disabled women (Table 2). This percentage was about the same as CVD. Because about half of newly disabled elderly individuals had difficulty with daily living as a result of low-level disability, prevention of low-level disability could have a substantial effect on extending healthy life expectancy. In order to prevent low-level disability, especially among women, it is important to address arthropathy, fracture, and dementia in addition to CVD.

Because our analysis was conducted retrospectively, we could not detect the exact risk of having each disease on disability. In order to better demonstrate the importance of disease prevention, prospective observations are necessary. Further, the data were obtained from one prefecture, and thus, we cannot apply the findings to other Japanese regions or other countries.

In conclusion, we found that CVD was the most common disease in the 6 months preceding disability among elderly individuals across most age and disability groups. In low-level disabled women, arthropathy and fracture were as common as CVD was. Because the frequency of low-level disability was three times greater than that of high-level disability in women, this finding emphasizes the need to consider arthropathy and fracture as well as CVD in order to prevent disability.

Acknowledgements

Financial support for this study was provided by the Health Labor Sciences Research program in 2013 and 2014, and a Grant-in-Aid for Scientific Research (KAKENHI), in 2013, Japan. Professor Yasushi

Iwamoto of The University of Tokyo was the chief of the study team for the claim data analysis, Fukui Gerontology Study. Associate Professor Ryoko Morozumi of the University of Toyama and Associate Professor Michio Yuda of Chukyo University were the board members of the Fukui Gerontology Study. They contributed to the claim data collection in this study. The authors would like to thank the staff of Fukui prefecture and the Institute of Gerontology at The University of Tokyo for their assistance in carrying out this research project.

References

1. Tsutsui T, Muramatsu N. Japan's universal long-term care system reform of 2005: Containing costs and realizing a vision. J Am Geriatr Soc. 2007; 55:1458-1463.
2. Adamson J, Beswick A, Ebrahim S. Is stroke the most common cause of disability? J Stroke Cerebrovasc Dis. 2004; 13:171-177.
3. American Stroke Association. About stroke. *http://www.strokeassociation.org/STROKEORG/AboutStroke/About-Stroke_UCM_308529_SubHomePage.jsp* (accessed March 30, 2015).
4. Ministry of Health, Labour and Welfare. Comprehensive Survey of Living Conditions (2013). *http://www.mhlw.go.jp/toukei/saikin/hw/k-tyosa/k-tyosa13/* (accessed March 30, 2015).
5. Newman AB, Brach JS. Gender gap in longevity and disability in older persons. Epidemiol Rev. 2001; 23:343-350.
6. Reeves MJ, Bushnell CD, Howard G, Gargano JW, Duncan PW, Lynch G, Khatiwoda A, Lisabeth L. Sex differences in stroke: Epidemiology, clinical presentation, medical care, and outcomes. Lancet Neurol. 2008; 7:915-926.
7. Kadushin G. Home health care utilization: A review of the research for social work. Health Soc Work. 2004; 29:219-244.
8. Liu Y, Arai A, Obayashi Y, Kanda K, Boostrom E, Lee RB, Tamashiro H. Trends of gender gaps in life expectancy in Japan, 1947-2010: Associations with gender mortality ratio and a social development index. Geriatr Gerontol. 2013; 13:92-97.
9. Naruse T, Nagata S, Taguchi A, Murashima S. Classification tree model identifies home-based service needs of Japanese long-term care insurance consumers. Public Health Nurs. 2010; 28:223-232.
10. Murray CJ, Lopez AD. Alternative projections of mortality and disability by cause 1990–2020: Global Burden of Disease Study. Lancet. 1997; 349:1498-1504.

(Received April 22, 2015; Revised June 15, 2015; Accepted June 18, 2015)

BST
BioScience Trends

Guide for Authors

1. Scope of Articles

BioScience Trends is an international peer-reviewed journal. BioScience Trends devotes to publishing the latest and most exciting advances in scientific research. Articles cover fields of life science such as biochemistry, molecular biology, clinical research, public health, medical care system, and social science in order to encourage cooperation and exchange among scientists and clinical researchers.

2. Submission Types

Original Articles should be well-documented, novel, and significant to the field as a whole. An Original Article should be arranged into the following sections: Title page, Abstract, Introduction, Materials and Methods, Results, Discussion, Acknowledgments, and References. Original articles should not exceed 5,000 words in length (excluding references) and should be limited to a maximum of 50 references. Articles may contain a maximum of 10 figures and/or tables.

Brief Reports definitively documenting either experimental results or informative clinical observations will be considered for publication in this category. Brief Reports are not intended for publication of incomplete or preliminary findings. Brief Reports should not exceed 3,000 words in length (excluding references) and should be limited to a maximum of 4 figures and/or tables and 30 references. A Brief Report contains the same sections as an Original Article, but the Results and Discussion sections should be combined.

Reviews should present a full and up-to-date account of recent developments within an area of research. Normally, reviews should not exceed 8,000 words in length (excluding references) and should be limited to a maximum of 100 references. Mini reviews are also accepted.

Policy Forum articles discuss research and policy issues in areas related to life science such as public health, the medical care system, and social science and may address governmental issues at district, national, and international levels of discourse. Policy Forum articles should not exceed 2,000 words in length (excluding references).

Case Reports should be detailed reports of the symptoms, signs, diagnosis, treatment, and follow-up of an individual patient. Case reports may contain a demographic profile of the patient but usually describe an unusual or novel occurrence. Unreported or unusual side effects or adverse interactions involving medications will also be considered. Case Reports should not exceed 3,000 words in length (excluding references).

News articles should report the latest events in health sciences and medical research from around the world. News should not exceed 500 words in length.

Letters should present considered opinions in response to articles published in BioScience Trends in the last 6 months or issues of general interest. Letters should not exceed 800 words in length and may contain a maximum of 10 references.

3. Editorial Policies

Ethics: BioScience Trends requires that authors of reports of investigations in humans or animals indicate that those studies were formally approved by a relevant ethics committee or review board.

Conflict of Interest: All authors are required to disclose any actual or potential conflict of interest including financial interests or relationships with other people or organizations that might raise questions of bias in the work reported. If no conflict of interest exists for each author, please state "There is no conflict of interest to disclose".

Submission Declaration: When a manuscript is considered for submission to BioScience Trends, the authors should confirm that 1) no part of this manuscript is currently under consideration for publication elsewhere; 2) this manuscript does not contain the same information in whole or in part as manuscripts that have been published, accepted, or are under review elsewhere, except in the form of an abstract, a letter to the editor, or part of a published lecture or academic thesis; 3) authorization for publication has been obtained from the authors' employer or institution; and 4) all contributing authors have agreed to submit this manuscript.

Cover Letter: The manuscript must be accompanied by a cover letter signed by the corresponding author on behalf of all authors. The letter should indicate the basic findings of the work and their significance. The letter should also include a statement affirming that all authors concur with the submission and that the material submitted for publication has not been published previously or is not under consideration for publication elsewhere. The cover letter should be submitted in PDF format. For example of Cover Letter, please visit http://www.biosciencetrends.com/downcentre.php (Download Centre).

Copyright: A signed JOURNAL PUBLISHING AGREEMENT (JPA) form must be provided by post, fax, or as a scanned file before acceptance of the article. Only forms with a hand-written signature are accepted. This copyright will ensure the widest possible dissemination of information. A form facilitating transfer of copyright can be downloaded by clicking the appropriate link and can be returned to the e-mail address or fax number noted on the form (Please visit Download Centre). Please note that your manuscript will not proceed to the next step in publication until the JPA Form is received. In addition, if excerpts from other copyrighted works are included, the author(s) must obtain written permission from the copyright owners and credit the source(s) in the article.

Suggested Reviewers: A list of up to 3 reviewers who are qualified to assess the scientific merit of the study is welcomed. Reviewer information including names, affiliations, addresses, and e-mail should be provided at the same time the manuscript is submitted online. Please do not suggest reviewers with known conflicts of interest, including participants or anyone with a stake in the proposed research; anyone from the same institution; former students, advisors, or research collaborators (within the last three years); or close personal contacts. Please note that the Editor-in-Chief may accept one or more of the proposed reviewers or may request a review by other qualified persons.

Language Editing: Manuscripts prepared by authors whose native language is not English should have their work proofread by a native English speaker before submission. If not, this might delay the publication of your manuscript in BioScience Trends.

The Editing Support Organization can provide English proofreading, Japanese-English translation, and Chinese-English translation services to authors who want to publish in BioScience Trends and need assistance before submitting a manuscript. Authors can visit this organization directly at http://www.iacmhr.com/iac-eso/support.php?lang=en. IAC-ESO was established to facilitate manuscript preparation by researchers whose native language is not English and to help edit works intended for international academic journals.

4. Manuscript Preparation

Manuscripts should be written in clear, grammatically correct English and submitted as a Microsoft Word file in a single-column format. Manuscripts must be paginated and typed in 12-point Times New Roman font with 24-point line spacing. Please do not embed figures in the text. Abbreviations should be used as little as possible and should be explained at first mention unless the term is a well-known abbreviation (*e.g.* DNA). Single words should not be abbreviated.

Title Page: The title page must include 1) the title of the paper (Please note the title should be short, informative, and contain the major key words); 2) full name(s) and affiliation(s) of the author(s), 3) abbreviated names of the author(s), 4) full name, mailing address, telephone/fax numbers, and e-mail address of the corresponding author; and 5) conflicts of interest (if you have an actual or potential conflict of interest to disclose, it must be included as a footnote on the title page of the manuscript; if no conflict of

interest exists for each author, please state "There is no conflict of interest to disclose"). Please visit Download Centre and refer to the title page of the manuscript sample.

Abstract: The abstract should briefly state the purpose of the study, methods, main findings, and conclusions. For article types including Original Article, Brief Report, Review, Policy Forum, and Case Report, a one-paragraph abstract consisting of no more than 250 words must be included in the manuscript. For News and Letters, a brief summary of main content in 150 words or fewer should be included in the manuscript. Abbreviations must be kept to a minimum and non-standard abbreviations explained in brackets at first mention. References should be avoided in the abstract. Key words or phrases that do not occur in the title should be included in the Abstract page.

Introduction: The introduction should be a concise statement of the basis for the study and its scientific context.

Materials and Methods: The description should be brief but with sufficient detail to enable others to reproduce the experiments. Procedures that have been published previously should not be described in detail but appropriate references should simply be cited. Only new and significant modifications of previously published procedures require complete description. Names of products and manufacturers with their locations (city and state/country) should be given and sources of animals and cell lines should always be indicated. All clinical investigations must have been conducted in accordance with Declaration of Helsinki principles. All human and animal studies must have been approved by the appropriate institutional review board(s) and a specific declaration of approval must be made within this section.

Results: The description of the experimental results should be succinct but in sufficient detail to allow the experiments to be analyzed and interpreted by an independent reader. If necessary, subheadings may be used for an orderly presentation. All figures and tables must be referred to in the text.

Discussion: The data should be interpreted concisely without repeating material already presented in the Results section. Speculation is permissible, but it must be well-founded, and discussion of the wider implications of the findings is encouraged. Conclusions derived from the study should be included in this section.

Acknowledgments: All funding sources should be credited in the Acknowledgments section. In addition, people who contributed to the work but who do not meet the criteria for authors should be listed along with their contributions.

References: References should be numbered in the order in which they appear in the text. Citing of unpublished results, personal communications, conference abstracts, and theses in the reference list is not recommended but these sources may be mentioned in the text. In the reference list, cite the names of all authors when there are fifteen or fewer authors; if there are sixteen or more authors, list the first three followed by *et al.* Names of journals should be abbreviated in the style used in PubMed. Authors are responsible for the accuracy of the references. Examples are given below:

Example 1 (Sample journal reference):
Inagaki Y, Tang W, Zhang L, Du GH, Xu WF, Kokudo N. Novel aminopeptidase N (APN/CD13) inhibitor 24F can suppress invasion of hepatocellular carcinoma cells as well as angiogenesis. Biosci Trends. 2010; 4:56-60.

Example 2 (Sample journal reference with more than 15 authors):
Darby S, Hill D, Auvinen A, *et al.* Radon in homes and risk of lung cancer: Collaborative analysis of individual data from 13 European case-control studies. BMJ. 2005; 330:223.

Example 3 (Sample book reference):
Shalev AY. Post-traumatic stress disorder: diagnosis, history and life course. In: Post-traumatic Stress Disorder, Diagnosis, Management and Treatment (Nutt DJ, Davidson JR, Zohar J, eds.). Martin Dunitz, London, UK, 2000; pp. 1-15.

Example 4 (Sample web page reference):
Ministry of Health, Labour and Welfare of Japan. Dietary reference intakes for Japanese. *http://www.mhlw.go.jp/houdou/2004/11/h1122-2a.html* (accessed June 14, 2010).

Tables: All tables should be prepared in Microsoft Word or Excel and should be arranged at the end of the manuscript after the References section. Please note that tables should not in image format. All tables should have a concise title and should be numbered consecutively with Arabic numerals. If necessary, additional information should be given below the table.

Figure Legend: The figure legend should be typed on a separate page of the main manuscript and should include a short title and explanation. The legend should be concise but comprehensive and should be understood without referring to the text. Symbols used in figures must be explained.

Figure Preparation: All figures should be clear and cited in numerical order in the text. Figures must fit a one- or two-column format on the journal page: 8.3 cm (3.3 in.) wide for a single column, 17.3 cm (6.8 in.) wide for a double column; maximum height: 24.0 cm (9.5 in.). Please make sure that the symbols and numbers appeared in the figures should be clear. Please make sure that artwork files are in an acceptable format (TIFF or JPEG) at minimum resolution (600 dpi for illustrations, graphs, and annotated artwork, and 300 dpi for micrographs and photographs). Please provide all figures as separate files. Please note that low-resolution images are one of the leading causes of article resubmission and schedule delays. All color figures will be reproduced in full color in the online edition of the journal at no cost to authors.

Units and Symbols: Units and symbols conforming to the International System of Units (SI) should be used for physicochemical quantities. Solidus notation (*e.g.* mg/kg, mg/mL, mol/mm^2/min) should be used. Please refer to the SI Guide www.bipm.org/en/si/ for standard units.

Supplemental data: Supplemental data might be useful for supporting and enhancing your scientific research and BioScience Trends accepts the submission of these materials which will be only published online alongside the electronic version of your article. Supplemental files (figures, tables, and other text materials) should be prepared according to the above guidelines, numbered in Arabic numerals (*e.g.*, Figure S1, Figure S2, and Table S1, Table S2) and referred to in the text. All figures and tables should have titles and legends. All figure legends, tables and supplemental text materials should be placed at the end of the paper. Please note all of these supplemental data should be provided at the time of initial submission and note that the editors reserve the right to limit the size and length of Supplemental Data.

5. Submission Checklist

The Submission Checklist will be useful during the final checking of a manuscript prior to sending it to BioScience Trends for review. Please visit Download Centre and download the Submission Checklist file.

6. Online Submission

Manuscripts should be submitted to BioScience Trends online at http://www.biosciencetrends.com. The manuscript file should be smaller than 5 MB in size. If for any reason you are unable to submit a file online, please contact the Editorial Office by e-mail at office@biosciencetrends.com.

7. Accepted Manuscripts

Proofs: Galley proofs in PDF format will be sent to the corresponding author via e-mail. Corrections must be returned to the editor (proof-editing@biosciencetrends.com) within 3 working days.

Offprints: Authors will be provided with electronic offprints of their article. Paper offprints can be ordered at prices quoted on the order form that accompanies the proofs.

Page Charge: Page charges will be levied on all manuscripts accepted for publication in BioScience Trends ($140 per page for black white pages; $340 per page for color pages). Under exceptional circumstances, the author(s) may apply to the editorial office for a waiver of the publication charges at the time of submission.

(*Revised February 2013*)

Editorial and Head Office:
Pearl City Koishikawa 603
2-4-5 Kasuga, Bunkyo-ku
Tokyo 112-0003 Japan
Tel: +81-3-5840-8764
Fax: +81-3-5840-8765
E-mail: office@biosciencetrends.com

BST
BioScience Trends

JOURNAL PUBLISHING AGREEMENT (JPA)

Manuscript No.:

Title:

Corresponding Author:

The International Advancement Center for Medicine & Health Research Co., Ltd. (IACMHR Co., Ltd.) is pleased to accept the above article for publication in BioScience Trends. The International Research and Cooperation Association for Bio & Socio-Sciences Advancement (IRCA-BSSA) reserves all rights to the published article. Your written acceptance of this JOURNAL PUBLISHING AGREEMENT is required before the article can be published. Please read this form carefully and sign it if you agree to its terms. The signed JOURNAL PUBLISHING AGREEMENT should be sent to the BioScience Trends office (Pearl City Koishikawa 603, 2-4-5 Kasuga, Bunkyo-ku, Tokyo 112-0003, Japan; E-mail: **office@biosciencetrends.com**; Tel: **+81-3-5840-8764**; Fax: **+81-3-5840-8765**).

1. Authorship Criteria

As the corresponding author, I certify on behalf of all of the authors that:

1) The article is an original work and does not involve fraud, fabrication, or plagiarism.
2) The article has not been published previously and is not currently under consideration for publication elsewhere. If accepted by BioScience Trends, the article will not be submitted for publication to any other journal.
3) The article contains no libelous or other unlawful statements and does not contain any materials that infringes upon individual privacy or proprietary rights or any statutory copyright.
4) I have obtained written permission from copyright owners for any excerpts from copyrighted works that are included and have credited the sources in my article.
5) All authors have made significant contributions to the study including the conception and design of this work, the analysis of the data, and the writing of the manuscript.
6) All authors have reviewed this manuscript and take responsibility for its content and approve its publication.
7) I have informed all of the authors of the terms of this publishing agreement and I am signing on their behalf as their agent.

2. Copyright Transfer Agreement

I hereby assign and transfer to IACMHR Co., Ltd. all exclusive rights of copyright ownership to the above work in the journal BioScience Trends, including but not limited to the right 1) to publish, republish, derivate, distribute, transmit, sell, and otherwise use the work and other related material worldwide, in whole or in part, in all languages, in electronic, printed, or any other forms of media now known or hereafter developed and the right 2) to authorize or license third parties to do any of the above.

I understand that these exclusive rights will become the property of IACMHR Co., Ltd., from the date the article is accepted for publication in the journal BioScience Trends. I also understand that IACMHR Co., Ltd. as a copyright owner has sole authority to license and permit reproductions of the article.

I understand that except for copyright, other proprietary rights related to the Work (*e.g.* patent or other rights to any process or procedure) shall be retained by the authors. To reproduce any text, figures, tables, or illustrations from this Work in future works of their own, the authors must obtain written permission from IACMHR Co., Ltd.; such permission cannot be unreasonably withheld by IACMHR Co., Ltd.

3. Conflict of Interest Disclosure

I confirm that all funding sources supporting the work and all institutions or people who contributed to the work but who do not meet the criteria for authors are acknowledged. I also confirm that all commercial affiliations, stock ownership, equity interests, or patent-licensing arrangements that could be considered to pose a financial conflict of interest in connection with the article have been disclosed.

Corresponding Author's Name (Signature):

Date: